Title: Immunomodulatory interactions of B cells in human gut-associated lymphoid tissue

Authors: Michael J. Pitcher[1], Xiaowen Sun[1], Chiara Dionisi[1], Lucia Montorsi[1], Sherine H. Kottoor[1], Jacqueline H.Y. Siu[2], Roman Laddach[3], Rosamond Nuamah[3], Gavin J. Pettigrew[4], Richard J. Ellis[5], Cynthia Bishop[5], Jahangir Sufi[5], Pawan Dhami[6], Heli Vaikkinen[6], Audrey Kelly[1], Anna Vossenkamper[7], Deena L. Gibbons[1], Jo Spencer[1]*.

Affiliations:

[1]School of Immunology and Microbial Sciences, King's College London; London, UK.

[2]The Kennedy Institute of Rheumatology, University of Oxford; Oxford, UK.

[3]School of Cancer and Pharmaceutical Sciences, King's College London; London, UK.

[4]Department of Surgery, University of Cambridge; Cambridge UK.

[5]Advanced Cytometry Platform, Guy's and St Thomas' NHS Foundation Trust; London, UK.

[6]Genomics Research Platform and Single Cell Laboratory at Guy's and St Thomas' NHS Foundation Trust; London, UK.

[7]Blizard Institute, Barts and the London School of Medicine and Dentistry, Queen Mary University London; London, UK.

*Corresponding author. Email: jo.spencer@kcl.ac.uk

Formatted: Font: 12 pt
Formatted: Font: (Default) Times New Roman, 12 pt
Formatted: Font: (Default) Times New Roman, 12 pt
Formatted: Font: (Default) Times New Roman, 12 pt
Formatted: Font: (Default) Times New Roman, 12 pt
Formatted: Font: (Default) Times New Roman, 12 pt
Formatted: Font: (Default) Times New Roman, 12 pt
Deleted: .
Formatted: Font: (Default) Times New Roman, 12 pt
Deleted: .
Formatted: Font: (Default) Times New Roman, 12 pt
Deleted: ONE-SENTENCE SUMMARY¶
Spatial transcriptomics enriched by single cell RNA sequencing data identifies that double negative 2 B cells that are located on the antigenic front line in human gut-associated lymphoid tissue, are highly interactive and immunomodulatory through their secretome and expression of receptors.¶
Formatted: Font: (Default) Times New Roman, 12 pt, Bold, Font colour: Text 1, English (US), Not Superscript/ Subscript
Formatted: Justified
Formatted: Font: (Default) Times New Roman, 12 pt
Deleted: ,
Deleted: United Kingdom
Formatted: Font: (Default) Times New Roman, 12 pt
Deleted: ¶
... [1]

ABSTRACT

Gut-associated lymphoid tissue (GALT) is organized lymphoid tissue that responds chronically to antigens, including whole bacteria, sampled from the gut lumen. The ensuing IgA plasma cell response disseminates to regulate bacterial populations and to mediate intestinal immune homeostasis. GALT has roles in the development of the innate like marginal zone B cell population and is also associated with a B cell mediated contribution to ulcerative colitis (UC) severity and response to therapy. Applying integrated multiomics methodologies, we identified key, spatially resolved interactions of B cell subsets including broad regulatory features of double negative 2 B cells with potential to maintain homeostasis on the microbe-rich mucosal front line. By contrast, GALT in UC is distorted in composition and spatial distribution of B cell subsets that have altered immunomodulatory potential compared to healthy GALT. Thus, we identify interactions of strategically located B cells as mediators of immunological equilibrium in human gut.

Deleted: s

Deleted: Superimposed on this,

Deleted: . It

Formatted: Font: (Default) Times New Roman, 12 pt

Deleted: Here by

Deleted: y

Formatted: Font: (Default) Times New Roman, 12 pt

Deleted: , by contrast,

Formatted: Font: (Default) Times New Roman, 12 pt

Deleted: The data we present provides a fundamental foundation for understanding the roles of B cells in human GALT.…

Formatted: Font: (Default) Times New Roman, 12 pt

ONE-SENTENCE SUMMARY

B cells on the antigenic front line in human gut-associated lymphoid tissue, are highly interactive and immunomodulatory.

Main text:

INTRODUCTION

Gut-associated lymphoid tissue (GALT) is active organized lymphoid tissue situated at the boundary between the intestinal microbiota and the host (1). Microbial antigens, including bacteria, are sampled from the gut lumen by the follicle associated epithelium (FAE) that overlies GALT and delivered to the subepithelial dome (SED) below (2-5). Ensuing B cell responses, both T-dependent and T-independent, can propagate the IgA plasma cell response that migrates from GALT to colonize the extensive lamina propria (LP) (6-8). The IgA secreted by LP plasma cells is actively transported across the intestinal epithelium where it maintains a healthy microbiota composition (9).

In addition to the generation of IgA plasma cells (10, 11), further functions of GALT have been identified including a role in supporting the maturation of innate-like marginal zone B cells (MZB) (12). Mature MZB, that circulate in the blood and locate mostly in the microanatomically defined marginal zone of the spleen, recognize antigens with repeating subunit structures and thus are protective against infections with bacteria that have repeating subunit antigens on their surface such as capsular polysaccharides (13). Some MZB that respond to pneumococcal vaccine have BCRs that also have specificity for antigens expressed on gut bacteria (12). Thus, the roles of GALT involve encountering and responding to microbial antigens. Yet, despite being rich in innate ligands, sampled microbes do not drive acute inflammation in the GALT microenvironment (1, 14).

To understand the interactions of B cells in GALT we studied human appendix that contains abundant well-orientated GALT. Data was acquired using the CosMx platform. Segmented single cells were aligned to different cell lineages. By integration with CITE-seq reference data, B cells belonging to different subsets were localized in GALT and imputed gene expression used to enrich the information provided by the CosMx platform. This allowed for exploration of B cell subset interactions with other lineages based on cell proximities. We observed that the SED is the zone with highest B cell interaction strengths. Double negative 2 (DN2) cells are relatively abundant in the SED and have strong cellular interactomes that are mostly immunosuppressive

Formatted: Font colour: Text 1

Formatted: Font: (Default) Times New Roman, 12 pt

Deleted: s…d lymphoid tissue situated at the boundary between the intestinal microbiota and the host ... [2]

Formatted ... [3]

Deleted: microfold (M) cells within the specialised epithelial monolayer termed …he follicle associated epithelium (FAE) that overlies GALT . Bacteria are ... [4]

Deleted: transported …o the subepithelial dome (SED) ... [5]

Formatted: Font: (Default) Times New Roman, 12 pt

Formatted ... [6]

Deleted: s… the extensive lamina propria (LP) ... [7]

Formatted: Font: Not Italic

Formatted ... [8]

Deleted:

Formatted ... [9]

Deleted: Whilst …n addition tothe role of GALT in…the generation of IgA plasma cells has been known for de ... [10]

Formatted ... [11]

Deleted: more recently …ncluding a role for GALT …n supporting the maturation of innate- ... [12]

Formatted ... [13]

Deleted: s… antigens with repeating subunit structures and thus are protective against infections with bacteria that have repeating subunit antigens on their surface such as capsular polysaccharides ... [14]

Formatted ... [15]

Deleted:

Formatted: Font: (Default) Times New Roman, 12 pt

Formatted: Font: (Default) Times New Roman, 12 pt

Deleted: s

Deleted: X

Formatted ... [16]

(4). Interactions involving CD86, progranulin and Epstein-Barr virus induced gene 3 (EBI3) expressed by DN2 cells were validated by RNAscope and protein expression in the SED confirmed.

The appendix has been associated with the inflammatory bowel disease ulcerative colitis (UC) in several ways (15, 16). Peri-appendiceal 'red patches' can be observed endoscopically around the appendiceal orifice in UC, even when the inflammation is restricted to the distal colon and rectum (17). Also, it has been proposed that appendectomy in early life can be protective against subsequent development of UC, though this is debated (15, 16). Most recently, studies of the cellular content of GALT in UC identified variation associated with clinical response to the drug vedolizumab that blocks interactions between integrin α4β7 and its endothelial ligand mucosal addressin cell adhesion molecule 1 (MAdCAM1)(18). We observed that whilst B cell follicles are present in appendix in UC, the microanatomy is disrupted including altered distribution of DN2 cells and expression of immunomodulators.

Thus, the maintenance of a chronically active but uninflamed microenvironment in GALT includes the production of immunomodulators by B cells, the disruption of which may be involved with inflammatory processes in the gut.

RESULTS

Immune cell lineages in GALT visualized by spatial transcriptomics

The aim of this study was to identify cellular interactions of B cells in GALT microenvironments and the first step towards this goal was to identify cell lineages that could contribute to the interactome in data acquired by CosMx (Fig. 1A). After quality control (fig. S1, A and B), segmented cells from the CosMx output were clustered based on their transcripts (fig. S1C). Clusters of cells representing epithelial cells were identified and classified (fig. S1, D and E). Previously published single cell RNA sequencing (scRNA-seq) data acquired from B cells, plasma cells, T cells, myeloid cells, endothelial cells and mesenchymal cells from adult human appendix was used for further lineage classification (19). A weighted anchor-based data transfer method(20) was used to transfer cell lineage labels from the reference dataset to the query CosMx dataset based on transcriptomic similarity between the query CosMx cells and the

Deleted: e
Formatted: Font: (Default) Times New Roman, 12 pt
Formatted: Font: (Default) Times New Roman, 12 pt
Formatted: Font: (Default) Times New Roman, 12 pt
Formatted: Font: (Default) Times New Roman, 12 pt
Deleted:
Formatted: Font: (Default) Times New Roman, 12 pt
Formatted: Font: (Default) Times New Roman, 12 pt
Deleted:
Deleted: In addition
Formatted: Font: (Default) Times New Roman, 12 pt
Formatted: Font: (Default) Times New Roman, 12 pt
Formatted: Font: (Default) Times New Roman, 12 pt
Deleted:
Formatted: Font: (Default) Times New Roman, 12 pt
Formatted: Font: (Default) Times New Roman, 12 pt
Formatted: Font: 12 pt
Formatted: Font: (Default) Times New Roman, 12 pt
Formatted: Font: 12 pt
Formatted: Font: (Default) Times New Roman, 12 pt
Deleted:
Formatted: Font: (Default) Times New Roman, 12 pt
Formatted: Font: (Default) Times New Roman, 12 pt
Deleted: s
Deleted: towards
Deleted: The first step towards identifying B cell subsets interactions in GALT microenvironments was to identify cell lineages that could contribute to the interactome in data acquired by CosMx
Deleted:
Formatted: Font: (Default) Times New Roman, 12 pt
Formatted: Font: (Default) Times New Roman, 12 pt
Formatted: Font: (Default) Times New Roman, 12 pt
Deleted:
Formatted: Font: (Default) Times New Roman, 12 pt
Formatted: Font: (Default) Times New Roman, 12 pt

reference scRNA-seq cells (Fig. 1A). The lineage classifications were then visualized spatially (Fig. 1, B and C and fig. S1F) and validated on the images by comparison with module scores of lineage marker genes (Fig. 1D and data file S1) and average expression of lineage markers per classification (Fig. 1E). Clusters broadly aligned with single lineages (Fig. 1, F and fig. S1C), though endothelial cells did not cluster together. Samples displayed similar proportions of cell lineages (fig. S1G).

To compute the relative spatial distribution of cell lineages within the tissues, a neighbor graph was constructed with edges indicating which cells were adjacent to each other with potential for interaction (fig. S1H). Having identified neighboring cells, a metric of neighborhood similarity was calculated for each cell by comparing the proportion of neighboring cells which shared the same lineage as the target cell. When viewed spatially, this metric highlighted large regions of same-lineage interactions (Fig. 1G and fig. S1I). B cells and T cells had the highest neighborhood similarity, illustrating their tendency to reside in lineage-homotypic zones, whereas myeloid cells had the lowest metric, indicating a propensity to reside in regions comprised of different lineages (Fig. 1H). Statistical testing of cell lineage proximities found that all lineages were significantly in proximity to themselves across the samples (Fig. 1I). Mesenchymal cells showed positive interactions with myeloid and endothelial cells. B cells showed negative interactions with all other lineages, further confirming the tendency of most B cells to reside in zones comprised of mostly B cells.

Thus, lineage information was assigned to segmented cells in CosMx data to generate profiles consistent with published work(4, 19, 21).

B cell subset identification in normal human GALT

Human GALT contains many potentially interacting B cell subsets, the features which are described in data file S2. To identify the spatial distribution of B cell subsets in GALT within the CosMx data, the lineage-delineated CosMx data was initially filtered down to cells classified as B cells (Fig. 2A). The number and identity of the genes in the 1000 probe set used for CosMx data acquisition were not sufficient to identify the locations of B cells of each subset in the

Deleted: s

Deleted: table

Deleted: S

Formatted: Font: (Default) Times New Roman, 12 pt

Deleted: interestingly

Deleted: u

Deleted: u

Deleted: u

Deleted: u

Deleted:

Formatted: Font: (Default) Times New Roman, 12 pt

Formatted: Font: (Default) Times New Roman, 12 pt

Formatted: Font: (Default) Times New Roman, 12 pt

Deleted: F

Deleted: of the B cell subsets to be studied here

Formatted: Font: (Default) Times New Roman, 12 pt

Deleted: table S

CosMx data. Therefore, to identify B cell subsets, a CITE-seq dataset was generated to allow transfer of B cell subset information by anchor-based data transfer (Fig. 2A)

B cells were sorted from three biological replicates of human appendix, labelled with oligonucleotide tagged antibodies (antibody detection tag: ADT, table S1), and loaded into the controller for 10x Chromium 5' for single cell CITE-seq immune profiling. Gene expression and ADT libraries were prepared and sequenced. After quality control (fig. S2A), data were integrated for both the RNA and ADT assays separately to remove batch effects in each assay. Dimensionality reduction was performed using a weighted-nearest-neighbor approach, combining both the transcriptomic and proteomic data. From the resulting uniform manifold approximation and projection (UMAP), donor of origin was visualized to ensure cells did not separate due to sample (fig. S2B), and the expression of cell surface antibody markers was visualized on the UMAP (fig. S2C). A clustering algorithm assigned cells into 30 distinct clusters based on similarities within both the transcriptome and proteome (fig. S2D). The mean expression of all surface markers (fig. S2E) and a selection of B cell-subset defining transcripts by reference to published work (fig. S2F) were visualized. Where necessary, clusters which showed heterogeneous profiles were split into subclusters using the same method in order to provide greater resolution (fig. S2D-F). Clusters and subclusters which displayed similar profiles were merged and assigned B cell subset labels according to known markers. From within the larger pool of naïve cells, transitional cells were distinguished by their surface expression of CD10 (22), whilst activated naïve (aNAV) were differentiated by surface expression of CD11c and gene expression of FCRL5. Germinal center (GC) cells were divided by Ki67 gene expression into centroblasts ($Ki67^+$) and centrocytes ($Ki67^-$)(23). Centroblasts also showed a greater proportion of cells in the G2M phase of the cell cycle (fig. S2G). A double-negative 2 (DN2) subset of B cells was identified by low surface expression of CD27, IgD, C-X-C Motif Chemokine Receptor 5 (CXCR5) and CD21 and high CD11c surface expression (24). This subset also showed high surface expression of Fc receptor-like 4 (FCRL4) and high gene expression of *FCRL4* and Fc receptor-like 5 (*FCRL5*)(25). A subset of activated B cells, ActB3, previously identified in human tissue and blood samples was identified here by high Metastasis Associated Lung Adenocarcinoma Transcript 1 (*MALAT1*) gene expression(26). MZB were identified by high CD27 and IgM surface expression, whilst IgM-only cells were distinguished

Deleted:
Deleted: 3
Deleted: samples
Formatted: Font: (Default) Times New Roman, 12 pt
Formatted: Font: (Default) Times New Roman, 12 pt
Deleted:
Deleted: table S3
Deleted: according to the manufacturer's instructions
Deleted: u
Deleted: s
Deleted: s
Deleted: s
Formatted: Font: (Default) Times New Roman, 12 pt
Formatted: Font: (Default) Times New Roman, 12 pt
Deleted: centre
Formatted: Font: (Default) Times New Roman, 12 pt
Formatted: Font: (Default) Times New Roman, 12 pt
Formatted: Font: (Default) Times New Roman, 12 pt
Formatted: Font: (Default) Times New Roman, 12 pt
Formatted: Font: (Default) Times New Roman, 12 pt
Formatted: Font: (Default) Times New Roman, 12 pt
Formatted: Font: (Default) Times New Roman, 12 pt
Formatted: Font: (Default) Times New Roman, 12 pt
Formatted: Font: (Default) Times New Roman, 12 pt
Deleted:
Formatted: Font: (Default) Times New Roman, 12 pt, Italic
Formatted: Font: (Default) Times New Roman, 12 pt
Formatted: Font: (Default) Times New Roman, 12 pt, Italic
Formatted: Font: (Default) Times New Roman, 12 pt
Formatted: Font: (Default) Times New Roman, 12 pt
Deleted:
Deleted: arginal zone B cells
Formatted: Font: (Default) Times New Roman, 12 pt, Italic
Formatted: Font: (Default) Times New Roman, 12 pt
Formatted: Font: (Default) Times New Roman, 12 pt
Formatted: Font: (Default) Times New Roman, 12 pt

from MZB by lower expression of CD1c and IgD and visualized on the UMAP (Fig. 2, B and C)(27, 28). Class switched memory B cells were CD27^{+} and expressed immunoglobulin isotypes other than IgM and IgD(29). The average expression profile for each subset was visualized for both the surface markers (Fig. 2C) and genes (Fig. 2D and data file S3). By linking the spatial CosMx dataset to the single-cell CITE-seq data, ADT marker expression (fig. S3A), B cell subset labels (Fig. 2E) and a higher-depth RNA assay were imputed in the spatial data, allowing identification of spatial densities of B cells subsets (fig. S3B).

Statistical tests were applied to B cell subsets to identify significant proximities between B cell subsets and cells of other lineages (Fig. 2F). The only strong positive proximities observed were plasmablasts with plasma cells to which they are developmentally related(30), and DN2 B cells with myeloid cells that have previously been observed to interact in the SED region(4).

We compared the representation of each subset within the CITE-seq and CosMx data (Fig. 2G). GC cells were relatively more abundant in the CosMx data. Despite the relative depletion in the cell suspensions, the centroblasts and centrocytes that have known microanatomical compartments(31) were well positioned in the images relative to each other and other cell types following anchor-based transfer of information. Thus, the distribution of B cell subsets was transferred to allow analysis of interactions in a subset specific context.

Cellular interactions of B cells in GALT identified within the CosMx dataset

Having identified the locations of individual cells belonging to major lineages (Fig. 1) and B cells belonging to different subsets in the CosMx data (Fig. 2), we sought to identify interactions between B cells in each subset and neighboring cells of other lineages, in which the B cells could be the target or the source of the interacting factor (Fig. 3A). To achieve this, a reference database of potential "ligand and receptor" gene pairs was used to identify when cell partners within an interacting receptor-ligand pair were present across an edge(32). Here, we define an interaction as an edge between two cells where one cell has expression of a receptor for a ligand expressed by the cell at the other end of the edge. Imputed genes are those expressed by B cells in a subset (data file S4). To be accepted as an interaction, we stipulated that the ligand-receptor pair must involve at least 10% of the edges between the cell types (Fig. 3A).

Deleted: marginal zone cells
Deleted: s
Formatted: Font: (Default) Times New Roman, 12 pt
Deleted:
Formatted: Font: (Default) Times New Roman, 12 pt
Formatted: Font: (Default) Times New Roman, 12 pt
Formatted: Font: (Default) Times New Roman, 12 pt, Superscript
Formatted: Font: (Default) Times New Roman, 12 pt
Deleted:
Deleted: s
Formatted: Font: (Default) Times New Roman, 12 pt
Formatted: Font: (Default) Times New Roman, 12 pt
Deleted: table
Deleted: 4
Formatted: Font: (Default) Times New Roman, 12 pt
Deleted:
Formatted: Font: (Default) Times New Roman, 12 pt
Formatted: Font: (Default) Times New Roman, 12 pt
Deleted:
Formatted: Font: (Default) Times New Roman, 12 pt
Formatted: Font: (Default) Times New Roman, 12 pt
Deleted: erminal centre
Deleted:
Formatted: Font: Not Italic
Formatted: Font: (Default) Times New Roman, 12 pt
Deleted: ¶ ¶
Deleted: ur
Formatted: Font: (Default) Times New Roman, 12 pt
Deleted:
Formatted: Font: (Default) Times New Roman, 12 pt
Formatted: Font: (Default) Times New Roman, 12 pt
Deleted: table
Deleted: S
Deleted: 5
Formatted: Font: (Default) Times New Roman, 12 pt

When interactions were identified, interaction strengths were determined by factoring together normalized reads of the source at one cell on the edge and the target on the opposite cell of the edge (Fig. 3A and data file S5). The combined strength of all target/ source pairs for each edge was then visualized, and it was observed that the SED was associated with the highest interaction strength across the images (Fig. 3, B and C).

Of the B cell subsets, aNAV and DN2 were the two subsets with the greatest interaction strengths with non-B cell lineages, but with relatively few edges compared to the subsets containing more cells (Fig. 3D and fig S4A). This is consistent with the biased distribution of DN2 towards the SED and FAE that contain many cell types(4).

The strengths of interactions between B cell subsets and cells of other lineages were then determined. Relatively strong interactions of DN2 cells with CD4 T cells, CD8 T cells, mesenchymal and myeloid cells were observed, whether DN2 cells were the source cells or the targets of the interaction (Fig. 3E and fig. S4B). After determining imputed interactions between B cell subsets and other lineages, the genes imputed on the DN2 cells that were involved in cellular interactions were run through pathway analysis to determine associated cell function. This identified that the interactions of DN2 B cells were broadly associated with cytokine signaling, leukocyte activation, cell trafficking and cell migration (Fig. 3F). Interactions between DN2 B cells and myeloid cells (Fig. 3G) CD4 T cells (Fig. 3H) and CD8 T cells (fig. S4C) were identified and grouped according to pathways identified in Fig. 3F.

This initial screen of interactions of B cells in different subsets identified some interactions that were not driven by significant features of the B cell subset (data files S3 and S4). For example, *IL16* was identified as a mediator of interactions between DN2 B cells and CD4 expressing myeloid and T cells (Fig. 3, G and H), yet *IL16* is not a marker gene of DN2 B cells (data file S3). Using an IMC panel that incorporated an RNAscope probe targeting the gene encoding *IL16* (data file S6), we determined that *IL16* is expressed by most B cells (fig. S4, D to G), and that the interaction was likely due to the microenvironmental proximity of DN2 cells to $CD4^+$ T cells and myeloid cells in the SED (fig. S4, F and G). Thus, B cell derived IL16 interacting with the

Deleted: s

Deleted: table S

Deleted: 6

Deleted: s

Deleted: whether the B cells was the source or the target of the interaction

Deleted: , irrespective of whether the markers they expressed were classified as receptors or ligands in the database

Formatted: Font: (Default) Times New Roman, 12 pt

Formatted: Font: (Default) Times New Roman, 12 pt

Deleted: 1

Formatted: Font: (Default) Times New Roman, 12 pt

Deleted: , whilst potentially important properties of B cells,

Deleted: particular

Deleted: table

Deleted: 4

Deleted: table S

Deleted: 5

Formatted: Font: (Default) Times New Roman, 12 pt

Formatted: Font: (Default) Times New Roman, 12 pt, Italic

Formatted: Font: (Default) Times New Roman, 12 pt

Deleted: table

Formatted: Font: (Default) Times New Roman, 12 pt, Italic

Formatted: Font: (Default) Times New Roman, 12 pt

Formatted: Font: (Default) Times New Roman, 12 pt

Deleted: 4

Formatted: Font: (Default) Times New Roman, 12 pt, Italic

Formatted: Font: (Default) Times New Roman, 12 pt

Deleted: table

Deleted: 7

Formatted: Font: (Default) Times New Roman, 12 pt

Formatted: Font: (Default) Times New Roman, 12 pt, Italic

Formatted: Font: (Default) Times New Roman, 12 pt

Deleted: apparent

Formatted: Font: (Default) Times New Roman, 12 pt, Superscript

Formatted: Font: (Default) Times New Roman, 12 pt

Formatted: Font: (Default) Times New Roman, 12 pt

CD4 molecule may have functional relevance in tissues, but this is not an interaction specifically associated with any B cell subset.

B cell subset interactions involving significant markers of B cell subsets.

We next analyzed B cell subset-specific interactions. We filtered the information to interactions that involved genes that were statistically associated with B cell subsets in the CITE-seq data (Fig. 3A). We also split the types of interactions to focus on those we considered to have functional relevance distinct from cell migration, cell retention or antigen presentation (data files S7 and S8). The comprehensive diagram of interactions of the 5 B cell subsets that are enriched in SED in human GALT are represented in Fig. 4A and listed with interactions strengths in data file S7. In general B cell subsets had contrasting interaction profiles. For example, the interaction profile of naïve B cells was dominated by interactions of LTA with TNF receptors that are associated with lymphoid tissue homeostasis and negative regulation of inflammation(33)(34). An interaction between *NOTCH2* expressed by MZB and delta ligand like 1 (*DLL1*) expressed by mesenchymal cells was observed, consistent with the predicted potential of MZB to develop from precursors in GALT under the NOTCH2–DLL1 signaling pathway(12, 28, 35).

The most interactive B cells in Fig. 3D and E were the aNAV and DN2 subsets, of which the DN2 were relatively more abundant and localized to the SED. We therefore focused again on the DN2 interactome. Interactions specific to DN2 cells included *TNFRSF13B* with *TNFSF13B* which is a known pathway supporting T cell independent IgA class switching in the SED region(6, 36). Other interactions of DN2 B cells involve B cell expression of *CD86, GRN, EBI3* and *SIGLEC10* that encode immunomodulatory proteins (37-41). Imputed expression of these genes can be localized mostly to the SED and GC in the CosMx data (Fig. 4B). The strongest imputed interactions of DN2 B cells that had not been identified before were validated as described below. Reagents were not available to enable validation of expression or interactions of *SIGLEC10*.

Interactions of B cells expressing subset marker genes relating to cell migration, retention and antigen presentation are represented in fig. S5 and listed in data file S8. Of note, DN2 cells are enriched in interactions involving *HLA, B2M and CD74*, consistent with their expression of

Deleted: …ay have important ... [17]

Deleted: s

Deleted: To do this, w… filtered the information to interactions that involved genes that were statistically associated with B cell subsets in the CITE-seq data (Fig. 3A). We also split the types of interactions to focus on those we considered to have functional relevance distinct from cell migration, cell retention ... [18]

Deleted: maintenance

Deleted: tables…SS…8…and SS…9…. The comprehensive diagram of interactions of the 5 B cell subsets that are enriched in SED in human GALT with subsets of T cells, endothelial, epithelial mesenchymal and myeloid cells …re represented in Fig. 4A and listed with interactions strengths in data file Stable S…8… In general B cell subsets had contrasting interaction profiles. For example, the interaction profile of naïve B cells was dominated by interactions of LTA with TNF receptors that are associated with lymphoid tissue homeostasis and negative regulation of inflammation ... [19]

Formatted: Font: (Default) Times New Roman, 12 pt

Deleted:

Formatted: Font: (Default) Times New Roman, 12 pt

Formatted ... [20]

Formatted ... [21]

Deleted: marginal zone B cells

Formatted: Font: (Default) Times New Roman, 12 pt

Deleted: l…ing pathway ... [22]

Formatted: Font: (Default) Times New Roman, 12 pt

Formatted: Font: (Default) Times New Roman, 12 pt

Deleted: s

Formatted ... [23]

Deleted:

Formatted ... [24]

Deleted: are all

Deleted:

Formatted: Font: (Default) Times New Roman, 12 pt

Formatted: Font: Not Italic

Formatted: Font: (Default) Times New Roman, 12 pt

Deleted: s…d mostly to the SED and GC in the CosMx data (Fig. 4B). The strongest imputed interactions of DN2 B cells that had not been identified before by others …ere validated as described below. RUnfortunately, r ... [25]

Formatted ... [26]

Deleted: table S…9 ... [27]

Deleted: *b2*

Formatted: Font: (Default) Times New Roman, 12 pt, Italic

Formatted: Font: (Default) Times New Roman, 12 pt

CD86 and a potential role in antigen presentation(42, 43). The interaction of *CCR7* with *CCL19/21*, that mediates lymphocyte recirculation between lymphoid tissues and blood, is identified in MZB, memory B cells and IgM-only B cells although not in DN2, suggesting a difference in systemic circulation(44). Memory B cells have prominent ITGB1 associated interactions (fig. S5). Thus, analysis of interactions of B cell subsets in GALT considering specifically those involving marker genes of individual subsets identified known and previously unknown interactions of B cells relevant to local immune function and regulation.

DN2 cells express CD86 gene and protein

To validate expression and interactions of CD86, initially an IMC panel including probes for *CD86* and *CTLA4* was applied to FFPE sections of human appendix (data file S6). The structural features of human GALT including the distribution of E-cadherin, CD20, Ki67, FcRL4, CD3, CD31, and CD68 and CD38, were initially used to identify microanatomy such as the SED and GC (Fig. 5, A and B). DN2 cells were then identified by their co-expression of FcRL4 and CD11c (encoded by *ITGAX*) (Fig. 5C) and the relative expression of *CD86* and *CTLA4* was visualized (Fig. 5D). *CD86* message was observed in DN2 cells expressing *ITGAX* and FcRL4, including cells located in epithelium (Fig. 5E). CD4 T cells expressing *CTLA4* were observed in the SED in close proximity to *CD86* mRNA (Fig. 5F).

To determine whether CD86 protein is expressed by B cells in the SED and in the epithelium as predicted by gene expression, FFPE sections of appendix were stained with antibodies to CD86 and CD20 (table S2). Co-expression was observed in the intraepithelial and SED compartments by immunofluorescence (IF) (Fig. 5G). Because of the expression of CD86 by M cells that are in close proximity to B cells (5), confocal microscopy (CM) was used to confirm co-expression of CD86 and CD20 (Fig. 5H). Thus, CD86 expression by DN2 B cells and interaction with CTLA4 was validated.

DN2 cells express GRN gene and protein

To validate expression and interactions of *GRN*, initially an IMC panel including probes to detect mRNA encoding *GRN, TNFRSF1A and TNFRSF1B* was applied to FFPE sections of human appendix (data file S6). The structural features of human GALT including the distribution of E-

Deleted:
Formatted ... [28]
Formatted ... [29]
Deleted: marginal zone
Formatted: Font: (Default) Times New Roman, 12 pt
Deleted:
Formatted ... [30]
Deleted: Validation of interactions involving CD86 expressing
Formatted: Font: (Default) Times New Roman, 12 pt
Deleted: An
Formatted ... [31]
Deleted: table S…7, that includes description of antibody specificities and relevance of markers to the panel ... [32]
Formatted ... [33]
Deleted: s
Formatted ... [34]
Deleted: table …able S2S10…. Co- ... [35]
Formatted: Font: Not Italic
Formatted ... [36]
Deleted: Validation of interactions involving GRN expressing DN2 cells¶
Deleted: A
Formatted: Font: Italic
Formatted ... [37]
Deleted: table
Deleted: 7
Formatted: Font: (Default) Times New Roman, 12 pt

cadherin, CD20, Ki67, FcRL4, CD3, CD68 and CD38, were initially used to identify the SED and GC (Fig. 6, A and B). DN2 cells were identified by co-expression of CD11c and FcRL4 (Fig. 6C). Expression of *GRN* by DN2 cells was confirmed in the SED (Fig. 6D), though most *GRN* was not expressed by B cells. Expression of imputed targets of *GRN, TNFRSF1A and TNFRSF1B*, was observed in the SED alongside *GRN* (Fig. 6E). Cells from within Fig. 6E were further observed to confirm the expression of *TNFRSF1B* by CD68, CD4 and CD8 expressing cells in the same regions of the SED, where DN2 B cells expressed *GRN*. Expression of progranulin (that is encoded by the *GRN* gene) by B cells in the FAE and SED was confirmed by IF (Fig. 6I) and CM (Fig. 6J). Thus, *GRN* expression by DN2 B cells and interaction with *TNFRSF1A* and *TNFRSF1B* was validated.

DN2 cells express EBI3 gene and protein

EBI3 is a subunit of heterodimeric cytokines IL-27 (with the p28 subunit) and IL-35 (with the p35 subunit) (45). It was identified as an interacting partner because adjacent cells expressed the IL27 receptor component *IL27RA* and the signaling protein *IL6ST* that are known to be expressed abundantly(45). We asked whether the p28 subunit of IL27 or the p35 subunit of IL35, encoded by *IL27* and *IL12A* genes respectively, were expressed significantly by DN2 B cells and they were not (Fig 7A and data file S3). We therefore validated the expression of *EBI3* using an IMC panel including an RNAscope probe for *EBI3*.

The structure of GALT including the SED and GC was annotated by visualizing the distribution of E-cadherin, CD20, Ki67, CD3, CD68 and CD38 (Fig. 7B and C). Expression of *EBI3* gene by DN2 B cells, identified by co-expression of CD11c and FCRL4, was confirmed (Fig. 7D). Expression in the light zone of the GC was also observed consistent with gene expression information in Fig. 7A. Expression of EBI3 protein by B cells in SED was confirmed by IF (Fig. 7E) and CM (Fig. 7F). Thus, expression of EBI3, that itself can be immunomodulatory(46, 47), by DN2 B cells in the SED, was validated.

B cells in GALT in ulcerative colitis.

Appendix has been implicated in UC in several contrasting ways(15-18). We applied IMC to investigate cellular interactions in four samples of appendix from patients with severe UC who

Formatted ... [38]
Deleted: by
Formatted ... [39]
Formatted: Font: Not Italic
Deleted: ¶
Deleted: Validation of expression of EBI3 by DN2 ... [40]
Deleted: protein
Formatted ... [41]
Deleted: l
Formatted ... [42]
Formatted ... [43]
Deleted:
Formatted ... [44]
Deleted: table …34 ... [45]
Formatted ... [46]
Deleted: ¶
Formatted: Font: (Default) Times New Roman, 12 pt
Deleted: s
Formatted ... [47]
Formatted: Font: Not Italic
Formatted: Font: (Default) Times New Roman, 12 pt
Deleted:
Formatted ... [48]
Deleted: 4
Formatted: Font: (Default) Times New Roman, 12 pt

had surgical right hemicolectomy as part of disease management (data files S9 and table S3). Following data acquisition by IMC, cells in images were segmented, quality controlled (fig. S6A), and cell lineages were identified using a semi-supervised machine learning approach from manually gated data (fig. S6B).

The distribution of key lineage markers and markers indicating B cell zonation were visualized alongside computationally derived lineages to ensure they were consistent for HC appendix (Fig. 8A) and examples of appendix from patients with UC (Fig. 8, B and C). Neighborhood graphs were constructed per image, and the proportion of lineage neighbors per ROI was determined. A principal component analysis (PCA) constructed on the lineage-based edge types showed the HC samples were consistent in their neighborhood composition, whilst the UC samples exhibited much greater heterogeneity and were distinct from HC samples (Fig. 8D). Proximity testing performed to investigate this differential identified a greater tendency for B and T cells to be neighbors in UC compared to HC consistent with loss of B cell and T cell zonation (Fig. 8E). Comparison of the number of B cells with at least one T cell neighbor validated this (Fig. 8F).

B cell subsets were identified based on clustering the labelled B cells for HC (fig. S6, C to E) and UC (fig. S6, F to H). When DN2 cells were visualized on the images (Fig. 8, G and H), they clustered closer to the epithelium in HC than in UC, confirmed by a difference in distribution of DN2 when based on their minimum distance to an epithelial cell (Fig. 8I).

We determined the expression of CD86, EBI3 and progranulin by B cells in UC mucosa. Little or no B cell expression of CD86 could be observed in UC samples, despite detection of some non-B cells in epithelium expressing CD86 (Fig. 8J). In contrast, progranulin (Fig. 8K) and EBI3 (Fig. 8L) were both expressed abundantly by B cells located close to epithelium in UC.

Thus, we observed that cell lineages and B cell subsets had altered microarchitecture in GALT in UC. DN2 B cells that are the most interactive B cell subset in GALT in HC were not as localized to the SED in UC as they are in HC, and of the B cell associated immunomodulators described here CD86 was reduced and EBI3 and progranulin were over expressed by B cells in the UC samples. These findings overall establish a framework for understanding how B cell ecosystems

Deleted: table
Deleted: 11
Deleted: S12
Formatted: Font: (Default) Times New Roman, 12 pt
Formatted: Font: (Default) Times New Roman, 12 pt
Deleted: s
Deleted: u
Deleted: u
Formatted: Font: (Default) Times New Roman, 12 pt
Formatted: Font: (Default) Times New Roman, 12 pt
Deleted: u
Deleted: u
Deleted: of
Deleted: u
Deleted: s
Deleted: s

can preserve a microenvironment in GALT permissive for maintenance of active immune homeostasis and how their disruption may contribute to inflammatory bowel disease.

DISCUSSION

The FAE that overlies the lymphoid tissue in GALT actively samples microbes into lymphoid tissues(1). We wished to understand the interactions of B cells on this antigenic frontline that contribute to the maintenance of tissue homeostasis in the presence of innate ligands. We identified that the most interactive B cells in human GALT are aNAV and DN2 cells. Of these cell subtypes, DN2 are most abundant and localize in the SED region where the immune system encounters antigens, including bacteria actively sampled from the gut lumen. We therefore focused attention on this B cell subset and observed that the dominant interactions of DN2 cells are immunomodulatory.

There is already precedent for some imputed interactions from studies of in vivo mouse models and human cells in vitro(6, 36, 48, 49). For example, here we identify DN2 expression of TNFRSF13B that encodes transmembrane activator and CAML interactor (TACI) interacting with myeloid cell expressed TNFSF13B that encodes B-cell activating factor (BAFF). Such interactions of TACI have been linked with T-independent activation of B cells substituting for CD40L in the up-regulation of activation induced deaminase (AID) and class switch recombination in the SED where DN2 tend to locate(6, 36, 48, 49).

The interaction of DN2 expressing CD86 with CTLA4 expressed by CD4 T cells was observed in the SED and the FAE. Expression of CD86 by B cells in this microenvironment has been observed previously(50). Whilst this is likely an immunosuppressive interaction that down regulates T cell activity, CD86 has the potential to be proinflammatory when interacting with CD28. In addition, strong expression of genes encoding markers associated with antigen presentation by DN2 cells including *HLA-B* and *B2M* suggest that the expression of CD86 by B cells that is tightly associated with the antigenic front line and the GC here could be critical in deciding the directions of T cell responses in this microenvironment(40, 42, 43).

Formatted: Font: (Default) Times New Roman, 12 pt
Formatted: Font: Not Italic
Deleted: By combining CITE-seq and spatial transcriptomics data using anchor-based transfer, we have identified interactions of human B cell subsets with cells of other lineages in GALT. …
Deleted: T
Deleted: s
Deleted: T
Deleted: , we
Deleted: strong
Formatted: Font: (Default) Times New Roman, 12 pt, Not Italic
Formatted: Font: (Default) Times New Roman, 12 pt
Deleted:
Formatted: Font: (Default) Times New Roman, 12 pt, Not Italic
Formatted: Font: (Default) Times New Roman, 12 pt
Formatted: Font: (Default) Times New Roman, 12 pt
Formatted: Font: (Default) Times New Roman, 12 pt
Deleted:
Deleted: These observations are consistent with T-independent switching of B cells to IgA in the SED in humans as in mice (*7, 18, 36*) and the interactions observed implicate DN2 cells as a key cell type involved in this process in humans.
Deleted: (*7, 18, 36*) and the interactions observed implicate DN2 cells as a key cell type involved in this process in … [49]
Formatted: Font: (Default) Times New Roman, 12 pt
Deleted: and the interactions observed implicate DN2 … [50]
Formatted: Font: (Default) Times New Roman, 12 pt
Deleted: the
Formatted: Font: (Default) Times New Roman, 12 pt
Formatted: Font: (Default) Times New Roman, 12 pt
Formatted: Font: (Default) Times New Roman, 12 pt
Formatted: Font: (Default) Times New Roman, 12 pt
Deleted: *b*
Formatted: Font: (Default) Times New Roman, 12 pt, Italic
Formatted: Font: (Default) Times New Roman, 12 pt
Formatted: Font: Italic
Formatted: Font: (Default) Times New Roman, 12 pt
Deleted: a
Deleted:
Formatted: Font: (Default) Times New Roman, 12 pt
Formatted: Font: (Default) Times New Roman, 12 pt

Interactions between DN2 cells expressing GRN, and TNF receptors expressed by myeloid and CD4 and CD8 T cells were imputed and validated, though it should be noted that we observed both B cells and myeloid cells expressing GRN in the SED. It has been proposed that granulin can inhibit the interaction between TNF and receptors and thus it could be a significant negative regulator of proinflammatory TNF activity in the SED(37, 38, 51).

EBI3 was identified in the list of interactions by its association with IL27RA expressed by CD4 and CD8 T cells and IL6ST expressed by CD4 T cells, endothelial cells, mesenchymal and myeloid cells. *EBI3* encodes the B subunit of immunomodulatory cytokines IL27 and IL35(39, 45). However, only *EBI3* was expressed by DN2 cells and not p28 or p35 subunits of IL27 and IL35 respectively. The interactions with IL27RA and IL6ST were likely picked up because both IL27RA and IL6ST are reported to be widely expressed(45). Expression of EBI3 alone has been reported to have immunoregulatory functions(39, 46, 47). It can interfere with the binding of various cytokines to receptors, including the binding of IL6 for example, effectively forming a "cytokine sink", to prevent inflammatory responses.

In addition to the immunomodulatory interactions observed in this study, the significance of expression of FcRL4 should be noted. FcRL4 is an inhibitory receptor expressed by B cells in proximity to mucosal epithelium(52-55). The enriched expression of this receptor that dampens the consequences of BCR ligation by DN2 B cells is consistent with the immunosuppressive profile of B cells in the SED and further evidence of the importance of tightly regulated immune responses in this antigen-rich microenvironment.

We identify that the cytokine IL16, that is a chemoattractant for cells expressing CD4, is expressed by most B cells in GALT. It is possible that B cell derived IL16 could direct the migration of CD4 expressing cells in tissue microenvironments including the SED and contribute to intestinal homeostasis and inflammation(56, 57).

Our manuscript provides a resource of interactions of cells of each B cell subset with cells of other lineages. We identified that the *NOTCH2* gene is a significant marker of only MZB and that it has potential to interact with mesenchymal *DLL1* in GALT. These observations support

Deleted:
Formatted: Font: (Default) Times New Roman, 12 pt
Formatted: Font: (Default) Times New Roman, 12 pt
Deleted: is a significant marker gene of DN2 B cells. It
Formatted: Font: (Default) Times New Roman, 12 pt, Italic
Formatted: Font: (Default) Times New Roman, 12 pt
Deleted:
Formatted: Font: (Default) Times New Roman, 12 pt, Italic
Formatted: Font: (Default) Times New Roman, 12 pt
Formatted: Font: (Default) Times New Roman, 12 pt
Formatted: Font: (Default) Times New Roman, 12 pt
Formatted: Font: (Default) Times New Roman, 12 pt, Italic
Formatted: Font: (Default) Times New Roman, 12 pt
Deleted:
Formatted: Font: (Default) Times New Roman, 12 pt
Formatted: Font: (Default) Times New Roman, 12 pt
Deleted:
Formatted: Font: (Default) Times New Roman, 12 pt
Formatted: Font: (Default) Times New Roman, 12 pt
Deleted: also
Deleted: when they are
Deleted:
Formatted: Font: Not Italic
Formatted: Font: (Default) Times New Roman, 12 pt
Deleted:
Formatted: Font: (Default) Times New Roman, 12 pt
Deleted: predominantly by B cells and
Deleted:
Formatted: Font: (Default) Times New Roman, 12 pt
Formatted: Font: (Default) Times New Roman, 12 pt
Deleted: Whilst our manuscript focuses on the properties of DN2 B cells, it also
Formatted: Font: (Default) Times New Roman, 12 pt
Deleted: marginal zone B cells
Formatted: Font: (Default) Times New Roman, 12 pt, Italic
Formatted: Font: (Default) Times New Roman, 12 pt
Formatted: Font: (Default) Times New Roman, 12 pt
Formatted: Font: (Default) Times New Roman, 12 pt, Italic
Formatted: Font: (Default) Times New Roman, 12 pt

MZB development and maturation from precursors dependent on NOTCH2/ DLL1 in the GALT microenvironment(12, 28, 35). Also notable are interactions between naïve B cell LTA and TNF receptors. These interactions are associated with maintenance of lymphoid architecture and structure; in particular, of GALT and spleen(33, 34).

We identify parameters associated with cell migration and antigen presentation that can help our understanding of the orchestration of tissue architecture. For example, interaction of CCL21/ CCL19 with CCR7, that is associated with lymphocyte recirculation, was identified for MZB, class switched memory and IgM-only cells but not DN2(44). This suggests that DN2 cells are not migratory, consistent with their low frequencies in healthy blood(24, 44). An interaction between B cell CCR6 and mesenchymal CCL20 was observed for MZB and IgM-only cells. This interaction, that is implicated in cellular location in the SED in mice(58, 59), could be associated with the SED and perifollicular distribution of MZB and IgM-only cells, but not DN2 cells.

The appendix has been implicated in the disease process in UC. It has been proposed that appendectomy in early life can be protective against UC(15, 16, 60). Also, there is a reddening around the appendiceal orifice in UC termed "periappendiceal red patches", that can occur even when colitis is distal(17). The importance of GALT in UC has been demonstrated by the impact on GALT structure of cases that respond clinically to the drug vedolizumab that blocks the α4β7/ MAdCAM1 mediated homing into gut tissues(18). Here we observe that normal cellular interactions in GALT are disrupted in severe UC. In addition to the general lack of B cell and T cell zonation that increases the potential for B cell/ T cell interaction, we observed that DN2 B cells that express TACI and BCMA in health for example, lose their subepithelial location. In addition, B cell expression of CD86 is lost and progranulin and EBI3 become abundantly secreted by B cells. It is unclear if B cell derived EBI3 and progranulin contribute to the inflammatory response or else represent a compensatory response to curb inflammation. These observations highlight the importance of considering B cells as immunoregulators when working to understand lymphoid tissue function and mechanisms of inflammation.

This study has limitations including our analysis of only B cells and adjacent interacting partners. It is likely that the immunomodulatory capacity of B cells extends beyond the

Deleted: marginal zone B cell
Formatted: Font: (Default) Times New Roman, 12 pt
Deleted:
Deleted: ,
Deleted: is the range of
Formatted ... [51]
Formatted: Font: (Default) Times New Roman, 12 pt
Formatted: Font: (Default) Times New Roman, 12 pt
Deleted: ,
Deleted:
Deleted: LTA secretion can also be associated with immune suppression, but this may not be relevant to naïve B cells that are quiescent.
Formatted: Font: (Default) Times New Roman, 12 pt
Formatted ... [52]
Deleted:
Formatted ... [53]
Deleted:
Formatted ... [54]
Deleted:
Deleted:
Formatted: Font: (Default) Times New Roman, 12 pt
Formatted ... [55]
Deleted:
Deleted:
Formatted ... [56]
Deleted:
Deleted: more generally
Formatted ... [57]
Formatted ... [58]
Deleted:
Deleted: GALT can be observed in the appendix in severe UC but that
Formatted ... [59]
Formatted: Font: (Default) Times New Roman, 12 pt

Deleted: several

interactions observed here. Also, our analysis of UC is restricted to severe disease. UC is a chronic relapsing disease with various degrees of severity in individuals across a lifetime and the features of severe UC we describe here will not be observed in all patients. However, we identify potential roles that B cells could contribute to diseased mucosa outside antibody production.

In summary, by integrating multimodal data including CITE-seq and spatial transcriptomics to the study of human GALT, we have generated a spatial and functional atlas of local B cell interactions. The immunoregulatory features of DN2 B cells that preferentially locate in the SED are likely to make an important contribution to maintenance of lymphoid tissue homeostasis in a microenvironment rich in pathogen associated molecular patterns, thus allowing the chronic propagation of B cell responses to the bacterial surface, without inflammation(6, 7, 48).

MATERIALS AND METHODS

Study design

This study sought to understand the spatial localization and potential interactions of cells in human GALT to determine cell functionality and any changes that might be associated with the inflammatory bowel disease UC. Single cell transcriptomics was used to profile immune cells in GALT and investigate cell-cell communication, including coupling with single cell RNA-seq which allowed for increased depth of information with a spatial context. IMC incorporating RNAscope mRNA probes and fluorescence-based methods were used to validate interactions. IMC and IF methods were used to investigate interactions in UC mucosa to localize cell populations between conditions.

Experimental subject details

See table S3 for details of human samples used for this study. Human appendix cells for CITE-seq analysis were obtained from three deceased adult transplant organ donors with research ethics committee (REC) approval and informed consent from the donor family (reference 15/EE/0152, East of England Cambridge South Research Ethics Committee). The seven histologically normal FFPE appendix samples used for CosMx analysis were from a series of stored anonymous tissue donors who had undergone appendicectomy or right hemicolectomy.

Deleted: already

Deleted: samples

Deleted: The data we describe is extensive and we could not hope to validate everything of interest. It will therefore be important to validate further in the future.

Formatted: Font: (Default) Times New Roman, 12 pt

Deleted: be

Deleted: PAMPs

Formatted: Font: (Default) Times New Roman, 12 pt

Deleted:

Formatted: Font: (Default) Times New Roman, 12 pt

Formatted: Font: (Default) Times New Roman, 12 pt

Deleted: s

Deleted: s

Deleted: while

Formatted: Font: (Default) Times New Roman, 12 pt

Formatted: Font: (Default) Times New Roman, 12 pt

Deleted: .

Deleted: s

Deleted: table

Deleted: S12

Formatted: Font: (Default) Times New Roman, 12 pt

Deleted: 7

Formatted: Font: (Default) Times New Roman, 12 pt

Further samples of histologically normal FFPE appendix from the same collection were used for validation. Four samples from the same collection three of which had been used for CosMx and analyzed and one that had not were used for comparison with four samples of UC appendix. No information is available relating to the 11 normal tissue donors. Studies of human cells and tissues for this project was approved by London, Camberwell St Giles Research Ethics Committee (study 11/LO/1274 Immunology of the intestine; features associated with autoimmunity).

Sample processing

Appendix collected from three deceased transplant organ donors were processed as described previously (26, 61). All tissue preparation and lymphocyte isolation procedures were performed with RPMI 1640 (GIBCO; 61870-010) containing heat-inactivated 10% fetal bovine serum (FBS) (Sigma Aldrich; F7524), 2 mM l-glutamine, penicillin (100 IU/ml), and streptomycin (100 mg/ml; RPMI-P/S) (Merck Life Science UK; p4333) unless stated otherwise. Cells were cryopreserved in freezing medium of FBS + 10% dimethyl sulfoxide (DMSO) (Sigma Aldrich; D2650) in aliquots of 1×10^7 cells.

Cell sorting, CITE-seq staining and scRNA-seq library preparation

Cryopreserved samples were thawed in a 37°C water bath and washed in RPMI with penicillin and streptomycin. After cell counting, 3 x 10^6 cells per sample resuspended in PBS with 1% bovine serum albumin were transferred to Eppendorf LoBind Microcentrifuge tubes and washed. Cells were processed and stained with oligonucleotide tagged antibodies (Table S1).

Sorted $CD19^+$ cell populations from three donors were loaded onto a 10X Genomics Chromium controller, and the libraries [5′ gene expression, V(D)J, and ADT] were prepared according to the manufacturer’s guidelines. Sequencing data was generated using Illumina NextSeq 2000 platform (28-10-10-90 sequencing configuration). Transcript alignment and generation of feature barcode matrices for downstream analysis were performed using the 10X Genomics Cell Ranger workflow.

Analysis of CITE-seq data

Deleted: 4
Deleted: f
Deleted: 4
Deleted: were used for comparison with UC appendix,
Deleted: 3
Formatted: Font: (Default) Times New Roman, 12 pt
Formatted: Font: (Default) Times New Roman, 12 pt
Deleted: s
Formatted: Font: (Default) Times New Roman, 12 pt
Formatted: Font: (Default) Times New Roman, 12 pt
Formatted: Font: (Default) Times New Roman, 12 pt
Formatted: Font: (Default) Times New Roman, 12 pt
Formatted: Font: (Default) Times New Roman, 12 pt
Formatted: Font: (Default) Times New Roman, 12 pt
Formatted: Font: (Default) Times New Roman, 12 pt
Formatted: Font: (Default) Times New Roman, 12 pt
Deleted: million
Formatted: Font: (Default) Times New Roman, 12 pt
Deleted: table
Deleted: S3

Gene expression and surface antibody (ADT) levels for the $CD19^+$ cells were loaded into R using the Seurat package (version 5.0.3) (62). Quality control removed cells with high mitochondrial read percentage, low ribosomal read percentage, high or low gene counts and read counts, and cells with no expression of B cell lineage markers *CD79A, CD79B, CD19* and *MS4A1*.

Expression data was normalized for each sample (SCTransform for the RNA assay, CLR for the ADT assay). For the RNA assay, the top 3000 genes with the most variation excluding *IGHV* genes were used for PCA construction. A PCA was constructed for each of the ADT assays, and a weighted-nearest neighbors method (63) was used to integrate samples and produce PCA and UMAP dimensionality reductions using both assays combined.

Cells were then clustered based on the combined PCA and clusters were manually assigned a label based on the expression of known B cell subset genes and surface markers. Where necessary, clusters were further sub-clustered to provide better resolution. Gene markers for each B cell subset were calculated using the Seurat FindClusters function with default parameters (Wilcoxon rank sum test with correction for multiple comparisons).

CosMx sample processing

Sections from seven FFPE blocks of normal human appendix cut at 5 µm thickness were deparaffinized and subjected to target retrieval and proteinase-K digestion according to NanoString's instructions for appendix (Bruker Supplied Reagents: CosMx FFPE Slide Preparation Kit (RNA) item 121500006). For image registration, the concentration of fiducial was 0.0005%. The NanoString RNA probe set Human Universal Cell Characterization Panel 1000 plex (RNA) was applied to the slides. After washing and DAPI staining, sections were incubated in Human Universal Cell Segmentation Kit (RNA) consisting of CD298/B2M, PanCK and CD45. Flow cells were loaded on to slides, and the slides were loaded on to the CosMx SMI instrument. Data was acquired after pre-bleaching using profile A and cell segmentation using profile A (64). Data was acquired as z-stacks at 0.8 µm intervals (65). The detection of transcript dispersion and their removal in specific Z-slices was performed using the R package NoButter (66). Dispersion was observed in Z-slices higher than Z8, so all transcripts present in these slices

Formatted: Font: (Default) Times New Roman, 12 pt
Formatted: Font: (Default) Times New Roman, 12 pt
Formatted: Font: (Default) Times New Roman, 12 pt, Italic
Formatted: Font: (Default) Times New Roman, 12 pt
Deleted: principal component analysis (
Deleted:)
Deleted: u
Formatted: Font: (Default) Times New Roman, 12 pt
Formatted: Font: (Default) Times New Roman, 12 pt
Deleted: X
Deleted: 7
Formatted: Font: (Default) Times New Roman, 12 pt
Deleted: s
Deleted:
Formatted: Font: (Default) Times New Roman, 12 pt
Formatted: Font: (Default) Times New Roman, 12 pt
Formatted: Font: (Default) Times New Roman, 12 pt
Formatted: Font: (Default) Times New Roman, 12 pt
Formatted: Font: (Default) Times New Roman, 12 pt
Formatted: Font: (Default) Times New Roman, 12 pt
Formatted: Font: (Default) Times New Roman, 12 pt
Formatted: Font: (Default) Times New Roman, 12 pt

were removed. The resulting cell gene expression and spatial co-ordinates were used for downstream analysis.

Analysis of CosMx cell data

CosMx gene expression and spatial location data were loaded into R using the Seurat package. Quality control was performed on the cells to remove any cell with low or high gene reads, and to remove cells with a high proportion of reads corresponding to the negative control probes. The RNA assays of each of the CosMx samples were normalized individually using the SCTransform function, and PCA and UMAP dimensionality reductions were calculated for each sample. Distinct clusters exhibiting epithelial cell markers were identified and these were classified as epithelium. Other clusters exhibited mixed cell lineage markers and thus for the remaining cells, a label transfer method was used. Previously published, pre-labelled data taken from cells in the human intestinal tract (19) was used and filtered to only include cells corresponding to adult appendix to best match the CosMx samples. Epithelial and neuronal cells were removed resulting in a reference dataset containing cells labelled as B cells, T cells, Endothelial cells, Myeloid cells and Plasma cells. The data was normalized using SCTransform and a PCA was computed for this reference dataset using the top 3000 most variable genes. The FindTransferAnchors function in Seurat (20) was used to find anchors between cells in the CosMx and cells in the reference dataset based on transcriptomic similarity in the 480 genes present in both datasets. The TransferData function was then used to assign a lineage classification based on the classification of anchored reference cells.

Cell-cell proximity was determined using the imcRtools package (67), involving Delaunay triangulation with a cutoff to prevent proximities occurring across large distances. Edges were assigned between neighboring cells to construct a network, and a neighborhood lineage similarity metric was calculated by taking the proportion of each cell's neighbors which were the same lineage as the query cell. Proximity testing was performed using the testInteractions function in imcRtools; briefly, proximities between cells are each for each sample, and a bootstrapping approach was used whereby lineage classifications are shuffled and recorded 1000 times. Observed proximity numbers for each combination of lineages were then compared

Formatted: Font: (Default) Times New Roman, 12 pt
Formatted: Font: (Default) Times New Roman, 12 pt
Deleted: s
Deleted: X
Formatted: Font: (Default) Times New Roman, 12 pt
Formatted: Font: (Default) Times New Roman, 12 pt
Formatted: Font: (Default) Times New Roman, 12 pt
Formatted: Font: (Default) Times New Roman, 12 pt
Deleted: u
Deleted: u
Deleted: cells'
Deleted: u
Formatted: Font: (Default) Times New Roman, 12 pt

against the shuffled repetitions to give a positive, negative or neutral proximity inclination per sample. These values were then summed across samples to give a sum of significant proximity.

Analysis of CosMx B cell data

The CosMx data was filtered to only cells labelled as B cells, and the anchor-based data transfer approach was repeated, now using the CITE-seq human appendix data as the reference dataset using the 238 genes overlapping between the CosMx genes and the RNA-seq genes used for integration in order to match cells between the datasets based on their transcriptomic similarity. B cell subset labels were transferred, and an RNA assay expression was imputed using this approach, generating the spatial imputed gene expression within the CosMx B cell data of the 3000 genes used for integration in the CITE-seq B cell data. B cell subset proximities were calculated using the same bootstrapping method as described previously.

Analysis of CosMx ligand-receptor pairs

Ligand-receptor analysis was performed on the CosMx dataset. Firstly, the CellTalkDB database of known interacting source and target cell pairs was downloaded (32) and filtered based on whether the genes involved were present in the CosMx panel or in the imputed B cell RNA assay. Only ligand-receptor pairs with at least one gene in the CosMx panel ('observed') and one gene either observed or in the imputed RNA assay ('imputed') were retained. Each edge in the previously constructed cell-cell proximity network was converted to a directed network with two edges between neighbors – with one node designated a 'source' and the other designated a 'target'. For each edge, each ligand-receptor pair was given a strength at the edge based on the ligand expression at the source node and the receptor expression at the target node. Total strengths per edge were calculated by summing strengths across all ligand-receptor pairs. Ligand-receptor pairs were deemed to be present between cell types if the interaction strength was > 0 across at least 10% of edges between each cell type pair. For interaction analysis, B cells were divided into their assigned subsets, whilst cells classified as T cell were reclustered, with clusters identified as $CD4^+$ or $CD8^+$, and T cells subdivided along these lines into $CD4^+$ T cells and $CD8^+$ T cells. Mean interaction strength per edges between cell types were calculated, and total interaction strength across edges was visualized spatially. Pathway analysis was performed

Deleted: X

Formatted: Font: (Default) Times New Roman, 12 pt

Formatted: Font: (Default) Times New Roman, 12 pt

Formatted: Font: (Default) Times New Roman, 12 pt

Deleted: u

Deleted: s

using Metascape (68), whereby the inputs for each subset were the genes involved in interactions involving that subset.

To identify interactions associated with B cell subset function, individual ligand-receptor pairs were further filtered to only include pairs where the B cell gene was also present in the CITE-seq marker gene for the subset. The strength of these interactions was then visualized across B cell subsets and their interaction partners.

Mitigation of false positives from ligand–receptor analysis and prioritization of interactions for validation

We consider the following to be key for mitigations of false positives in the data: Accurate lineage designations at the outset; restricting the analysis to interactions involving at least 10% of edges between each cell type pair; using a database of interactions that was fully referenced and that could be filtered to interactions involving human cells; giving priority to interactions involving statistically significant marker genes of the B cell subsets; dividing the interactions into those involved in cell migration and/or maintenance, potential antigen presentation and immune function and focusing on the latter.

B cell subset interactions were initially identified by gene expression derived from scRNAseq data that was projected computationally onto the spatial transcriptomic data. It was therefore important to know if examples that we considered to be functionally relevant because of high interaction strength and association with B cell function in the SED could be identified directly and by gene and protein expression. Genes selected by these criteria and by availability of reagents for validation in the sections below were *CD86*, *GRN* and *EBI3*.

Tissue imaging

Immunofluorecence and confocal microscopic analysis of FFPE tissues (three biological replicates for each) was carried out as described previously using the Olympus BX51 fluorescence microscope and Nikon AXR inverted confocal microscope with Nikon Spatial Array Confocal respectively. Antibodies are detailed in table S2 (4). For IMC, sections were stained and data acquired as described previously using Hyperion Imaging System (three

Formatted: Font: (Default) Times New Roman, 12 pt
Formatted: Font: (Default) Times New Roman, 12 pt
Deleted: s
Formatted: Font: Bold, Not Italic
Formatted: Normal, Don't adjust right indent when grid is defined, Line spacing: single, Don't adjust space between Latin and Asian text, Don't adjust space between Asian text and numbers
Formatted: Font: (Default) Times New Roman, 12 pt
Deleted: s
Formatted: Font: (Default) Times New Roman, 12 pt
Deleted: .
Deleted: ,
Formatted: Font: (Default) Times New Roman, 12 pt
Deleted: using a
Deleted: table
Deleted: S10
Formatted: Font: (Default) Times New Roman, 12 pt
Formatted: Font: (Default) Times New Roman
Formatted: Font: (Default) Times New Roman, 12 pt
Formatted: Font: (Default) Times New Roman, 12 pt

biological replicates for each) (69). For the IMC-RNAScope combined protocol, expression of genes encoding *IL16, CD86, CTLA4, EBI3, IL27RA, GRN, TNFRSF1A, TNFRSF1B* was detected using RNAscope probes from Bio-Techne as described previously (4). Probes were detected by incorporation of metal tagged antibodies to digoxigenin, FITC and biotin into an IMC panel as described before (4) and detailed in data file S6.

IMC image data was pre-processed using IMCSegmentationPipeline(70, 71), and analyzed according to further established pipelines (67, 71)(72), as described previously(4).

A lineage classification approach was performed whereby cells were gated based on expression of lineage markers, with cells passing through multiple lineage gates left unlabeled. A population of B/T cells was gated based on double expression of CD3 and CD20. A random forest classifier was then trained on the gated cells to apply a label to the unlabeled cells. First, the B/T population was classified based on a classifier trained on the gated B and T cells, assigning cells from the B/T population into either B cell or T cell classifications. Then, a classifier was trained on the entire labeled population (excluding the B/T cells) and used to classify the remaining unlabeled cells. For both classifications, cells with an uncertain classification (defined as a maximum classification probability less than 33% greater than the second highest classification probability) were left unclassified. Proximity edges between cells was calculated based on a distance threshold and the number of edge types was determined for each ROI based on the lineages present on either end of the edge. This data was scaled per ROI and used to construct a PCA of cell proximities. Proximity testing was again performed using the testInteractions function for both health and UC; a proximity score was calculated by subtracting the UC score from the healthy score, giving a metric for determining if cell lineages are in closer proximity in health versus in UC.

The data was then filtered to B cells and re-clustered, with the markers used for clustering chosen for their B cell relevance and markers were excluded if they exhibited low signal-to-noise ratio in the healthy B cell data. Health and UC B cells were clustered separately, and B cell subset classifications were assigned based on marker expression, with clusters exhibiting no

Formatted: Font: (Default) Times New Roman, 12 pt
Formatted: Font: (Default) Times New Roman, 12 pt
Formatted: Font: (Default) Times New Roman, 12 pt
Formatted: Font: (Default) Times New Roman, 12 pt, Italic
Formatted: Font: (Default) Times New Roman, 12 pt
Deleted: b
Deleted: t
Formatted: Font: (Default) Times New Roman, 12 pt
Formatted: Font: (Default) Times New Roman, 12 pt
Deleted: table
Deleted: 7
Formatted: Font: Not Italic
Formatted: Font: (Default) Times New Roman, 12 pt
Formatted: Font: (Default) Times New Roman, 12 pt
Deleted: (*70*)
Deleted: (*70*)
Deleted: s
Formatted: Font: Not Italic
Formatted: Font: (Default) Times New Roman, 12 pt
Deleted: according to
Deleted: (*67, 72*),
Deleted: (*67, 72*),
Deleted: ,
Deleted:
Formatted: Font: (Default) Times New Roman, Highlight
Formatted: Highlight
Formatted: Highlight
Formatted: Highlight
Formatted: Highlight
Formatted: Highlight
Formatted: Highlight
Formatted: Highlight
Formatted: Font: (Default) Times New Roman, 12 pt
Formatted: Font: (Default) Times New Roman, 12 pt
Formatted: Font: (Default) Times New Roman, 12 pt
Deleted: l
Deleted: l
Deleted: l
Deleted: l

positive expression left as unknown. For DN2 B cells, the minDistToCells function in imcRTools was used to determine the minimum distance of each DN2 cell to epithelial cells.

Code and Data availability (to be released on acceptance of the manuscript).

Code is available at (73). CITEseq data is available on GEO, accession numbers GSM9656504 to GSM9656515. CosMx and IMC data are available at (74).

Statistics

For differential gene expression in RNA-seq and CosMx data, Wilcoxon tests with Bonferroni correction for multiple comparisons were used in the Seurat package in R version 4.3.1. All other statistical tests were done in Prism v10. Two-tailed paired t tests were performed using parametric tests for comparisons of health and UC in mass cytometry data.

SUPPLEMENTARY MATERIALS

fig S1 Computational analysis of cells in GALT using CosMx

fig S2 Computational analysis of B cells in GALT using CITE-seq

fig S3 Validation of imputed B cell subsets in GALT using CosMx

fig S4 Imputed interaction networks of B cell subsets and spatial validation of IL16 gene expression in follicular microenvironments

fig S5 Imputed interactions associated with antigen presentation and cell migration and/or maintenance function of significant B cell marker genes across selected B cell subsets

fig S6 Computational comparisons of GALT cells from ulcerative colitis patients and healthy controls

Table S1. Antibodies used in CITEseq experiment

Table S2. Antibodies used for IF/confocal validation of interactions

Table S3. Sample information

Data fileS1. Lineage gene markers

Data file S2. Definitions of human B cell subsets

Data file S3. B cell subset markers

Data file S4. Genes expressed by B cell subsets

Data file S5. Imputed ligand-receptor interactions occurring between B cells and other cell types

Deleted: https://github.com/jspencer-lab/GALT_CosMX_IMC. …

Formatted: Font: (Default) Times New Roman

Formatted: Not Highlight

Deleted: xxxx.

Deleted: on zenodo at https://doi.org/10.5281/zenodo.18405128…

Deleted: ¶ ¶

Formatted: Font: (Default) Times New Roman

Formatted: Font: (Default) Times New Roman

Deleted: X

Data file S6. Antibodies used for IMC validation of interactions

Data file S7. Imputed ligand-receptor interactions associated with immune function occurring between B cells and other cell types.

Data file S8. Imputed ligand-receptor interactions involving antigen presentation and cells migration or retention occurring between B cells and other cell types

Data file S9. Antibodies used for imaging mass cytometry analysis of UC samples from right hemicolectomies and controls

Raw figure data file

Deleted:

Deleted: migtation

Moved (insertion) [2]

REFERENCES

1. U. M. Morbe, P. B. Jorgensen, T. M. Fenton, N. von Burg, L. B. Riis, J. Spencer, W. W. Agace, Human gut-associated lymphoid tissues (GALT); diversity, structure, and function. *Mucosal Immunol* **14**, 793-802 (2021).
2. N. Torow, R. Li, T. C. A. Hitch, C. Mingels, S. Al Bounny, N. van Best, E. L. Stange, B. Simons, T. Maie, L. Ruttger, N. Gubbi, D. A. Abbott, A. Benabid, M. Gadermayr, S. Runge, N. Treichel, D. Merhof, S. P. Rosshart, N. Jehmlich, T. W. Hand, M. von Bergen, F. Heymann, O. Pabst, T. Clavel, F. Tacke, H. Lelouard, I. G. Costa, M. W. Hornef, M cell maturation and cDC activation determine the onset of adaptive immune priming in the neonatal Peyer's patch. *Immunity*, (2023).
3. H. Lelouard, M. Fallet, B. de Bovis, S. Meresse, J. P. Gorvel, Peyer's patch dendritic cells sample antigens by extending dendrites through M cell-specific transcellular pores. *Gastroenterology* **142**, 592-601 e593 (2012).
4. L. Montorsi, M. J. Pitcher, Y. Zhao, C. Dionisi, A. Demonti, T. J. Tull, P. Dhami, R. J. Ellis, C. Bishop, J. D. Sanderson, S. Jain, D. D'Cruz, D. L. Gibbons, T. H. Winkler, M. Bemark, F. D. Ciccarelli, J. Spencer, Double-negative B cells and DNASE1L3 colocalise with microbiota in gut-associated lymphoid tissue. *Nat Commun* **15**, 4051 (2024).
5. D. Wang, S. Lim, W. J. van de Wetering, C. Lopez-Iglesias, Y. Okura, Y. Teranishi-Ikawa, A. Mizoroki, W. K. Spoelstra, T. Dayton, G. J. F. van Son, A. Pronk, N. Smakman, G. B. C. Gonera-de Jong, S. Withoff, I. H. Jonkers, J. S. van Zon, S. J. Tans, P. J. Peters, J. H. van Es, H. Clevers, Human gut M cells resemble dendritic cells and present gluten antigen. *Nature*, (2025).
6. E. K. Grasset, A. Chorny, S. Casas-Recasens, C. Gutzeit, G. Bongers, I. Thomsen, L. Chen, Z. He, D. B. Matthews, M. A. Oropallo, P. Veeramreddy, M. Uzzan, A. Mortha, J. Carrillo, B. S. Reis, M. Ramanujam, J. Sintes, G. Magri, P. J. Maglione, C. Cunningham-Rundles, R. J. Bram, J. Faith, S. Mehandru, O. Pabst, A. Cerutti, Gut T cell-independent IgA responses to commensal bacteria require engagement of the TACI receptor on B cells. *Sci Immunol* **5**, (2020).
7. P. Bergqvist, A. Stensson, N. Y. Lycke, M. Bemark, T cell-independent IgA class switch recombination is restricted to the GALT and occurs prior to manifest germinal center formation. *J Immunol* **184**, 3545-3553 (2010).
8. A. Cerutti, The regulation of IgA class switching. *Nat Rev Immunol* **8**, 421-434 (2008).
9. O. Pabst, V. Cerovic, M. Hornef, Secretory IgA in the Coordination of Establishment and Maintenance of the Microbiota. *Trends Immunol* **37**, 287-296 (2016).

10. P. Brandtzaeg, I. N. Farstad, F. E. Johansen, H. C. Morton, I. N. Norderhaug, T. Yamanaka, The B-cell system of human mucosae and exocrine glands. *Immunol Rev* **171**, 45-87 (1999).
11. D. K. Dunn-Walters, P. G. Isaacson, J. Spencer, Sequence analysis of human IgVH genes indicates that ileal lamina propria plasma cells are derived from Peyer's patches. *Eur J Immunol* **27**, 463-467 (1997).
12. S. Weller, D. Sterlin, T. Fadeev, E. Coignard, A. Verge de Los Aires, C. Goetz, R. Fritzen, M. Bahuaud, F. Batteux, G. Gorochov, J. C. Weill, C. A. Reynaud, T-independent responses to polysaccharides in humans mobilize marginal zone B cells prediversified against gut bacterial antigens. *Sci Immunol* **8**, eade1413 (2023).
13. J. C. Weill, S. Weller, C. A. Reynaud, Human marginal zone B cells. *Annu Rev Immunol* **27**, 267-285 (2009).
14. J. Spencer, L. M. Sollid, The human intestinal B-cell response. *Mucosal Immunol* **9**, 1113-1124 (2016).
15. R. E. Andersson, G. Olaison, C. Tysk, A. Ekbom, Appendectomy and protection against ulcerative colitis. *N Engl J Med* **344**, 808-814 (2001).
16. M. G. Russel, E. Dorant, R. J. Brummer, M. A. van de Kruijs, J. W. Muris, J. M. Bergers, J. Goedhard, R. W. Stockbrugger, Appendectomy and the risk of developing ulcerative colitis or Crohn's disease: results of a large case-control study. South Limburg Inflammatory Bowel Disease Study Group. *Gastroenterology* **113**, 377-382 (1997).
17. M. A. Reijntjes, L. Heuthorst, K. Gecse, A. Mookhoek, W. A. Bemelman, C. J. Buskens, Clinical relevance of endoscopic peri-appendiceal red patch in ulcerative colitis patients. *Therap Adv Gastroenterol* **15**, 17562848221098849 (2022).
18. P. Canales-Herrerias, M. Uzzan, A. Seki, R. S. Czepielewski, B. Verstockt, A. E. Livanos, F. Raso, A. Dunn, D. Dai, A. Wang, Z. Al-Taie, J. Martin, T. Laurent, H. M. Ko, M. Tokuyama, M. Tankelevich, H. Meringer, F. Cossarini, D. Jha, A. Krek, J. D. Paulsen, M. D. Taylor, M. Z. Nakadar, J. Wong, E. C. Erlich, R. L. Mintz, E. J. Onufer, B. A. Helmink, K. Sharma, A. Rosenstein, D. Ganjian, G. Chung, T. Dawson, J. Juarez, V. Yajnik, A. Cerutti, J. J. Faith, M. Suarez-Farinas, C. Argmann, F. Petralia, G. J. Randolph, A. D. Polydorides, A. Reboldi, J. F. Colombel, S. Mehandru, Gut-associated lymphoid tissue attrition associates with response to anti-alpha4beta7 therapy in ulcerative colitis. *Sci Immunol* **9**, eadg7549 (2024).
19. R. Elmentaite, N. Kumasaka, K. Roberts, A. Fleming, E. Dann, H. W. King, V. Kleshchevnikov, M. Dabrowska, S. Pritchard, L. Bolt, S. F. Vieira, L. Mamanova, N. Huang, F. Perrone, I. Goh Kai'En, S. N. Lisgo, M. Katan, S. Leonard, T. R. W. Oliver, C. E. Hook, K. Nayak, L. S. Campos, C. Dominguez Conde, E. Stephenson, J. Engelbert, R. A. Botting, K. Polanski, S. van Dongen, M. Patel, M. D. Morgan, J. C. Marioni, O. A. Bayraktar, K. B. Meyer, X. He, R. A. Barker, H. H. Uhlig, K. T. Mahbubani, K. Saeb-Parsy, M. Zilbauer, M. R. Clatworthy, M. Haniffa, K. R. James, S. A. Teichmann, Cells of the human intestinal tract mapped across space and time. *Nature* **597**, 250-255 (2021).
20. T. Stuart, A. Butler, P. Hoffman, C. Hafemeister, E. Papalexi, W. M. Mauck, 3rd, Y. Hao, M. Stoeckius, P. Smibert, R. Satija, Comprehensive Integration of Single-Cell Data. *Cell* **177**, 1888-1902 e1821 (2019).
21. R. Elmentaite, C. Dominguez Conde, L. Yang, S. A. Teichmann, Single-cell atlases: shared and tissue-specific cell types across human organs. *Nat Rev Genet*, (2022).
22. A. Palanichamy, J. Barnard, B. Zheng, T. Owen, T. Quach, C. Wei, R. J. Looney, I. Sanz, J. H. Anolik, Novel human transitional B cell populations revealed by B cell depletion therapy. *J Immunol* **182**, 5982-5993 (2009).
23. G. D. Victora, D. Dominguez-Sola, A. B. Holmes, S. Deroubaix, R. Dalla-Favera, M. C. Nussenzweig, Identification of human germinal center light and dark zone cells and their relationship to human B-cell lymphomas. *Blood* **120**, 2240-2248 (2012).

24. S. A. Jenks, K. S. Cashman, E. Zumaquero, U. M. Marigorta, A. V. Patel, X. Wang, D. Tomar, M. C. Woodruff, Z. Simon, R. Bugrovsky, E. L. Blalock, C. D. Scharer, C. M. Tipton, C. Wei, S. S. Lim, M. Petri, T. B. Niewold, J. H. Anolik, G. Gibson, F. E. Lee, J. M. Boss, F. E. Lund, I. Sanz, Distinct Effector B Cells Induced by Unregulated Toll-like Receptor 7 Contribute to Pathogenic Responses in Systemic Lupus Erythematosus. *Immunity* **49**, 725-739 e726 (2018).
25. G. R. Ehrhardt, R. S. Davis, J. T. Hsu, C. M. Leu, A. Ehrhardt, M. D. Cooper, The inhibitory potential of Fc receptor homolog 4 on memory B cells. *Proc Natl Acad Sci U S A* **100**, 13489-13494 (2003).
26. J. H. Y. Siu, M. J. Pitcher, T. J. Tull, R. L. Velounias, W. Guesdon, L. Montorsi, K. T. Mahbubani, R. Ellis, P. Dhami, K. Todd, U. D. Kadolsky, M. Kleeman, D. P. D'Cruz, K. Saeb-Parsy, M. Bemark, G. J. Pettigrew, J. Spencer, Two subsets of human marginal zone B cells resolved by global analysis of lymphoid tissues and blood. *Sci Immunol* **7**, eabm9060 (2022).
27. Y. Zhao, M. Uduman, J. H. Y. Siu, T. J. Tull, J. D. Sanderson, Y. B. Wu, J. Q. Zhou, N. Petrov, R. Ellis, K. Todd, K. M. Chavele, W. Guesdon, A. Vossenkamper, W. Jassem, D. P. D'Cruz, D. J. Fear, S. John, D. Scheel-Toellner, C. Hopkins, E. Moreno, N. L. Woodman, F. Ciccarelli, S. Heck, S. H. Kleinstein, M. Bemark, J. Spencer, Spatiotemporal segregation of human marginal zone and memory B cell populations in lymphoid tissue. *Nat Commun* **9**, 3857 (2018).
28. T. J. Tull, M. J. Pitcher, W. Guesdon, J. H. Y. Siu, C. Lebrero-Fernandez, Y. Zhao, N. Petrov, S. Heck, R. Ellis, P. Dhami, U. D. Kadolsky, M. Kleeman, Y. Kamra, D. J. Fear, S. John, W. Jassem, R. W. Groves, J. D. Sanderson, M. G. Robson, D. P. D'Cruz, M. Bemark, J. Spencer, Human marginal zone B cell development from early T2 progenitors. *J Exp Med* **218**, (2021).
29. C. A. Perugino, H. Liu, J. Feldman, J. Marbourg, T. V. Guy, A. Hui, N. Ingram, J. Liebaert, N. Chaudhary, W. Tao, C. Jacob-Dolan, B. M. Hauser, Z. Mian, A. Nathan, Z. Zhao, C. Kaseke, R. Tano-Menka, M. A. Getz, F. Senjobe, C. Berrios, O. Ofoman, Z. Manickas-Hill, D. R. Wesemann, J. E. Lemieux, M. B. Goldberg, K. Nundel, A. Moormann, A. Marshak-Rothstein, R. C. Larocque, E. T. Ryan, J. A. Iafrate, D. Lingwood, G. Gaiha, R. Charles, A. B. Balazs, A. Pandit, V. Naranbhai, A. G. Schmidt, S. Pillai, Two distinct durable human class-switched memory B cell populations are induced by vaccination and infection. *Cell Rep* **44**, 115472 (2025).
30. H. E. Mei, T. Yoshida, W. Sime, F. Hiepe, K. Thiele, R. A. Manz, A. Radbruch, T. Dorner, Blood-borne human plasma cells in steady state are derived from mucosal immune responses. *Blood* **113**, 2461-2469 (2009).
31. G. D. Victora, M. C. Nussenzweig, Germinal Centers. *Annu Rev Immunol* **40**, 413-442 (2022).
32. X. Shao, J. Liao, C. Li, X. Lu, J. Cheng, X. Fan, CellTalkDB: a manually curated database of ligand-receptor interactions in humans and mice. *Brief Bioinform* **22**, (2021).
33. V. Upadhyay, Y. X. Fu, Lymphotoxin organizes contributions to host defense and metabolic illness from innate lymphoid cells. *Cytokine Growth Factor Rev* **25**, 227-233 (2014).
34. V. Upadhyay, Y. X. Fu, Lymphotoxin signalling in immune homeostasis and the control of microorganisms. *Nat Rev Immunol* **13**, 270-279 (2013).
35. M. Descatoire, S. Weller, S. Irtan, S. Sarnacki, J. Feuillard, S. Storck, A. Guiochon-Mantel, J. Bouligand, A. Morali, J. Cohen, E. Jacquemin, M. Iascone, C. Bole-Feysot, N. Cagnard, J. C. Weill, C. A. Reynaud, Identification of a human splenic marginal zone B cell precursor with NOTCH2-dependent differentiation properties. *J Exp Med* **211**, 987-1000 (2014).

36. J. Liu, Z. Shulman, Affinity-based clonal selection in Peyer's patches. *Curr Opin Immunol* **74**, 100-105 (2022).
37. W. Tang, Y. Lu, Q. Y. Tian, Y. Zhang, F. J. Guo, G. Y. Liu, N. M. Syed, Y. Lai, E. A. Lin, L. Kong, J. Su, F. Yin, A. H. Ding, A. Zanin-Zhorov, M. L. Dustin, J. Tao, J. Craft, Z. Yin, J. Q. Feng, S. B. Abramson, X. P. Yu, C. J. Liu, The growth factor progranulin binds to TNF receptors and is therapeutic against inflammatory arthritis in mice. *Science* **332**, 478-484 (2011).
38. Y. P. Zhao, B. Liu, Q. Y. Tian, J. L. Wei, B. Richbourgh, C. J. Liu, Progranulin protects against osteoarthritis through interacting with TNF-alpha and beta-Catenin signalling. *Ann Rheum Dis* **74**, 2244-2253 (2015).
39. H. Yoshida, C. A. Hunter, The immunobiology of interleukin-27. *Annu Rev Immunol* **33**, 417-443 (2015).
40. K. Vandenborre, S. W. Van Gool, A. Kasran, J. L. Ceuppens, M. A. Boogaerts, P. Vandenberghe, Interaction of CTLA-4 (CD152) with CD80 or CD86 inhibits human T-cell activation. *Immunology* **98**, 413-421 (1999).
41. R. E. Forgione, C. Di Carluccio, J. Guzman-Caldentey, R. Gaglione, F. Battista, F. Chiodo, Y. Manabe, A. Arciello, P. Del Vecchio, K. Fukase, A. Molinaro, S. Martin-Santamaria, P. R. Crocker, R. Marchetti, A. Silipo, Unveiling Molecular Recognition of Sialoglycans by Human Siglec-10. *iScience* **23**, 101231 (2020).
42. T. S. Lim, J. K. Goh, A. Mortellaro, C. T. Lim, G. J. Hammerling, P. Ricciardi-Castagnoli, CD80 and CD86 differentially regulate mechanical interactions of T-cells with antigen-presenting dendritic cells and B-cells. *PLoS One* **7**, e45185 (2012).
43. G. Baravalle, H. Park, M. McSweeney, M. Ohmura-Hoshino, Y. Matsuki, S. Ishido, J. S. Shin, Ubiquitination of CD86 is a key mechanism in regulating antigen presentation by dendritic cells. *J Immunol* **187**, 2966-2973 (2011).
44. E. S. Baekkevold, T. Yamanaka, R. T. Palframan, H. S. Carlsen, F. P. Reinholt, U. H. von Andrian, P. Brandtzaeg, G. Haraldsen, The CCR7 ligand elc (CCL19) is transcytosed in high endothelial venules and mediates T cell recruitment. *J Exp Med* **193**, 1105-1112 (2001).
45. S. Kang, M. Narazaki, H. Metwally, T. Kishimoto, Historical overview of the interleukin-6 family cytokine. *J Exp Med* **217**, (2020).
46. E. N. Scott, C. Ye, H. Yano, Z. Lipatova, E. Brunazzi, K. M. Vignali, C. J. Workman, D. A. A. Vignali, Ebi3 Binding to IFN-gamma and IL-10 Limits Their Function. *J Immunol* **213**, 1115-1124 (2024).
47. K. Hildenbrand, S. Bohnacker, P. R. Menon, A. Kerle, U. F. Prodjinotho, F. Hartung, P. C. Strasser, D. A. M. Catici, F. Ruhrnossl, M. Haslbeck, K. Schumann, S. I. Muller, C. P. da Costa, J. Esser-von Bieren, M. J. Feige, Human interleukin-12alpha and EBI3 are cytokines with anti-inflammatory functions. *Sci Adv* **9**, eadg6874 (2023).
48. M. B. Litinskiy, B. Nardelli, D. M. Hilbert, B. He, A. Schaffer, P. Casali, A. Cerutti, DCs induce CD40-independent immunoglobulin class switching through BLyS and APRIL. *Nat Immunol* **3**, 822-829 (2002).
49. A. Biram, A. Stromberg, E. Winter, L. Stoler-Barak, R. Salomon, Y. Addadi, R. Dahan, G. Yaari, M. Bemark, Z. Shulman, BCR affinity differentially regulates colonization of the subepithelial dome and infiltration into germinal centers within Peyer's patches. *Nat Immunol* **20**, 482-492 (2019).
50. T. Yamanaka, A. Straumfors, H. Morton, O. Fausa, P. Brandtzaeg, I. Farstad, M cell pockets of human Peyer's patches are specialized extensions of germinal centers. *Eur J Immunol* **31**, 107-117 (2001).
51. J. C. Kennedy, S. O. Vargas, M. P. Fishman, N. Alesi, S. H. Baek, D. Khabibillin, C. D. Platt, C. Garcia-de-Alba, P. B. Agrawal, N. E. Carmichael, L. A. Henderson, A. Wehrman, S. Boland, T. Walther, R. V. Farese, Jr., A. M. H. Casey, J. P. Manis, L. V. Collen, M.

Lvova, A. Barbieri, B. Sullivan, B. A. Raby, A progranulin variant causing childhood interstitial lung disease responsive to anti-TNF-alpha biologic therapy. *Med*, 100607 (2025).
52. B. Falini, E. Tiacci, A. Pucciarini, B. Bigerna, J. Kurth, G. Hatzivassiliou, S. Droetto, B. V. Galletti, M. Gambacorta, A. Orazi, L. Pasqualucci, I. Miller, R. Kuppers, R. Dalla-Favera, G. Cattoretti, Expression of the IRTA1 receptor identifies intraepithelial and subepithelial marginal zone B cells of the mucosa-associated lymphoid tissue (MALT). *Blood* **102**, 3684-3692 (2003).
53. G. R. Ehrhardt, J. T. Hsu, L. Gartland, C. M. Leu, S. Zhang, R. S. Davis, M. D. Cooper, Expression of the immunoregulatory molecule FcRH4 defines a distinctive tissue-based population of memory B cells. *J Exp Med* **202**, 783-791 (2005).
54. G. Hatzivassiliou, I. Miller, J. Takizawa, N. Palanisamy, P. H. Rao, S. Iida, S. Tagawa, M. Taniwaki, J. Russo, A. Neri, G. Cattoretti, R. Clynes, C. Mendelsohn, R. S. Chaganti, R. Dalla-Favera, IRTA1 and IRTA2, novel immunoglobulin superfamily receptors expressed in B cells and involved in chromosome 1q21 abnormalities in B cell malignancy. *Immunity* **14**, 277-289 (2001).
55. Y. Liu, J. R. McDaniel, S. Khan, P. Campisi, E. J. Propst, T. Holler, E. Grunebaum, G. Georgiou, G. C. Ippolito, G. R. A. Ehrhardt, Antibodies Encoded by FCRL4-Bearing Memory B Cells Preferentially Recognize Commensal Microbial Antigens. *J Immunol* **200**, 3962-3969 (2018).
56. D. Seegert, P. Rosenstiel, H. Pfahler, P. Pfefferkorn, S. Nikolaus, S. Schreiber, Increased expression of IL-16 in inflammatory bowel disease. *Gut* **48**, 326-332 (2001).
57. P. Middel, K. Reich, F. Polzien, V. Blaschke, B. Hemmerlein, J. Herms, M. Korabiowska, H. J. Radzun, Interleukin 16 expression and phenotype of interleukin 16 producing cells in Crohn's disease. *Gut* **49**, 795-803 (2001).
58. A. Reboldi, T. I. Arnon, L. B. Rodda, A. Atakilit, D. Sheppard, J. G. Cyster, IgA production requires B cell interaction with subepithelial dendritic cells in Peyer's patches. *Science* **352**, aaf4822 (2016).
59. R. J. Komban, A. Stromberg, A. Biram, J. Cervin, C. Lebrero-Fernandez, N. Mabbott, U. Yrlid, Z. Shulman, M. Bemark, N. Lycke, Activated Peyer's patch B cells sample antigen directly from M cells in the subepithelial dome. *Nat Commun* **10**, 2423 (2019).
60. A. Parian, B. Limketkai, J. Koh, S. R. Brant, A. Bitton, J. H. Cho, R. H. Duerr, D. P. McGovern, D. D. Proctor, M. D. Regueiro, J. D. Rioux, P. Schumm, K. D. Taylor, M. S. Silverberg, A. H. Steinhart, R. Hernaez, M. Lazarev, Appendectomy does not decrease the risk of future colectomy in UC: results from a large cohort and meta-analysis. *Gut*, (2016).
61. J. H. Southard, F. O. Belzer, Organ preservation. *Annu Rev Med* **46**, 235-247 (1995).
62. Y. Hao, T. Stuart, M. H. Kowalski, S. Choudhary, P. Hoffman, A. Hartman, A. Srivastava, G. Molla, S. Madad, C. Fernandez-Granda, R. Satija, Dictionary learning for integrative, multimodal and scalable single-cell analysis. *Nat Biotechnol* **42**, 293-304 (2024).
63. Y. Hao, S. Hao, E. Andersen-Nissen, W. M. Mauck, 3rd, S. Zheng, A. Butler, M. J. Lee, A. J. Wilk, C. Darby, M. Zager, P. Hoffman, M. Stoeckius, E. Papalexi, E. P. Mimitou, J. Jain, A. Srivastava, T. Stuart, L. M. Fleming, B. Yeung, A. J. Rogers, J. M. McElrath, C. A. Blish, R. Gottardo, P. Smibert, R. Satija, Integrated analysis of multimodal single-cell data. *Cell* **184**, 3573-3587 e3529 (2021).
64. C. Stringer, T. Wang, M. Michaelos, M. Pachitariu, Cellpose: a generalist algorithm for cellular segmentation. *Nat Methods* **18**, 100-106 (2021).
65. S. He, R. Bhatt, C. Brown, E. A. Brown, D. L. Buhr, K. Chantranuvatana, P. Danaher, D. Dunaway, R. G. Garrison, G. Geiss, M. T. Gregory, M. L. Hoang, R. Khafizov, E. E. Killingbeck, D. Kim, T. K. Kim, Y. Kim, A. Klock, M. Korukonda, A. Kutchma, Z. R. Lewis, Y. Liang, J. S. Nelson, G. T. Ong, E. P. Perillo, J. C. Phan, T. Phan-Everson, E. Piazza, T.

Rane, Z. Reitz, M. Rhodes, A. Rosenbloom, D. Ross, H. Sato, A. W. Wardhani, C. A. Williams-Wietzikoski, L. Wu, J. M. Beechem, High-plex imaging of RNA and proteins at subcellular resolution in fixed tissue by spatial molecular imaging. *Nat Biotechnol* **40**, 1794-1806 (2022).
66. R. L. Béibhinn O'Hora, Rosamond Nuamah, Elena Alberts, Isobelle Wall, Joseph Bell, David A Johnston, Sonya James, Jeanette Norman, Mark G. Jones, Ciro Chiappini, Anita Grigoriadis, Jelmar Quist, NoButter: An R package for reducing transcript dispersion in CosMx Spatial Molecular Imaging Data. *BioRxiv*, (2024).
67. J. Windhager, V. R. T. Zanotelli, D. Schulz, L. Meyer, M. Daniel, B. Bodenmiller, N. Eling, An end-to-end workflow for multiplexed image processing and analysis. *Nat Protoc* **18**, 3565-3613 (2023).
68. Y. Zhou, B. Zhou, L. Pache, M. Chang, A. H. Khodabakhshi, O. Tanaseichuk, C. Benner, S. K. Chanda, Metascape provides a biologist-oriented resource for the analysis of systems-level datasets. *Nat Commun* **10**, 1523 (2019).
69. M. Bortolomeazzi, M. R. Keddar, L. Montorsi, A. Acha-Sagredo, L. Benedetti, D. Temelkovski, S. Choi, N. Petrov, K. Todd, P. Wai, J. Kohl, T. Denner, E. Nye, R. Goldstone, S. Ward, G. A. Wilson, M. Al Bakir, C. Swanton, S. John, J. Miles, B. Larijani, V. Kunene, E. Fontana, H. T. Arkenau, P. J. Parker, M. Rodriguez-Justo, K. K. Shiu, J. Spencer, F. D. Ciccarelli, Immunogenomics of Colorectal Cancer Response to Checkpoint Blockade: Analysis of the KEYNOTE 177 Trial and Validation Cohorts. *Gastroenterology* **161**, 1179-1193 (2021).
70. V. R. T. Zanotelli, ; Bodenmiller, B., in *https://zenodo.org/record/3841961*. (Zenodo, 2022).
71. S. Berg, D. Kutra, T. Kroeger, C. N. Straehle, B. X. Kausler, C. Haubold, M. Schiegg, J. Ales, T. Beier, M. Rudy, K. Eren, J. I. Cervantes, B. Xu, F. Beuttenmueller, A. Wolny, C. Zhang, U. Koethe, F. A. Hamprecht, A. Kreshuk, ilastik: interactive machine learning for (bio)image analysis. *Nat Methods* **16**, 1226-1232 (2019).
72. N. Eling, in *https://bodenmillergroup.github.io/IMCDataAnalysis/*. (2023).
73. M. J. Pitcher, in *https://github.com/jspencer-lab/GALT_CosMX_IMC*. (2026).
74. M. J. Pitcher, Sun, X., in *https://doi.org/10.5281/zenodo.18405128*. (2026).
75. M. J. Pitcher, in *https://BioRender.com/vmhd0uc*. (2026).

Formatted: German
Formatted: German
Formatted: German
Field Code Changed

ACKNOWLEDGEMENTS

We thank Dr Jelmar Quist for supporting the design and initial analysis of the spatial transcriptomics experiment, and Dr Sahil Jain for supporting the acquisition of confocal images.

Funding:

This work was supported by an Investigator Award to Jo Spencer from the Wellcome Trust reference 220872/Z/20/Z.

Author contributions:

Conceptualization: J.Spencer, M.J.P., L.M., D.L.G. **Funding acquisition:** J. Spencer **Investigation:** M.J.P., X.S., C.D., L.M., S.H.K., J.H.Y.S., R.L., R.N., G.J.P., R.J.E., C.B., J. Sufi, H.V., A.K., A.V. **Development of methodology:** R.L., M.J.P. X.S., P.D., R.J.E., G.J.P., J.H.Y.S. **Data analysis:** M.J.P., X.S., R.L. **Critical review of data:** J. Spencer, D.L.G., A.V., **Writing—original draft:** J.S., M.J.P., X.S. **Writing—review and editing:** D.L.G., A.V., J.Spencer, M.J.P., X.S., J.H.Y.S., G.J.P.

Competing interests:

The authors have no competing interests to declare.

Data, code, and materials

All data are available in the data files, in the supplementary material or through links provided in the manuscript.

FIGURE LEGENDS

Fig 1 Spatial composition of immune cell lineages in GALT derived using CosMx spatial transcriptomics

(A) Schematic of CosMx cell lineage classification. Appendix samples (n=7) were processed using CosMx Spatial Molecular Imager. The resulting image data was segmented using surface proteins for cell boundaries, and for each cell, x and y coordinates and expression of 1000 genes was derived. The cell expression data was anchored to a published atlas of immune cells in human appendix pre-labeled for cell lineages (Epithelial, endothelial, B cells, T cells, mesenchymal, plasma cells and myeloid cells), with anchoring based on transcriptomic similarity of cells in the CosMx with reference data. Lineage labels were transferred from reference to CosMx data based on the anchors. (B) Cell lineages visualized spatially in one of the CosMx samples (left) and split by each lineage (right). (C) Lineage classifications of a lymphoid follicle are shown in (B). (D) Expression of module scores of marker genes for each lineage derived from annotated reference data, on the whole tissue and inset in (B) and (C) respectively. (E) Heatmap of gene expression in the CosMx data showing top 10 markers for each lineage. (F) UMAP visualization of lineage classified cells for a representative sample of the CosMx data.

Deleted: J
Formatted ... [60]
Formatted ... [61]
Formatted ... [62]
Formatted ... [63]
Formatted ... [64]
Formatted ... [65]
Formatted ... [66]
Formatted ... [67]
Formatted ... [68]
Deleted: X
Deleted: X
Deleted: from
Deleted: donors
Formatted ... [69]
Deleted: X
Deleted: cell
Deleted: to give
Deleted: gene
Formatted ... [70]
Formatted ... [71]
Deleted: l
Deleted: X
Deleted: the
Deleted: Cell l
Deleted: then
Deleted: the
Deleted: the
Deleted: X
Deleted: s
Deleted: X
Formatted ... [72]
Deleted: as
Formatted ... [73]
Formatted ... [74]
Deleted: the
Deleted: as shown
Deleted: X
Deleted: derived from annotated reference data
Deleted: s
Deleted: single
Deleted: X

(G) Percentage of neighbors of each cell sharing the same lineage as the cell, across the whole tissue (left) and a lymphoid follicle (right, same region as in (C)). Regions consisting mostly of T cells (green) and B cells (blue) were manually annotated. (H) Boxplot of proportion of neighbors of the same lineage, split by lineage. (I) Heatmap of sum of significant proximities across lineages (p values generated by comparing observed with permuted interactions). Positive sum values indicate a tendency for lineages to be in proximity to each other across samples; negative values indicate a tendency for lineages to not be near each other. Schematic created in BioRender.com(*75*).

Fig 2 Single cell analysis of B cell subpopulations in human GALT

(A) Schematic representation of pipeline. B cells were selected from the total CosMx cellular output. A CITEseq data set was generated from human appendix cells (n=3 biological replicates) that included RNA sequencing data and ADT markers that allowed B cells to be designated into subsets. Common genes between the cells in the CosMx and CITEseq data set allowed transfer of cell subset information from CITEseq to CosMx. (B) UMAP visualization of B cell composition in GALT colored by subset (TS = Transitional, aNAV = Activated Naïve, ActB3 = Activated B cell 3, MZ = Marginal Zone, CSM = class-switched memory, DN2 = Double Negative 2, PB = Plasmablast). (C) Dot plot of surface antibody expression of ADT markers on B cell subsets. (D) Dot plot of gene expression of selected genes on B cell subsets. (E) A lymphoid follicle from a representative CosMx sample is shown, with manual annotation of the B cell follicle, the follicle-associated epithelium and sub-epithelial dome (SED). Color code bar identifies B cell subsets and epithelium. (F) Heatmap of sum of significant proximities across B cell subsets with cell lineages and B cell subsets. Positive sum values indicate a tendency for cell lineages to be in proximity to each other across samples; negative values indicate a tendency for cell lineages to not be in proximity to each other. (G) Comparison of frequencies of B cell subsets observed using CITE-seq and CosMx modalities with the same color code as E.

Fig 3 Interaction profile of B cells in GALT derived using ligand-receptor analysis

(A) Diagram showing derivation of ligand-receptor interactions from CosMx data and the pipelines leading to outputs in Figs. 3 and 4. (B) Ligand-receptor strength between B cells and interacting cells at each edge visualized spatially. Edge positions are mid-point of edge between

Deleted: u
Deleted: which share
Formatted: Font: (Default) Times New Roman, 12 pt
Deleted: u
Deleted: with
Deleted: as the cell
Formatted: Font: (Default) Times New Roman, 12 pt
Formatted: Highlight
Formatted: Font: (Default) Times New Roman, 12 pt
Deleted: cell
Deleted: cell
Deleted: in proximity to
Formatted: Font: (Default) Times New Roman, 12 pt
Formatted: Font: (Default) Times New Roman, 12 pt
Formatted: Font: (Default) Times New Roman, 12 pt
Deleted: s
Deleted: u
Deleted: X
Formatted: Font: (Default) Times New Roman, 12 pt
Deleted: Schematic created in BioRender.com.
Formatted: Font: (Default) Times New Roman, 12 pt
Deleted: X
Deleted: s

two cells; strengths are calculate based on sum of all strengths of ligand-receptor pairs for each edge. (C) Expression across a single follicle with manually annotated sub-epithelial dome (SED) and germinal center (GC). (D) Scatter plot showing interaction profile of B cell subsets, showing number of edges (horizontal axis) and mean interaction strength (vertical axis). (E) Dot plot for B cell subset interactions with B cells as source (expressing ligand). (F) Results of pathway analysis run on genes present in the imputed interactions of DN2 B cells in CosMx data. Top 7 pathways (with negative log10 P value > 20) are highlighted in color. (G) Ligand-receptor pairs present on DN2 interactions with Myeloid and (H) $CD4^+$ T cells.

Fig. 4 Interactions of five B cell subsets in GALT with cells of other lineages

(A) Interaction strengths between marker genes of five B cell subsets identified in the CITE-seq data (n=3 biological replicates) and target cells of other lineages in the CosMx data (n=7 biological replicates) as described in Fig. 3A. Interacting pairs are ranked according to the strength of interactions observed between DN2 B cells and cells of other lineages. (B) Spatial analysis of imputed expression of CD86, GRN, EBI3 and SIGLEC10 that are associated with DN2 interactions. Each is enriched in the SED and GC (white arrows).

Fig 5 Validation of CD86 gene and protein expression in the SED of GALT

(A) and (B) Imaging mass cytometry illustration of features of the microanatomy of GALT identifying the SED region with a dotted line and the GC with a solid line. (C) Location of key markers FcRL4 and *ITGAX* that have enriched expression in DN2 B cells. (D) Expression of *CD86* is concentrated in the GC and SED. The *CTLA4* binding partner of *CD86* has a perifollicular and subepithelial distribution. (E) Illustration of *CD86* expression by B cells with features of DN2 cells in the SED. Arrows in inserts identify an example of an intraepithelial DN2 cell expressing *CD86*. (F) Illustration of *CTLA4* expression by CD4 T cells in the immediate microenvironments as *CD86* expressing B cells microenvironments (Compare distribution of cells in boxes in inserts in E and F that are included to aid identification of individual cells). Example is from one of 3 biological replicates. (G) Immunofluorescence and (H) confocal microscopy (representative image of 3 biological replicates), illustrating the co-expression of CD86 protein by B cells in the FAE of GALT (arrows). Scale bars = 50 µm (A-F) and 30 µm (G, H).

Deleted: re

Deleted: X

Deleted: 5

Formatted: Font: (Default) Times New Roman, 12 pt

Deleted: u

Deleted: .

Formatted: Font: (Default) Times New Roman, 12 pt

Formatted: Font: (Default) Times New Roman, 12 pt

Formatted: Font: (Default) Times New Roman, 12 pt, Italic

Formatted: Font: (Default) Times New Roman, 12 pt

Formatted: Font: (Default) Times New Roman, 12 pt, Italic

Formatted: Font: (Default) Times New Roman, 12 pt

Formatted: Font: (Default) Times New Roman, 12 pt, Italic

Formatted: Font: (Default) Times New Roman, 12 pt

Formatted: Font: (Default) Times New Roman, 12 pt, Italic

Formatted: Font: (Default) Times New Roman, 12 pt

Formatted: Font: (Default) Times New Roman, 12 pt, Italic

Formatted: Font: (Default) Times New Roman, 12 pt

Formatted: Font: (Default) Times New Roman, 12 pt, Italic

Formatted: Font: (Default) Times New Roman, 12 pt

Formatted: Font: (Default) Times New Roman, 12 pt, Italic

Formatted: Font: (Default) Times New Roman, 12 pt

Formatted: Font: (Default) Times New Roman, 12 pt, Highlight

Formatted: Highlight

Formatted: Font: (Default) Times New Roman, 12 pt, Highlight

Formatted: Highlight

Formatted: Highlight

Formatted: Font: (Default) Times New Roman, 12 pt

Formatted: Highlight

Formatted: Font: (Default) Times New Roman, 12 pt

Formatted: Font: (Default) Times New Roman, 12 pt, Highlight

Deleted: add for inserts

Formatted: Font: (Default) Times New Roman, 12 pt

Fig 6 Validation of GRN gene and protein expression in the SED of GALT

(A) and (B) Imaging mass cytometry illustration of features of the microanatomy of GALT identifying the SED region with a dotted line and the GC with a solid line. (C) Location of key markers FcRL4 and CD11c that have enriched expression in DN2 B cells. (D) Expression of *GRN* by B cells expressing the FcRL4 and CD11c markers of DN2 cells. (E) Identification of *GRN* expression alongside expression of binding partners *TNFRSF1A* and *TNFRSF1B* showing proximity of expression. Compare staining in shapes in inserts in (D) and (E) that aid identification of *GRN* association with cells expressing identifiers of DN2 B cells. (F) Expression of *TNFRSF1B* by CD68 expressing myeloid cells in the SED (G) Expression of *TNFRSF1B* by CD4 expressing cells in the SED and (H) Expression of *TNFRSF1B* by CD8 T cells. Example is from one of 3 biological replicates. (I) Immunofluorescence and (J) confocal microscopy to identify expression of progranulin protein by B cells in the SED. (Representative image from one of 3 biological replicates). Scale bars = 100 µm (A-H) and 30 µm (I, J).

Fig 7 Validation of EBI3 gene and protein expression in the SED of GALT

(A) Although *EBI3* is a marker gene of DN2 B cells and is significantly expressed by DN2 cells and centrocytes, in neither case is expression of IL27 or IL12A observed that are chains that can bind EBI3 to make IL27 or IL35. (B) and (C) Imaging mass cytometry illustration of features of the microanatomy of GALT identifying the SED region with a dotted line and the GC with a solid line. (D) Selective expression of *EBI3* in the SED and GC alongside FcRL4 and CD11c that are enriched in DN2 cells. Example is from one of 3 biological replicates. (E) Immunofluorescence and (F) confocal microscopy demonstration that the EBI3 protein is expressed by B cells in the SED of GALT. Example is an image from one of 3 biological replicates. Scale bars = 100 µm (B-D) and 30 µm (E, F).

Fig 8 Analysis of B cell subsets in Ulcerative Colitis

(A) IMC staining of healthy appendix (one of 4 biological replicates), showing lineage markers (left) and computational classification of cells from the same ROI. (B and C) IMC staining two different UC appendix samples (out of 4 biological replicates), showing lineage markers (left) and computational classification of cells from the same ROI in each. (D) PCA plot constructed

Deleted: GRN
Formatted: Font: (Default) Times New Roman, 12 pt, Italic
Formatted: Font: (Default) Times New Roman, 12 pt
Formatted: Font: (Default) Times New Roman, 12 pt
Formatted: Font: (Default) Times New Roman, 12 pt, Italic
Formatted: Font: (Default) Times New Roman, 12 pt
Formatted: Font: (Default) Times New Roman, 12 pt, Italic
Formatted: Font: (Default) Times New Roman, 12 pt
Formatted: Font: (Default) Times New Roman, 12 pt, Italic
Formatted: Font: (Default) Times New Roman, 12 pt
Deleted: *identify*
Formatted: Font: (Default) Times New Roman, 12 pt
Formatted: Font: (Default) Times New Roman, 12 pt, Italic
Formatted: Font: (Default) Times New Roman, 12 pt
Formatted: Font: (Default) Times New Roman, 12 pt, Italic
Formatted: Font: (Default) Times New Roman, 12 pt
Formatted: Font: (Default) Times New Roman, 12 pt, Italic
Formatted: Font: (Default) Times New Roman, 12 pt
Formatted: Font: (Default) Times New Roman, 12 pt
Deleted: r
Formatted: Font: (Default) Times New Roman, 12 pt
Formatted: Font: (Default) Times New Roman, 12 pt, Italic
Formatted: Font: (Default) Times New Roman, 12 pt
Formatted: Font: (Default) Times New Roman, 12 pt, Italic
Formatted: Font: (Default) Times New Roman, 12 pt
Formatted: Font: (Default) Times New Roman, 12 pt
Formatted: Highlight
Formatted: Font: (Default) Times New Roman, 12 pt
Deleted: representative
Deleted: sample
Formatted: Highlight
Formatted: Highlight
Formatted: Font: (Default) Times New Roman, 12 pt, Highlight
Formatted: Font: (Default) Times New Roman, 12 pt
Deleted: of representative
Formatted: Font: (Default) Times New Roman, 12 pt
Formatted: Highlight
Formatted: Font: (Default) Times New Roman, 12 pt, Highlight
Formatted: Font: (Default) Times New Roman, 12 pt
Formatted: Font: (Default) Times New Roman, 12 pt

on scaled number of proximities between lineages within each ROI. (E) Proximity score between lineages based on interaction score testing between lineages in health and UC. (F) Dot plot of percentage of B cells with at least 1 T cell neighbor in HC and UC (2 biological replicates 2 tailed t-test). (G) IMC staining of DN2 markers (left) and visualization of computationally derived DN2 B cells (epithelial cells for reference) (right) from healthy appendix. (H) IMC staining of key DN2 markers (left) and visualization of computationally derived DN2 B cells, (epithelial cells for reference) (right) from a representative UC appendix sample. Insert shows DN2 cells scattered through the follicle in UC rather than subepithelial clustering. (I) Density plot showing distribution of DN2 B cells based on minimum distance from an epithelial cell, split by HC and UC. (J) Immunofluorescence illustrating distribution of CD86 expression in UC appendix. Representative images of three replicates shown. Expression of CD86 was sparse and not localized to epithelium or SED as observed in health (Fig. 5). (K) Immunofluorescence illustrating distribution of progranulin expression in UC appendix. Expression of progranulin by B cells was more extensive than in health (Fig. 5), though still a feature of the subepithelial region. (L) Immunofluorescence illustrating distribution of EBI3 expression in UC appendix. Expression of EBI3 by B cells was more extensive than observed in health (Fig. 5), though was still a feature of the subepithelial region. Scale bars = 100 μm.

Deleted: which have
Deleted: u
Deleted: which is a T cell,
Deleted: split by
Formatted: Font: (Default) Times New Roman, 12 pt
Formatted: Font: (Default) Times New Roman, 12 pt
Formatted: Font: (Default) Times New Roman, 12 pt
Formatted: Highlight
Deleted: key
Deleted: s
Formatted: Font: (Default) Times New Roman, 12 pt, Highlight
Formatted: Font: (Default) Times New Roman, 12 pt
Deleted: , with
Deleted: a
Deleted: sample
Formatted: Font: (Default) Times New Roman, 12 pt
Deleted: s
Deleted: with
Deleted: e with i
Formatted: Font: (Default) Times New Roman, 12 pt
Deleted: ing
Deleted: with
Formatted: Font: (Default) Times New Roman, 12 pt
Deleted: their
Deleted: staining
Formatted: Highlight
Formatted: Font: (Default) Times New Roman, 12 pt
Deleted: s
Deleted: the
Deleted: in
Deleted: .
Deleted: staining
Deleted: observed
Deleted: in
Formatted: Font: (Default) Times New Roman, 12 pt
Deleted: staining
Deleted: in
Formatted: Font: (Default) Times New Roman, 12 pt
Moved (insertion) [1]
Deleted: ¶ ... [75]

Page 1: [1] Deleted **Jo Spencer** **02/04/2026 13:28:00**

Page 3: [2] Deleted **Jo Spencer** **02/04/2026 13:52:00**

Page 3: [2] Deleted **Jo Spencer** **02/04/2026 13:52:00**

Page 3: [3] Formatted **Jo Spencer** **03/04/2026 15:46:00**

Font: (Default) Times New Roman, 12 pt

Page 3: [3] Formatted **Jo Spencer** **03/04/2026 15:46:00**

Font: (Default) Times New Roman, 12 pt

Page 3: [4] Deleted **Jo Spencer** **08/04/2026 16:31:00**

Page 3: [4] Deleted **Jo Spencer** **08/04/2026 16:31:00**

Page 3: [5] Deleted **Jo Spencer** **09/04/2026 15:24:00**

Page 3: [5] Deleted **Jo Spencer** **09/04/2026 15:24:00**

Page 3: [6] Formatted **Jo Spencer** **02/04/2026 13:27:00**

Font: (Default) Times New Roman, 12 pt

Page 3: [6] Formatted **Jo Spencer** **02/04/2026 13:27:00**

Font: (Default) Times New Roman, 12 pt

Page 3: [7] Deleted **Jo Spencer** **02/04/2026 13:53:00**

Page 3: [7] Deleted **Jo Spencer** **02/04/2026 13:53:00**

Page 3: [8] Formatted **Jo Spencer** **02/04/2026 13:27:00**

Font: 12 pt

Page 3: [8] Formatted **Jo Spencer** **02/04/2026 13:27:00**

Font: 12 pt

Page 3: [9] Formatted **Jo Spencer** **02/04/2026 13:27:00**

Font: (Default) Times New Roman, 12 pt

Page 3: [9] Formatted **Jo Spencer** **02/04/2026 13:27:00**

Font: (Default) Times New Roman, 12 pt

Page 3: [10] Deleted **Jo Spencer** **02/04/2026 13:53:00**

Page 3: [10] Deleted **Jo Spencer** **02/04/2026 13:53:00**

Page 3: [10] Deleted **Jo Spencer** **02/04/2026 13:53:00**

Page 3: [11] Formatted **Jo Spencer** **03/04/2026 15:47:00**

Font: (Default) Times New Roman, 12 pt

Page 3: [11] Formatted **Jo Spencer** **03/04/2026 15:47:00**

Font: (Default) Times New Roman, 12 pt

Page 3: [11] Formatted **Jo Spencer** **03/04/2026 15:47:00**

Font: (Default) Times New Roman, 12 pt

Page 3: [12] Deleted **Jo Spencer** **07/04/2026 13:41:00**

Page 3: [12] Deleted **Jo Spencer** **07/04/2026 13:41:00**

Page 3: [12] Deleted **Jo Spencer** **07/04/2026 13:41:00**

Page 3: [13] Formatted **Jo Spencer** **03/04/2026 15:47:00**

Font: (Default) Times New Roman, 12 pt

Page 3: [13] Formatted **Jo Spencer** **03/04/2026 15:47:00**

Font: (Default) Times New Roman, 12 pt

Page 3: [14] Deleted **Jo Spencer** **02/04/2026 14:00:00**

Page 3: [14] Deleted **Jo Spencer** **02/04/2026 14:00:00**

Page 3: [15] Formatted **Jo Spencer** **03/04/2026 15:47:00**

Font: (Default) Times New Roman, 12 pt

Page 3: [15] Formatted **Jo Spencer** **03/04/2026 15:47:00**

Font: (Default) Times New Roman, 12 pt

Page 3: [15] Formatted **Jo Spencer** **03/04/2026 15:47:00**

Font: (Default) Times New Roman, 12 pt

Page 3: [15] Formatted **Jo Spencer** **03/04/2026 15:47:00**

Font: (Default) Times New Roman, 12 pt

Page 3: [16] Formatted **Jo Spencer** **02/04/2026 13:27:00**

Font: (Default) Times New Roman, 12 pt

Page 3: [16] Formatted **Jo Spencer** **02/04/2026 13:27:00**

Font: (Default) Times New Roman, 12 pt

Page 9: [17] Deleted **Jo Spencer** **05/04/2026 07:37:00**

Page 9: [17] Deleted **Jo Spencer** **05/04/2026 07:37:00**

Page 9: [18] Deleted **Jo Spencer** **08/04/2026 16:19:00**

Page 9: [18] Deleted **Jo Spencer** **08/04/2026 16:19:00**

Page 9: [19] Deleted **Jo Spencer** **07/04/2026 15:56:00**

Page 9: [19] Deleted **Jo Spencer** **07/04/2026 15:56:00**

Page 9: [19] Deleted **Jo Spencer** **07/04/2026 15:56:00**

Page 9: [19] Deleted **Jo Spencer** **07/04/2026 15:56:00**

Page 9: [19] Deleted **Jo Spencer** **07/04/2026 15:56:00**

Page 9: [19] Deleted **Jo Spencer** **07/04/2026 15:56:00**

Page 9: [19] Deleted **Jo Spencer** **07/04/2026 15:56:00**

Page 9: [19] Deleted **Jo Spencer** **07/04/2026 15:56:00**

Page 9: [19] Deleted **Jo Spencer** **07/04/2026 15:56:00**

Page 9: [19] Deleted **Jo Spencer** **07/04/2026 15:56:00**

Page 9: [20] Formatted **Xiaowen Sun** **13/04/2026 14:01:00**

Font: (Default) Times New Roman, 12 pt

Page 9: [20] Formatted **Xiaowen Sun** **13/04/2026 14:01:00**

Font: (Default) Times New Roman, 12 pt

Page 9: [21] Formatted **Jo Spencer** **02/04/2026 13:27:00**

Font: (Default) Times New Roman, 12 pt

Page 9: [21] Formatted **Jo Spencer** **02/04/2026 13:27:00**

Font: (Default) Times New Roman, 12 pt

Page 9: [21] Formatted **Jo Spencer** **02/04/2026 13:27:00**

Font: (Default) Times New Roman, 12 pt

Page 9: [21] Formatted **Jo Spencer** **02/04/2026 13:27:00**

Font: (Default) Times New Roman, 12 pt

Page 9: [21] Formatted **Jo Spencer** **02/04/2026 13:27:00**

Font: (Default) Times New Roman, 12 pt

Page 9: [22] Deleted **Jo Spencer** **02/04/2026 14:14:00**

Page 9: [22] Deleted **Jo Spencer** **02/04/2026 14:14:00**

Page 9: [23] Formatted **Jo Spencer** **07/04/2026 13:56:00**

Font: (Default) Times New Roman, 12 pt, Italic

Page 9: [23] Formatted **Jo Spencer** **07/04/2026 13:56:00**

Font: (Default) Times New Roman, 12 pt, Italic

Page 9: [23] Formatted **Jo Spencer** **07/04/2026 13:56:00**

Font: (Default) Times New Roman, 12 pt, Italic

Page 9: [23] Formatted **Jo Spencer** **07/04/2026 13:56:00**

Font: (Default) Times New Roman, 12 pt, Italic

Page 9: [24] Formatted **Jo Spencer** **02/04/2026 13:27:00**

Font: (Default) Times New Roman, 12 pt

Page 9: [24] Formatted **Jo Spencer** **02/04/2026 13:27:00**

Font: (Default) Times New Roman, 12 pt

Page 9: [24] Formatted **Jo Spencer** **02/04/2026 13:27:00**

Font: (Default) Times New Roman, 12 pt

Page 9: [24] Formatted **Jo Spencer** **02/04/2026 13:27:00**

Font: (Default) Times New Roman, 12 pt

Page 9: [24] Formatted **Jo Spencer** **02/04/2026 13:27:00**

Font: (Default) Times New Roman, 12 pt

Page 9: [24] Formatted **Jo Spencer** **02/04/2026 13:27:00**

Font: (Default) Times New Roman, 12 pt

Page 9: [25] Deleted **Jo Spencer** **02/04/2026 14:14:00**

Page 9: [25] Deleted **Jo Spencer** **02/04/2026 14:14:00**

Page 9: [25] Deleted **Jo Spencer** **02/04/2026 14:14:00**

Page 9: [26] Formatted **Jo Spencer** **07/04/2026 13:57:00**

Font: (Default) Times New Roman, 12 pt, Italic

Page 9: [26] Formatted **Jo Spencer** **07/04/2026 13:57:00**

Font: (Default) Times New Roman, 12 pt, Italic

Page 9: [27] Deleted **Jo Spencer** **07/04/2026 15:56:00**

Page 9: [27] Deleted **Jo Spencer** **07/04/2026 15:56:00**

Page 10: [28] Formatted **Jo Spencer** **07/04/2026 14:58:00**

Font: (Default) Times New Roman, 12 pt, Italic

Page 10: [28] Formatted **Jo Spencer** **07/04/2026 14:58:00**

Font: (Default) Times New Roman, 12 pt, Italic

Page 10: [29] Formatted **Jo Spencer** **02/04/2026 13:27:00**

Font: (Default) Times New Roman, 12 pt

Page 10: [29] Formatted **Jo Spencer** **02/04/2026 13:27:00**

Font: (Default) Times New Roman, 12 pt

Page 10: [29] Formatted **Jo Spencer** **02/04/2026 13:27:00**

Font: (Default) Times New Roman, 12 pt

Page 10: [29] Formatted **Jo Spencer** **02/04/2026 13:27:00**

Font: (Default) Times New Roman, 12 pt

Page 10: [29] Formatted **Jo Spencer** **02/04/2026 13:27:00**

Font: (Default) Times New Roman, 12 pt

Page 10: [29] Formatted **Jo Spencer** **02/04/2026 13:27:00**

Font: (Default) Times New Roman, 12 pt

Page 10: [30] Formatted **Jo Spencer** **02/04/2026 13:27:00**

Font: (Default) Times New Roman, 12 pt

Page 10: [30] Formatted **Jo Spencer** **02/04/2026 13:27:00**

Font: (Default) Times New Roman, 12 pt

Page 10: [30] Formatted **Jo Spencer** **02/04/2026 13:27:00**

Font: (Default) Times New Roman, 12 pt

Page 10: [30] Formatted **Jo Spencer** **02/04/2026 13:27:00**

Font: (Default) Times New Roman, 12 pt

Page 10: [31] Formatted **Jo Spencer** **02/04/2026 13:27:00**

Font: (Default) Times New Roman, 12 pt

Page 10: [31] Formatted **Jo Spencer** **02/04/2026 13:27:00**

Font: (Default) Times New Roman, 12 pt

Page 10: [31] Formatted **Jo Spencer** **02/04/2026 13:27:00**

Font: (Default) Times New Roman, 12 pt

Page 10: [31] Formatted **Jo Spencer** **02/04/2026 13:27:00**

Font: (Default) Times New Roman, 12 pt

Page 10: [31] Formatted **Jo Spencer** **02/04/2026 13:27:00**

Font: (Default) Times New Roman, 12 pt

Page 10: [32] Deleted **Jo Spencer** **07/04/2026 15:56:00**

Page 10: [32] Deleted **Jo Spencer** **07/04/2026 15:56:00**

Page 10: [33] Formatted **Jo Spencer** **05/04/2026 08:17:00**

Font: (Default) Times New Roman, 12 pt, Italic

Page 10: [33] Formatted **Jo Spencer** **05/04/2026 08:17:00**

Font: (Default) Times New Roman, 12 pt, Italic

Page 10: [33] Formatted **Jo Spencer** **05/04/2026 08:17:00**

Font: (Default) Times New Roman, 12 pt, Italic

Page 10: [33] Formatted **Jo Spencer** **05/04/2026 08:17:00**

Font: (Default) Times New Roman, 12 pt, Italic

Page 10: [33] Formatted **Jo Spencer** **05/04/2026 08:17:00**

Font: (Default) Times New Roman, 12 pt, Italic

Page 10: [33] Formatted **Jo Spencer** **05/04/2026 08:17:00**

Font: (Default) Times New Roman, 12 pt, Italic

Page 10: [33] Formatted **Jo Spencer** **05/04/2026 08:17:00**

Font: (Default) Times New Roman, 12 pt, Italic

Page 10: [34] Formatted **Jo Spencer** **05/04/2026 08:17:00**

Font: (Default) Times New Roman, 12 pt, Italic

Page 10: [34] Formatted **Jo Spencer** **05/04/2026 08:17:00**

Font: (Default) Times New Roman, 12 pt, Italic

Page 10: [34] Formatted **Jo Spencer** **05/04/2026 08:17:00**

Font: (Default) Times New Roman, 12 pt, Italic

Page 10: [34] Formatted **Jo Spencer** **05/04/2026 08:17:00**

Font: (Default) Times New Roman, 12 pt, Italic

Page 10: [34] Formatted **Jo Spencer** **05/04/2026 08:17:00**

Font: (Default) Times New Roman, 12 pt, Italic

Page 10: [34] Formatted **Jo Spencer** **05/04/2026 08:17:00**

Font: (Default) Times New Roman, 12 pt, Italic

Page 10: [34] Formatted **Jo Spencer** **05/04/2026 08:17:00**

Font: (Default) Times New Roman, 12 pt, Italic

Page 10: [34] Formatted **Jo Spencer** **05/04/2026 08:17:00**

Font: (Default) Times New Roman, 12 pt, Italic

Page 10: [35] Deleted **Jo Spencer** **07/04/2026 15:57:00**

Page 10: [35] Deleted **Jo Spencer** **07/04/2026 15:57:00**

Page 10: [35] Deleted **Jo Spencer** **07/04/2026 15:57:00**

Page 10: [36] Formatted **Jo Spencer** **02/04/2026 13:27:00**

Font: (Default) Times New Roman, 12 pt

Page 10: [36] Formatted **Jo Spencer** **02/04/2026 13:27:00**

Font: (Default) Times New Roman, 12 pt

Page 10: [37] Formatted **Jo Spencer** **05/04/2026 08:23:00**

Font: (Default) Times New Roman, 12 pt, Italic

Page 10: [37] Formatted **Jo Spencer** **05/04/2026 08:23:00**

Font: (Default) Times New Roman, 12 pt, Italic

Page 11: [38] Formatted **Jo Spencer** **05/04/2026 08:23:00**

Font: (Default) Times New Roman, 12 pt, Italic

Page 11: [38] Formatted **Jo Spencer** **05/04/2026 08:23:00**

Font: (Default) Times New Roman, 12 pt, Italic

Page 11: [38] Formatted **Jo Spencer** **05/04/2026 08:23:00**

Font: (Default) Times New Roman, 12 pt, Italic

Page 11: [38] Formatted **Jo Spencer** **05/04/2026 08:23:00**

Font: (Default) Times New Roman, 12 pt, Italic

Page 11: [38] Formatted **Jo Spencer** **05/04/2026 08:23:00**

Font: (Default) Times New Roman, 12 pt, Italic

Page 11: [38] Formatted **Jo Spencer** **05/04/2026 08:23:00**

Font: (Default) Times New Roman, 12 pt, Italic

Page 11: [38] Formatted **Jo Spencer** **05/04/2026 08:23:00**

Font: (Default) Times New Roman, 12 pt, Italic

Page 11: [38] Formatted **Jo Spencer** **05/04/2026 08:23:00**

Font: (Default) Times New Roman, 12 pt, Italic

Page 11: [38] Formatted **Jo Spencer** **05/04/2026 08:23:00**

Font: (Default) Times New Roman, 12 pt, Italic

Page 11: [38] Formatted **Jo Spencer** **05/04/2026 08:23:00**

Font: (Default) Times New Roman, 12 pt, Italic

Page 11: [38] Formatted **Jo Spencer** **05/04/2026 08:23:00**

Font: (Default) Times New Roman, 12 pt, Italic

Page 11: [38] Formatted **Jo Spencer** **05/04/2026 08:23:00**

Font: (Default) Times New Roman, 12 pt, Italic

Page 11: [38] Formatted **Jo Spencer** **05/04/2026 08:23:00**

Font: (Default) Times New Roman, 12 pt, Italic

Page 11: [39] Formatted **Jo Spencer** **02/04/2026 13:27:00**

Font: (Default) Times New Roman, 12 pt

Page 11: [39] Formatted **Jo Spencer** **02/04/2026 13:27:00**

Font: (Default) Times New Roman, 12 pt

Page 11: [39] Formatted **Jo Spencer** **02/04/2026 13:27:00**

Font: (Default) Times New Roman, 12 pt

Page 11: [39] Formatted **Jo Spencer** **02/04/2026 13:27:00**

Font: (Default) Times New Roman, 12 pt

Page 11: [40] Deleted **Jo Spencer** **06/04/2026 07:44:00**

Page 11: [40] Deleted **Jo Spencer** **06/04/2026 07:44:00**

Page 11: [41] Formatted **Jo Spencer** **02/04/2026 13:27:00**

Font: (Default) Times New Roman, 12 pt

Page 11: [41] Formatted **Jo Spencer** **02/04/2026 13:27:00**

Font: (Default) Times New Roman, 12 pt

Page 11: [42] Formatted **Jo Spencer** **07/04/2026 15:19:00**

Font: (Default) Times New Roman, 12 pt, Italic

Page 11: [42] Formatted **Jo Spencer** **07/04/2026 15:19:00**

Font: (Default) Times New Roman, 12 pt, Italic

Page 11: [43] Formatted **Jo Spencer** **07/04/2026 15:19:00**

Font: (Default) Times New Roman, 12 pt, Italic

Page 11: [43] Formatted **Jo Spencer** **07/04/2026 15:19:00**

Font: (Default) Times New Roman, 12 pt, Italic

Page 11: [44] Formatted **Jo Spencer** **02/04/2026 13:27:00**

Font: (Default) Times New Roman, 12 pt

Page 11: [44] Formatted **Jo Spencer** **02/04/2026 13:27:00**

Font: (Default) Times New Roman, 12 pt

Page 11: [44] Formatted **Jo Spencer** **02/04/2026 13:27:00**

Font: (Default) Times New Roman, 12 pt

Page 11: [44] Formatted **Jo Spencer** **02/04/2026 13:27:00**

Font: (Default) Times New Roman, 12 pt

Page 11: [44] Formatted **Jo Spencer** **02/04/2026 13:27:00**

Font: (Default) Times New Roman, 12 pt

Page 11: [44] Formatted **Jo Spencer** **02/04/2026 13:27:00**

Font: (Default) Times New Roman, 12 pt

Page 11: [45] Deleted **Jo Spencer** **07/04/2026 15:57:00**

Page 11: [45] Deleted **Jo Spencer** **07/04/2026 15:57:00**

Page 11: [46] Formatted **Jo Spencer** **07/04/2026 15:20:00**

Font: (Default) Times New Roman, 12 pt, Italic

Page 11: [46] Formatted **Jo Spencer** **07/04/2026 15:20:00**

Font: (Default) Times New Roman, 12 pt, Italic

Page 11: [46] Formatted **Jo Spencer** **07/04/2026 15:20:00**

Font: (Default) Times New Roman, 12 pt, Italic

Page 11: [46] Formatted **Jo Spencer** **07/04/2026 15:20:00**

Font: (Default) Times New Roman, 12 pt, Italic

Page 11: [47] Formatted **Jo Spencer** **07/04/2026 15:20:00**

Font: (Default) Times New Roman, 12 pt, Italic

Page 11: [47] Formatted **Jo Spencer** **07/04/2026 15:20:00**

Font: (Default) Times New Roman, 12 pt, Italic

Page 11: [47] Formatted **Jo Spencer** **07/04/2026 15:20:00**

Font: (Default) Times New Roman, 12 pt, Italic

Page 11: [48] Formatted **Jo Spencer** **02/04/2026 13:27:00**

Font: (Default) Times New Roman, 12 pt

Page 11: [48] Formatted **Jo Spencer** **02/04/2026 13:27:00**

Font: (Default) Times New Roman, 12 pt

Page 13: [49] Deleted **Jo Spencer** **07/04/2026 10:41:00**

Page 13: [50] Deleted **Jo Spencer** **07/04/2026 10:41:00**

Page 15: [51] Formatted **Jo Spencer** **02/04/2026 13:27:00**

Font: (Default) Times New Roman, 12 pt

Page 15: [51] Formatted **Jo Spencer** **02/04/2026 13:27:00**

Font: (Default) Times New Roman, 12 pt

Page 15: [52] Formatted **Jo Spencer** **02/04/2026 13:27:00**

Font: (Default) Times New Roman, 12 pt

Page 15: [52] Formatted **Jo Spencer** **02/04/2026 13:27:00**

Font: (Default) Times New Roman, 12 pt

Page 15: [53] Formatted **Jo Spencer** **02/04/2026 13:27:00**

Font: (Default) Times New Roman, 12 pt

Page 15: [53] Formatted **Jo Spencer** **02/04/2026 13:27:00**

Font: (Default) Times New Roman, 12 pt

Page 15: [54] Formatted **Jo Spencer** **02/04/2026 13:27:00**

Font: (Default) Times New Roman, 12 pt

Page 15: [54] Formatted **Jo Spencer** **02/04/2026 13:27:00**

Font: (Default) Times New Roman, 12 pt

Page 15: [55] Formatted **Jo Spencer** **02/04/2026 13:27:00**

Font: (Default) Times New Roman, 12 pt

Page 15: [55] Formatted **Jo Spencer** **02/04/2026 13:27:00**

Font: (Default) Times New Roman, 12 pt

Page 15: [56] Formatted **Jo Spencer** **02/04/2026 13:27:00**

Font: (Default) Times New Roman, 12 pt

Page 15: [56] Formatted **Jo Spencer** **02/04/2026 13:27:00**

Font: (Default) Times New Roman, 12 pt

Page 15: [57] Formatted **Jo Spencer** **02/04/2026 13:27:00**

Font: (Default) Times New Roman, 12 pt

Page 15: [57] Formatted **Jo Spencer** **02/04/2026 13:27:00**

Font: (Default) Times New Roman, 12 pt

Page 15: [58] Formatted **Jo Spencer** **02/04/2026 13:27:00**

Font: 12 pt

Page 15: [58] Formatted **Jo Spencer** **02/04/2026 13:27:00**

Font: 12 pt

Page 15: [58] Formatted **Jo Spencer** **02/04/2026 13:27:00**

Font: 12 pt

Page 15: [58] Formatted **Jo Spencer** **02/04/2026 13:27:00**

Font: 12 pt

Page 15: [58] Formatted **Jo Spencer** **02/04/2026 13:27:00**

Font: 12 pt

Page 15: [58] Formatted **Jo Spencer** **02/04/2026 13:27:00**

Font: 12 pt

Page 15: [59] Formatted **Jo Spencer** **02/04/2026 13:27:00**

Font: (Default) Times New Roman, 12 pt

Page 15: [59] Formatted **Jo Spencer** **02/04/2026 13:27:00**

Font: (Default) Times New Roman, 12 pt

Page 30: [60] Formatted **Jo Spencer** **08/04/2026 13:32:00**

Justified

Page 30: [61] Formatted **Jo Spencer** **08/04/2026 13:33:00**

Font: Not Bold

Page 30: [62] Formatted **Jo Spencer** **08/04/2026 13:32:00**

Font: 12 pt, Not Highlight

Page 30: [63] Formatted **Jo Spencer** **08/04/2026 13:32:00**

Font: (Default) Times New Roman, 12 pt

Page 30: [64] Formatted **Jo Spencer** **08/04/2026 13:32:00**

EndNote Bibliography, Indent: Left: 0 cm, Hanging: 1.27 cm, Line spacing: single

Page 30: [65] Formatted **Jo Spencer** **08/04/2026 13:32:00**

Font: (Default) Times New Roman, 12 pt, Not Bold, Font colour: Text 1

Page 30: [66] Formatted **Jo Spencer** **08/04/2026 13:32:00**

Font: (Default) Times New Roman, 12 pt, Not Bold, Font colour: Text 1

Page 30: [67] Formatted **Jo Spencer** **08/04/2026 13:32:00**

Font: (Default) Times New Roman, 12 pt, Not Bold, Font colour: Text 1

Page 30: [68] Formatted	**Jo Spencer**	**02/04/2026 13:27:00**

Font: (Default) Times New Roman, 12 pt

Page 30: [69] Formatted	**Jo Spencer**	**02/04/2026 13:27:00**

Font: (Default) Times New Roman, 12 pt

Page 30: [70] Formatted	**Jo Spencer**	**02/04/2026 13:27:00**

Font: (Default) Times New Roman, 12 pt

Page 30: [71] Formatted	**Jo Spencer**	**02/04/2026 13:27:00**

Font: (Default) Times New Roman, 12 pt

Page 30: [72] Formatted	**Jo Spencer**	**02/04/2026 13:27:00**

Font: (Default) Times New Roman, 12 pt

Page 30: [73] Formatted	**Jo Spencer**	**02/04/2026 13:27:00**

Font: (Default) Times New Roman, 12 pt

Page 30: [74] Formatted	**Jo Spencer**	**02/04/2026 13:27:00**

Font: (Default) Times New Roman, 12 pt

Page 34: [75] Deleted	**Jo Spencer**	**08/04/2026 13:38:00**

Fig. 1

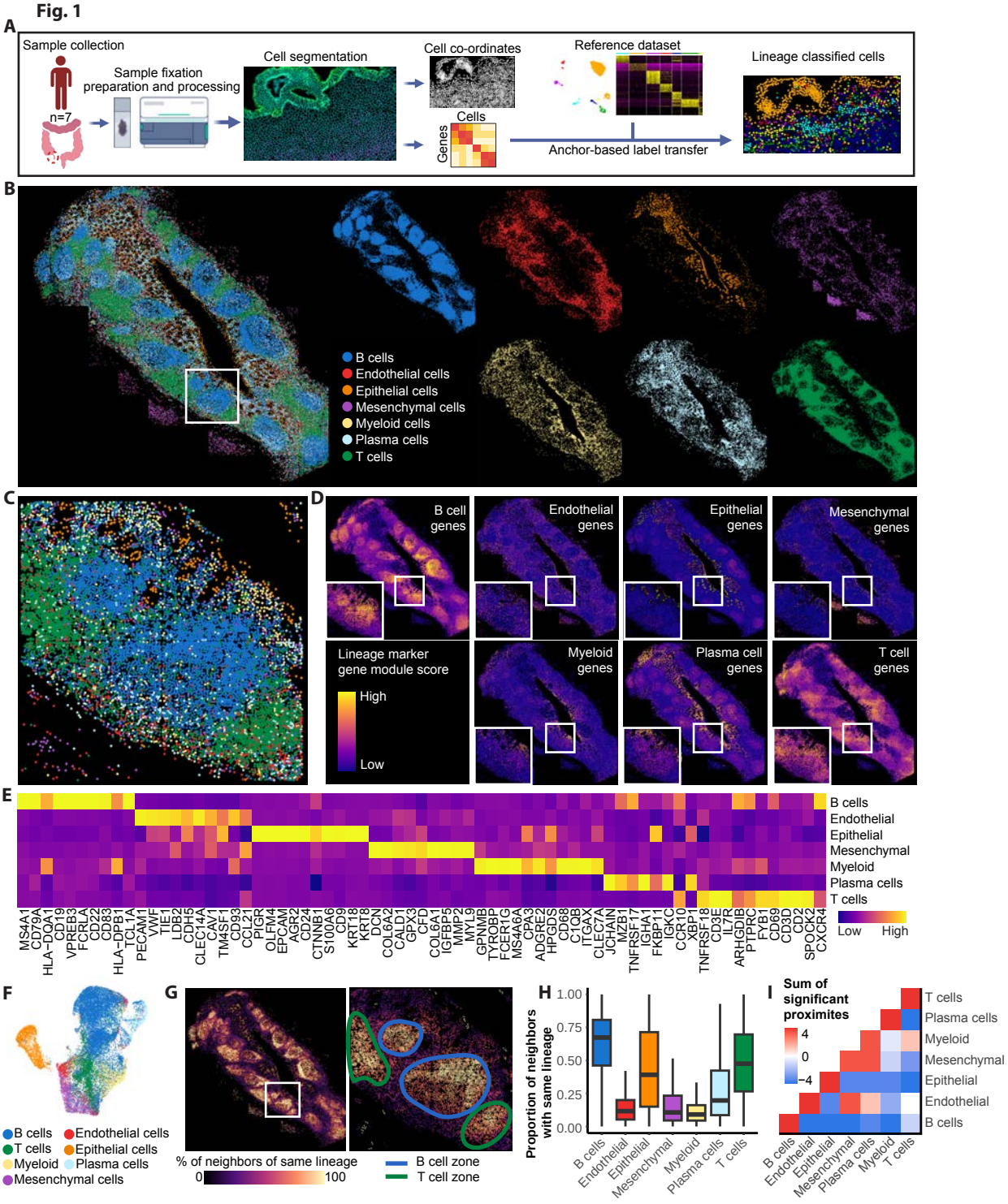

A
Sample collection
n=7
Sample fixation
preparation and processing
Cell segmentation
Cell co-ordinates
Cells
Genes
Reference dataset
Anchor-based label transfer
Lineage classified cells
B
B cells
Endothelial cells
Epithelial cells
Mesenchymal cells
Myeloid cells
Plasma cells
T cells
C
D
B cell genes
Endothelial genes
Epithelial genes
Mesenchymal genes
Lineage marker gene module score
High
Low
Myeloid genes
Plasma cell genes
T cell genes
E
B cells
Endothelial
Epithelial
Mesenchymal
Myeloid
Plasma cells
T cells
Low
High
MS4A1 CD79A HLA−DQA1 CD19 VPREB3 FCRLA CD22 CD83 HLA−DPB1 TCL1A PECAM1 VWF TIE1 LDB2 CDH5 CLEC14A CAV1 TM4SF1 CD93 CCL21 PIGR OLFM4 EPCAM AGR2 CD24 CTNNB1 S100A6 CD9 KRT18 KRT8 DCN COL6A2 CALD1 GPX3 CFD COL6A1 IGFBP5 MMP2 MYL9 GPNMB TYROBP FCER1G MS4A6A CPA3 ADGRE2 HPGDS CD68 C1QB ITGAX CLEC7A JCHAIN MZB1 TNFRSF17 IGHA1 FKBP11 IGKC CCR10 XBP1 TNFRSF18 CD3E IL7R ARHGDIB PTPRC FYB1 CD69 CD3D CD2 SPOCK2 CXCR4
F
B cells
Endothelial cells
T cells
Epithelial cells
Myeloid
Plasma cells
Mesenchymal cells
G
% of neighbors of same lineage
0
100
B cell zone
T cell zone
H
Proportion of neighbors with same lineage
1.00
0.75
0.50
0.25
0.00
B cells
Endothelial
Epithelial
Mesenchymal
Myeloid
Plasma cells
T cells
I
Sum of significant proximites
4
0
−4
T cells
Plasma cells
Myeloid
Mesenchymal
Epithelial
Endothelial
B cells

Fig. 2

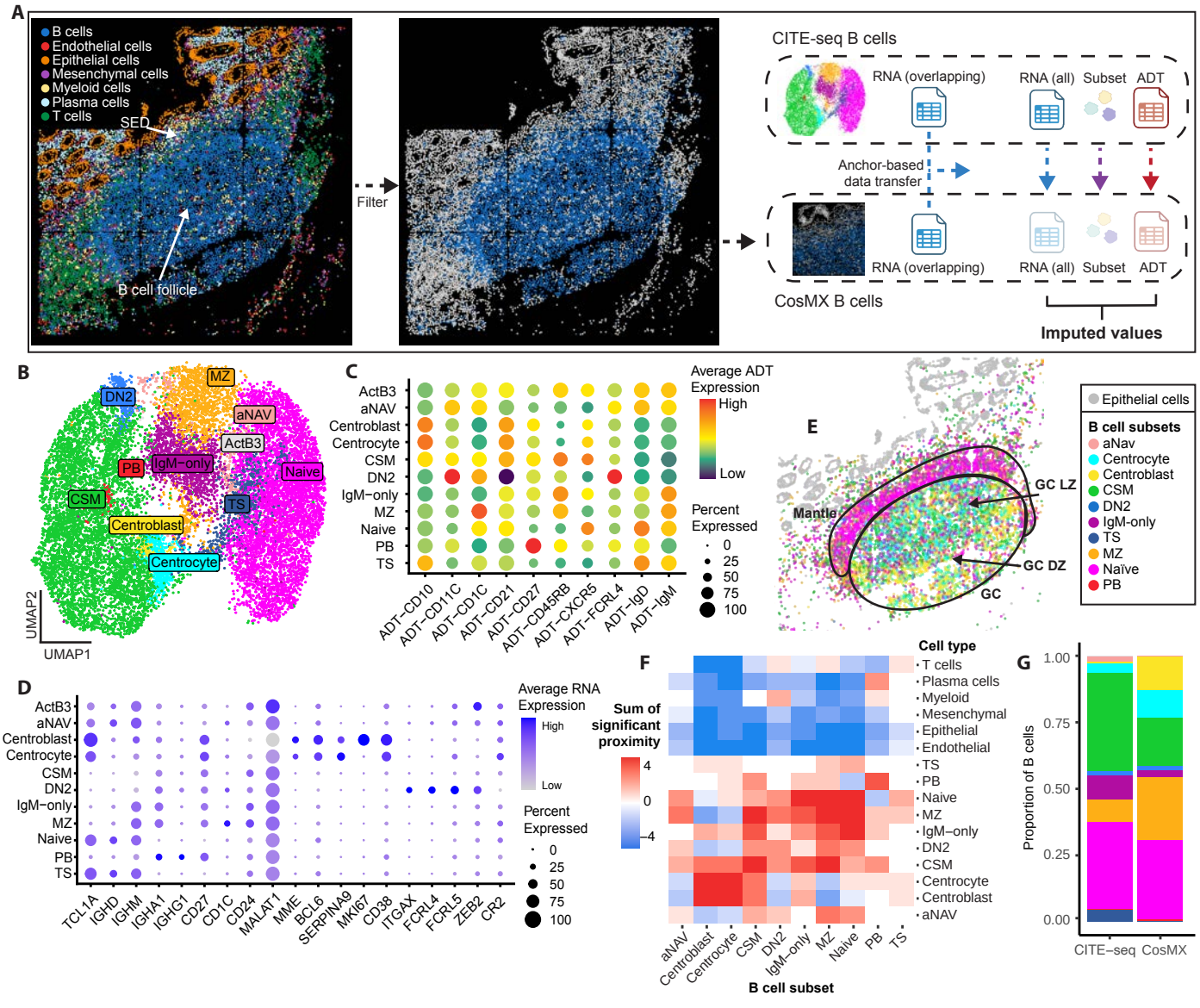
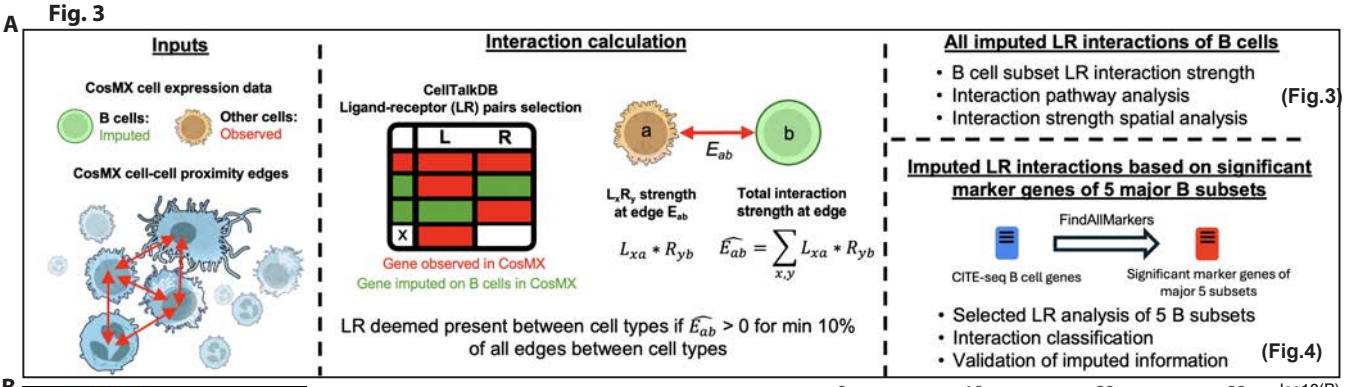
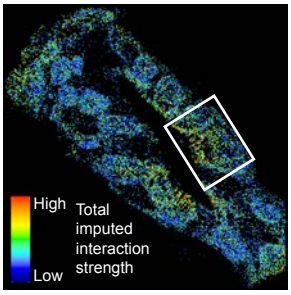
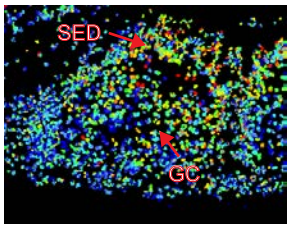
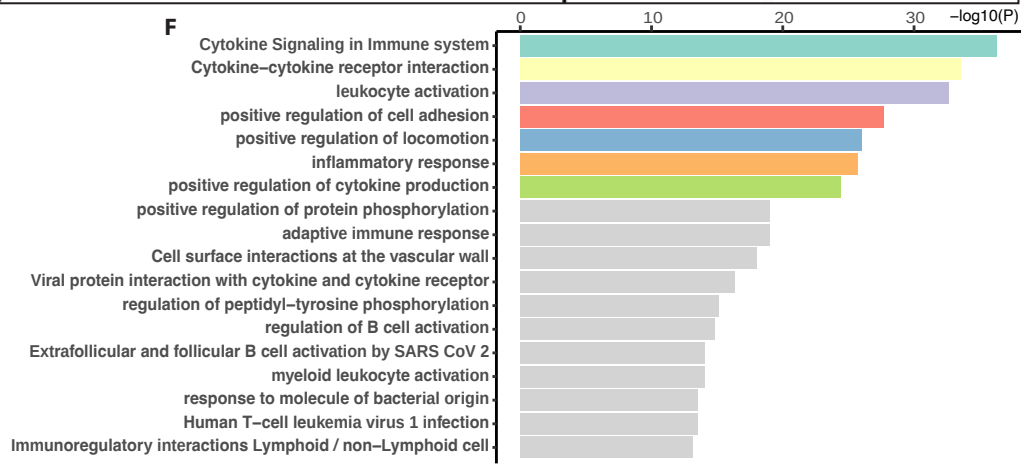

A
B cells
Endothelial cells
Epithelial cells
Mesenchymal cells
Myeloid cells
Plasma cells
T cells
SED
B cell follicle
Filter
CITE-seq B cells
RNA (overlapping)
RNA (all)
Subset
ADT
Anchor-based data transfer
CosMX B cells
Imputed values
B
DN2
MZ
aNAV
ActB3
PB
IgM−only
Naive
CSM
TS
Centroblast
Centrocyte
UMAP2
UMAP1
C
ActB3
aNAV
Centroblast
Centrocyte
CSM
DN2
IgM−only
MZ
Naive
PB
TS
ADT−CD10
ADT−CD11C
ADT−CD1C
ADT−CD21
ADT−CD27
ADT−CD45RB
ADT−CXCR5
ADT−FCRL4
ADT−IgD
ADT−IgM
Average ADT Expression
High
Low
Percent Expressed
0
25
50
75
100
E
Mantle
GC LZ
GC DZ
GC
Epithelial cells
B cell subsets
aNav
Centrocyte
Centroblast
CSM
DN2
IgM-only
TS
MZ
Naïve
PB
D
ActB3
aNAV
Centroblast
Centrocyte
CSM
DN2
IgM−only
MZ
Naive
PB
TS
TCL1A
IGHD
IGHM
IGHA1
IGHG1
CD27
CD1C
CD24
MALAT1
MME
BCL6
SERPINA9
MKI67
CD38
ITGAX
FCRL4
FCRL5
ZEB2
CR2
Average RNA Expression
High
Low
Percent Expressed
0
25
50
75
100
F
Sum of significant proximity
4
0
−4
Cell type
T cells
Plasma cells
Myeloid
Mesenchymal
Epithelial
Endothelial
TS
PB
Naive
MZ
IgM−only
DN2
CSM
Centrocyte
Centroblast
aNAV
aNAV
Centroblast
Centrocyte
CSM
DN2
IgM−only
MZ
Naive
PB
TS
B cell subset
G
Proportion of B cells
1.00
0.75
0.50
0.25
0.00
CITE−seq
CosMX

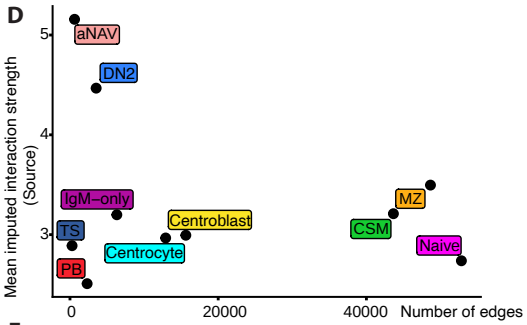
Fig. 3

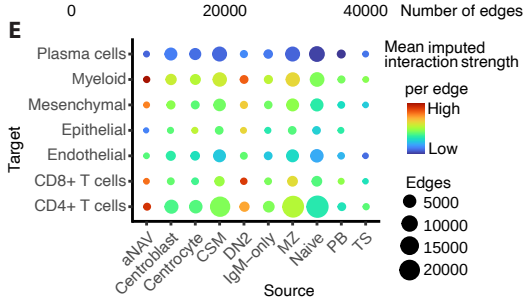

A
Inputs
CosMX cell expression data
B cells: Imputed
Other cells: Observed
CosMX cell-cell proximity edges
Interaction calculation
CellTalkDB
Ligand-receptor (LR) pairs selection
L
R
X
Gene observed in CosMX
Gene imputed on B cells in CosMX
a
b
E_{ab}
L_xR_y strength at edge E_{ab}
$L_{xa} * R_{yb}$
Total interaction strength at edge
$\widehat{E_{ab}} = \sum_{x,y} L_{xa} * R_{yb}$
LR deemed present between cell types if $\widehat{E_{ab}} > 0$ for min 10% of all edges between cell types
All imputed LR interactions of B cells
• B cell subset LR interaction strength
• Interaction pathway analysis
• Interaction strength spatial analysis
(Fig.3)
Imputed LR interactions based on significant marker genes of 5 major B subsets
FindAllMarkers
CITE-seq B cell genes
Significant marker genes of major 5 subsets
• Selected LR analysis of 5 B subsets
• Interaction classification
• Validation of imputed information
(Fig.4)

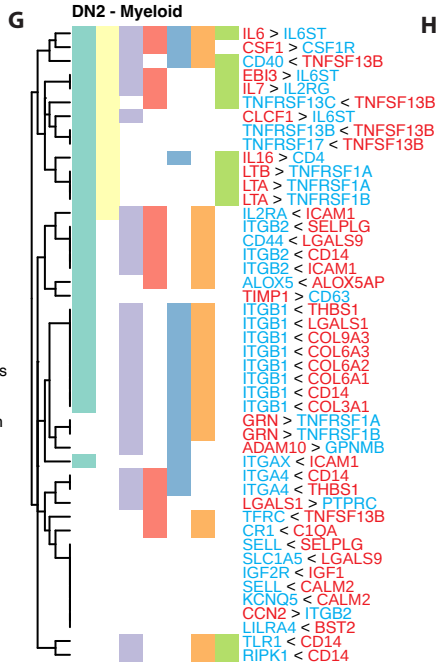

B
High
Low
Total imputed interaction strength


C
SED
GC


F
0
10
20
30
–log10(P)
Cytokine Signaling in Immune system
Cytokine–cytokine receptor interaction
leukocyte activation
positive regulation of cell adhesion
positive regulation of locomotion
inflammatory response
positive regulation of cytokine production
positive regulation of protein phosphorylation
adaptive immune response
Cell surface interactions at the vascular wall
Viral protein interaction with cytokine and cytokine receptor
regulation of peptidyl–tyrosine phosphorylation
regulation of B cell activation
Extrafollicular and follicular B cell activation by SARS CoV 2
myeloid leukocyte activation
response to molecule of bacterial origin
Human T–cell leukemia virus 1 infection
Immunoregulatory interactions Lymphoid / non–Lymphoid cell


D
Mean imputed interaction strength (Source)
aNAV
DN2
IgM–only
Centroblast
TS
Centrocyte
PB
MZ
CSM
Naive
0
20000
40000
Number of edges


E
Target
Plasma cells
Myeloid
Mesenchymal
Epithelial
Endothelial
CD8+ T cells
CD4+ T cells
aNAV
Centroblast
Centrocyte
CSM
DN2
IgM–only
MZ
Naive
PB
TS
Source
Mean imputed interaction strength
per edge
High
Low
Edges
5000
10000
15000
20000


G
DN2 - Myeloid
IL6 > IL6ST
CSF1 > CSF1R
CD40 < TNFSF13B
EBI3 > IL6ST
IL7 > IL2RG
TNFRSF13C < TNFSF13B
CLCF1 > IL6ST
TNFRSF13B < TNFSF13B
TNFRSF17 < TNFSF13B
IL16 > CD4
LTB > TNFRSF1A
LTA > TNFRSF1A
LTA > TNFRSF1B
IL2RA < ICAM1
ITGB2 < SELPLG
CD44 < LGALS9
ITGB2 < CD14
ITGB2 < ICAM1
ALOX5 < ALOX5AP
TIMP1 > CD63
ITGB1 < THBS1
ITGB1 < LGALS1
ITGB1 < COL9A3
ITGB1 < COL6A3
ITGB1 < COL6A2
ITGB1 < COL6A1
ITGB1 < CD14
ITGB1 < COL3A1
GRN > TNFRSF1A
GRN > TNFRSF1B
ADAM10 > GPNMB
ITGAX < ICAM1
ITGA4 < CD14
ITGA4 < THBS1
LGALS1 > PTPRC
TFRC < TNFSF13B
CR1 < C1QA
SELL < SELPLG
SLC1A5 < LGALS9
IGF2R < IGF1
SELL < CALM2
KCNQ5 < CALM2
CCN2 > ITGB2
LILRA4 < BST2
TLR1 < CD14
RIPK1 < CD14

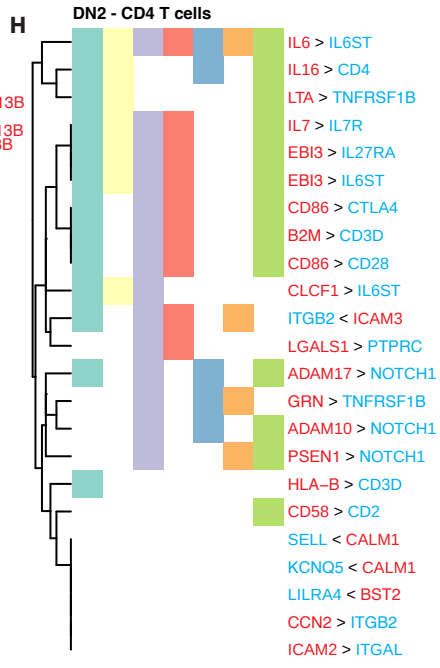
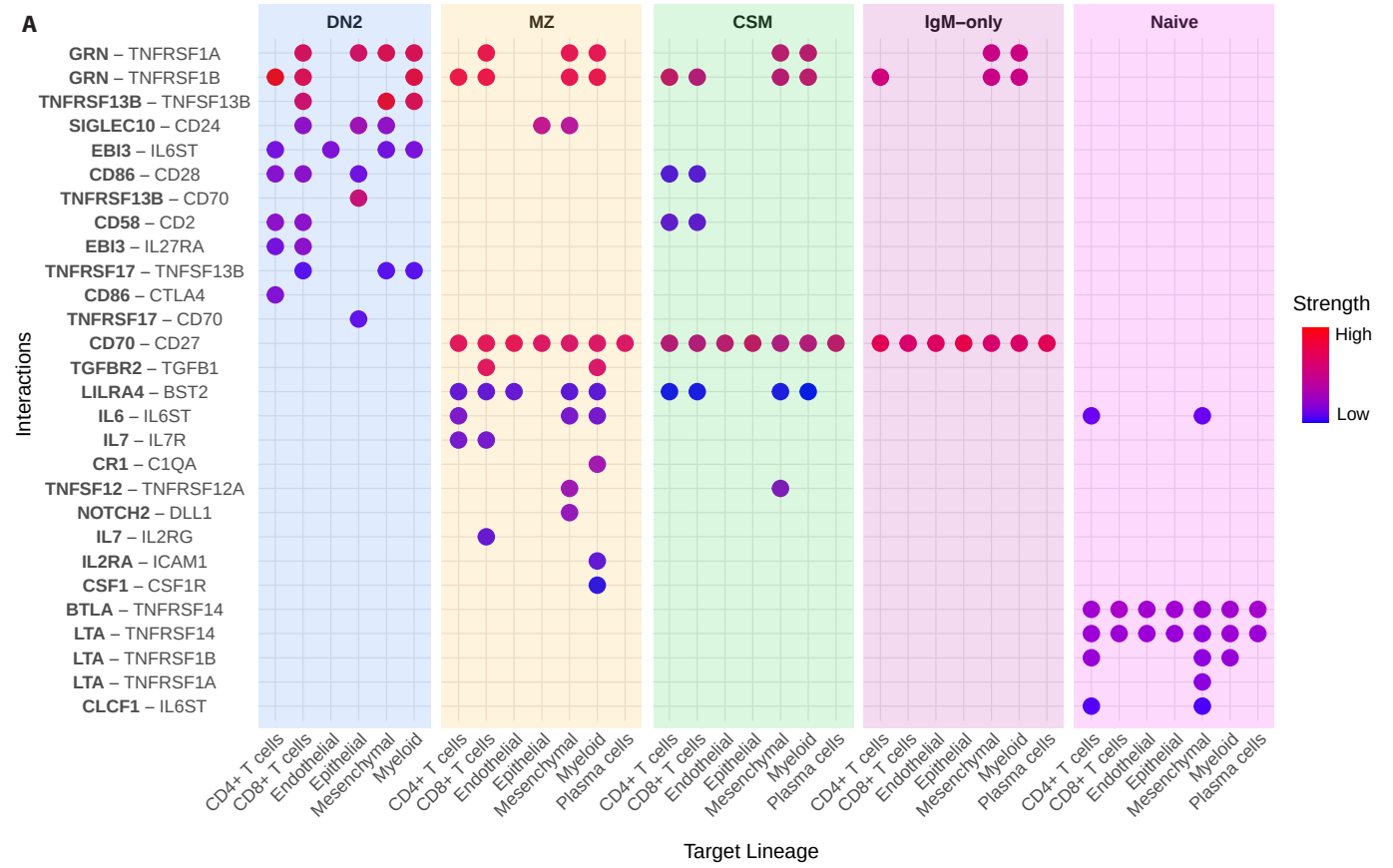

H
DN2 - CD4 T cells
IL6 > IL6ST
IL16 > CD4
LTA > TNFRSF1B
IL7 > IL7R
EBI3 > IL27RA
EBI3 > IL6ST
CD86 > CTLA4
B2M > CD3D
CD86 > CD28
CLCF1 > IL6ST
ITGB2 < ICAM3
LGALS1 > PTPRC
ADAM17 > NOTCH1
GRN > TNFRSF1B
ADAM10 > NOTCH1
PSEN1 > NOTCH1
HLA–B > CD3D
CD58 > CD2
SELL < CALM1
KCNQ5 < CALM1
LILRA4 < BST2
CCN2 > ITGB2
ICAM2 > ITGAL

Fig. 4


A
DN2
MZ
CSM
IgM–only
Naive
GRN – TNFRSF1A
GRN – TNFRSF1B
TNFRSF13B – TNFSF13B
SIGLEC10 – CD24
EBI3 – IL6ST
CD86 – CD28
TNFRSF13B – CD70
CD58 – CD2
EBI3 – IL27RA
TNFRSF17 – TNFSF13B
CD86 – CTLA4
TNFRSF17 – CD70
CD70 – CD27
TGFBR2 – TGFB1
LILRA4 – BST2
IL6 – IL6ST
IL7 – IL7R
CR1 – C1QA
TNFSF12 – TNFRSF12A
NOTCH2 – DLL1
IL7 – IL2RG
IL2RA – ICAM1
CSF1 – CSF1R
BTLA – TNFRSF14
LTA – TNFRSF14
LTA – TNFRSF1B
LTA – TNFRSF1A
CLCF1 – IL6ST
Interactions
CD4+ T cells
CD8+ T cells
Endothelial
Epithelial
Mesenchymal
Myeloid
Plasma cells
Target Lineage
Strength
High
Low

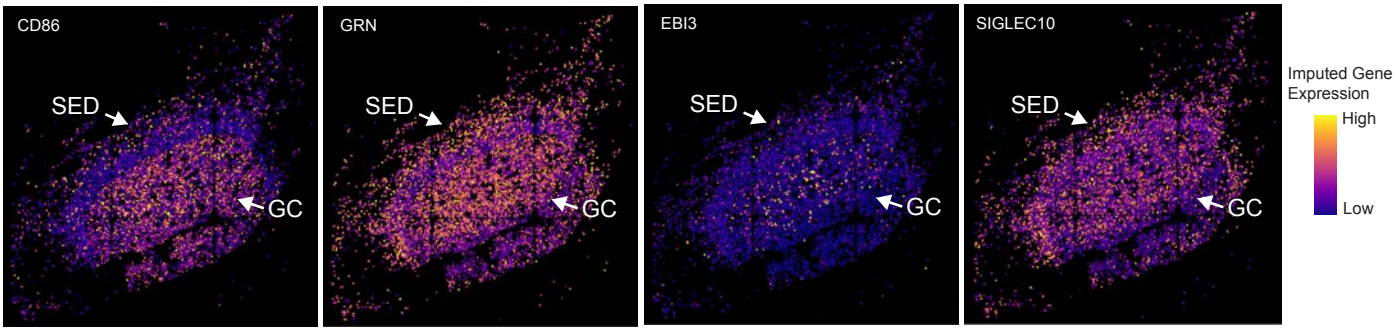

B
CD86
GRN
EBI3
SIGLEC10
SED
GC
Imputed Gene Expression
High
Low

Fig. 5

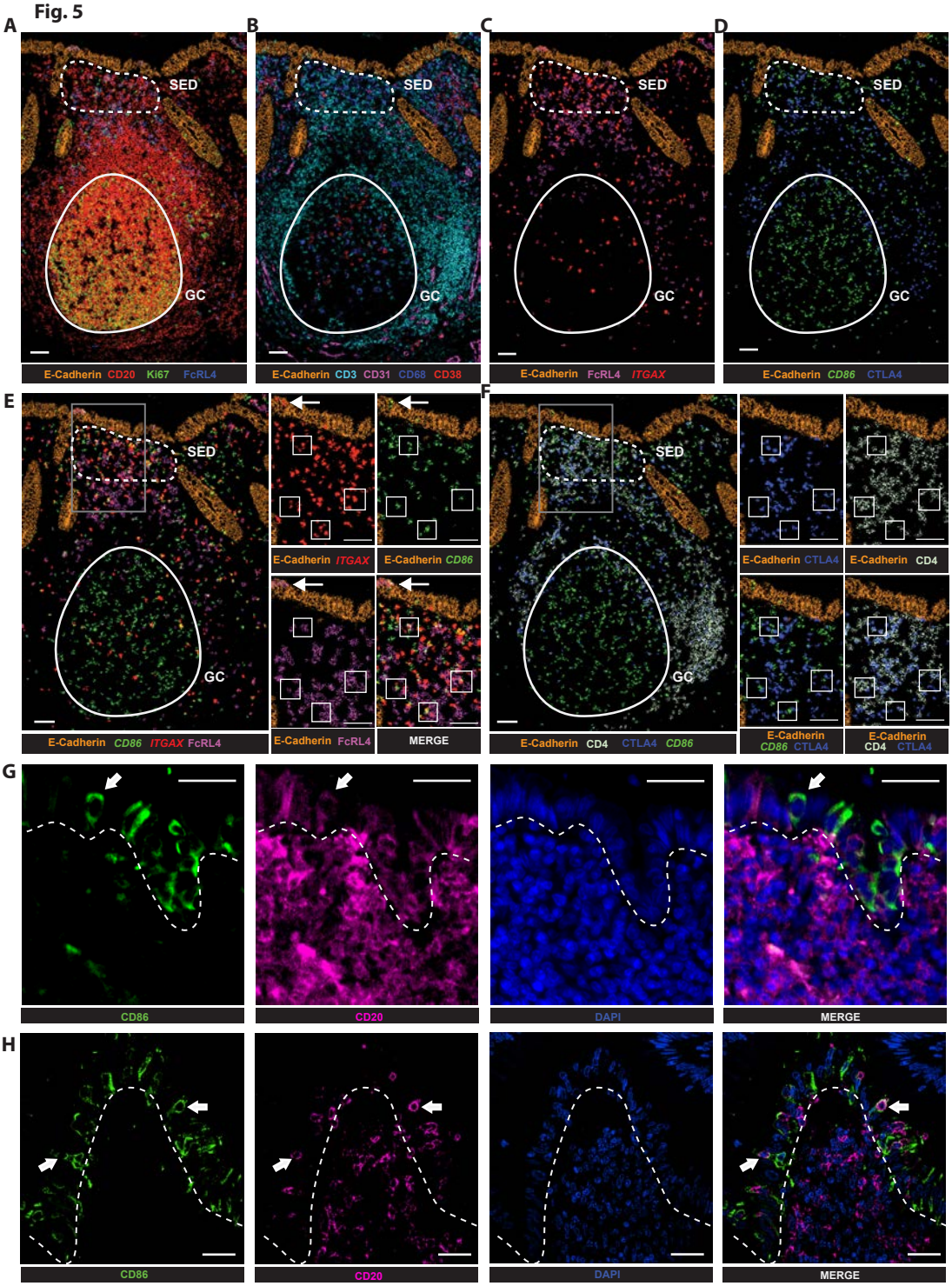

A
SED
GC
E-Cadherin CD20 Ki67 FcRL4
B
SED
GC
E-Cadherin CD3 CD31 CD68 CD38
C
SED
GC
E-Cadherin FcRL4 ITGAX
D
SED
GC
E-Cadherin CD86 CTLA4
E
SED
GC
E-Cadherin CD86 ITGAX FcRL4
E-Cadherin ITGAX
E-Cadherin CD86
E-Cadherin FcRL4
MERGE
F
SED
GC
E-Cadherin CD4 CTLA4 CD86
E-Cadherin CTLA4
E-Cadherin CD4
E-Cadherin CD86 CTLA4
E-Cadherin CD4 CTLA4
G
CD86
CD20
DAPI
MERGE
H
CD86
CD20
DAPI
MERGE

Fig. 6

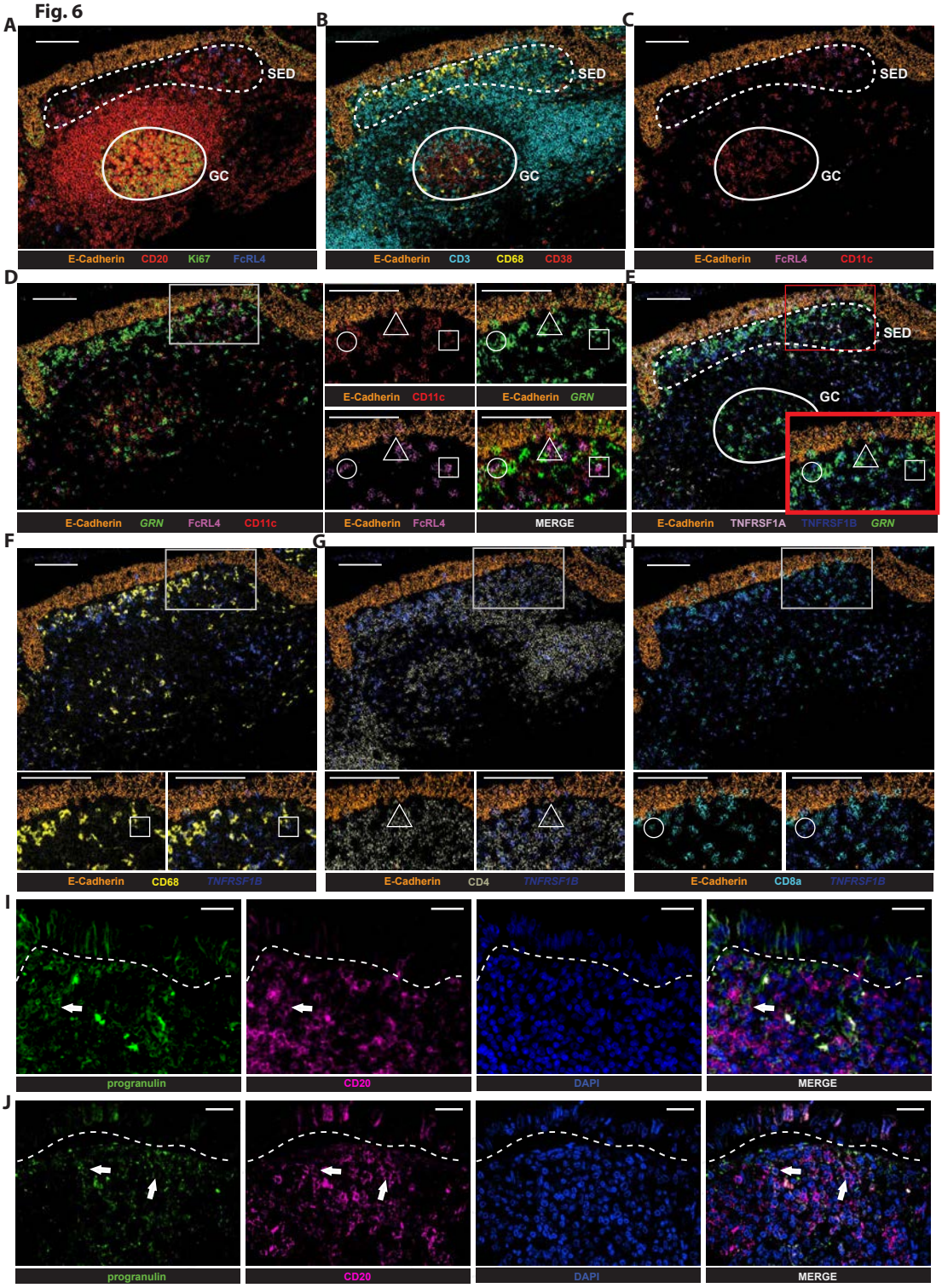

A
SED
GC
E-Cadherin CD20 Ki67 FcRL4
B
SED
GC
E-Cadherin CD3 CD68 CD38
C
SED
GC
E-Cadherin FcRL4 CD11c
D
E-Cadherin GRN FcRL4 CD11c
E-Cadherin CD11c
E-Cadherin GRN
E-Cadherin FcRL4
MERGE
E
SED
GC
E-Cadherin TNFRSF1A TNFRSF1B GRN
F
E-Cadherin CD68 TNFRSF1B
G
E-Cadherin CD4 TNFRSF1B
H
E-Cadherin CD8a TNFRSF1B
I
progranulin
CD20
DAPI
MERGE
J
progranulin
CD20
DAPI
MERGE

Fig. 7

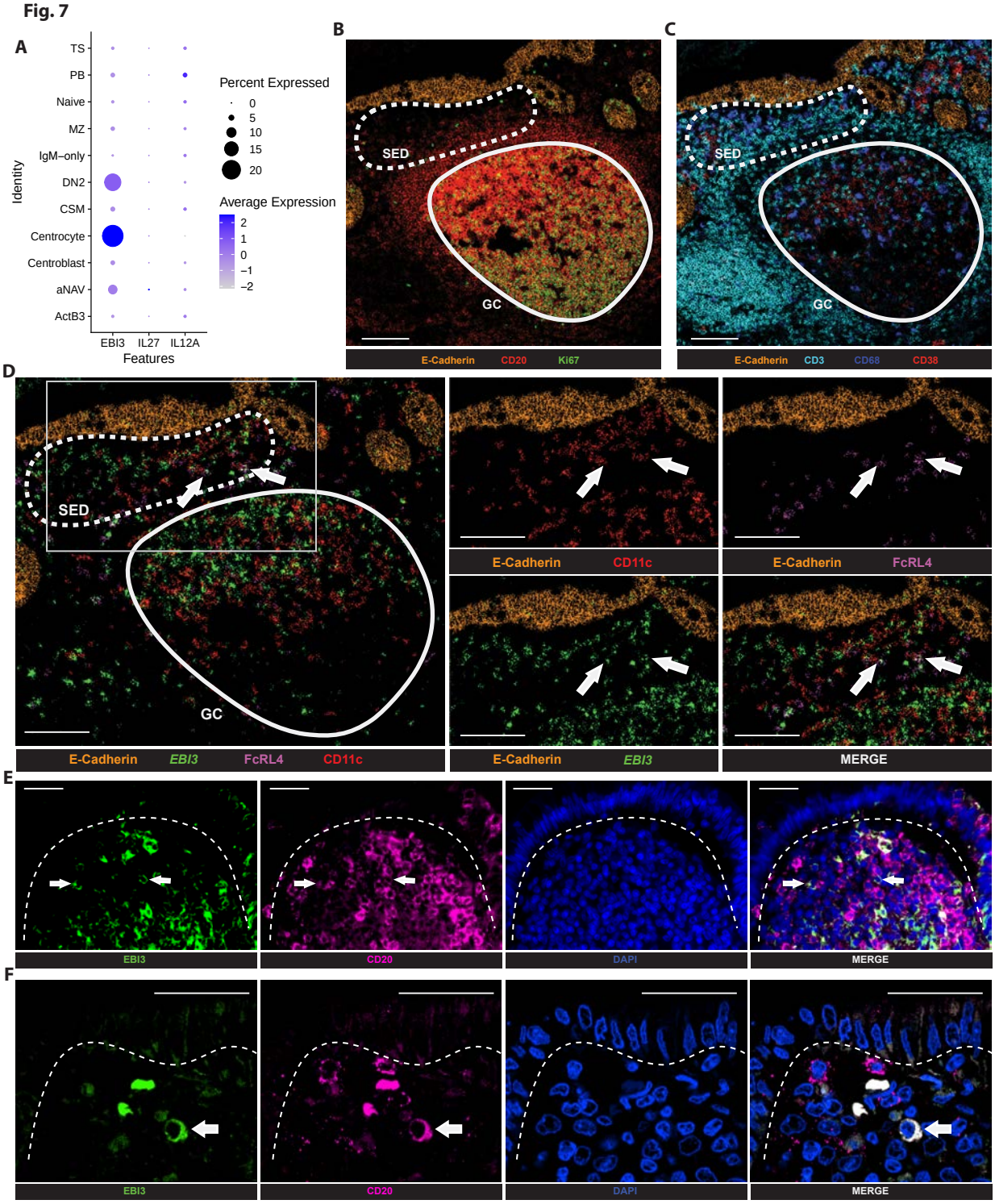
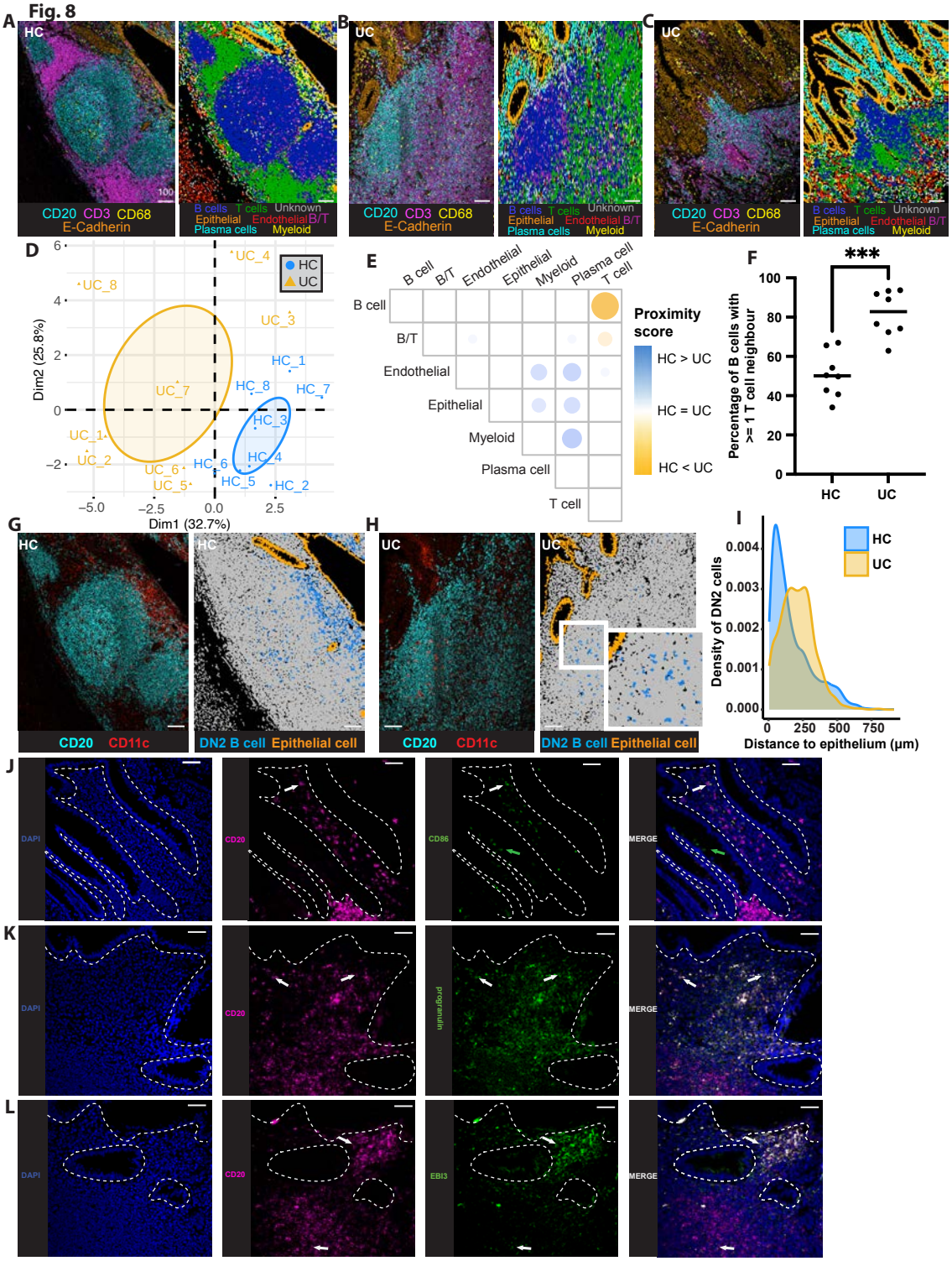

A
TS
PB
Naive
MZ
IgM–only
DN2
CSM
Centrocyte
Centroblast
aNAV
ActB3
Identity
EBI3
IL27
IL12A
Features
Percent Expressed
0
5
10
15
20
Average Expression
2
1
0
−1
−2
B
SED
GC
E-Cadherin
CD20
Ki67
C
SED
GC
E-Cadherin
CD3
CD68
CD38
D
SED
GC
E-Cadherin
EBI3
FcRL4
CD11c
E-Cadherin
CD11c
E-Cadherin
FcRL4
E-Cadherin
EBI3
E-Cadherin
EBI3
MERGE
E
EBI3
CD20
DAPI
MERGE
F
EBI3
CD20
DAPI
MERGE

Fig. 8


A
HC
CD20 CD3 CD68
E-Cadherin
B cells T cells Unknown
Epithelial Endothelial B/T
Plasma cells Myeloid
B
UC
C
UC
D
HC
UC
Dim2 (25.8%)
Dim1 (32.7%)
E
B cell
B/T
Endothelial
Epithelial
Myeloid
Plasma cell
T cell
Proximity score
HC > UC
HC = UC
HC < UC
F
***
Percentage of B cells with >= 1 T cell neighbour
HC
UC
G
CD20 CD11c
DN2 B cell Epithelial cell
H
I
Density of DN2 cells
Distance to epithelium (μm)
J
DAPI
CD20
CD86
MERGE
K
programulin
L
EBI3

Supplementary Materials for

Immunomodulatory interactions of B cells in human gut-associated lymphoid tissue

Michael J Pitcher, Xiaowen Sun, Chiara Dionisi, Lucia Montorsi, Sherine H Kottoor, Jacqueline HY Siu, Roman Laddach, Rosamond Nuamah, Gavin J Pettigrew, Richard J. Ellis, Cynthia Bishop, Jahangir Sufi, Pawan Dhami, Heli Vaikkinen, Audrey Kelly, Anna Vossenkamper, Deena L. Gibbons, Jo Spencer
Corresponding author: jo.spencer@kcl.ac.uk

The PDF file includes:

Figs. S1 to S6
Tables S1 to S3

Other Supplementary Materials for this manuscript include the following:

Data files 1-9.
Raw figure data file.
MDAR Reproducibility Checklist

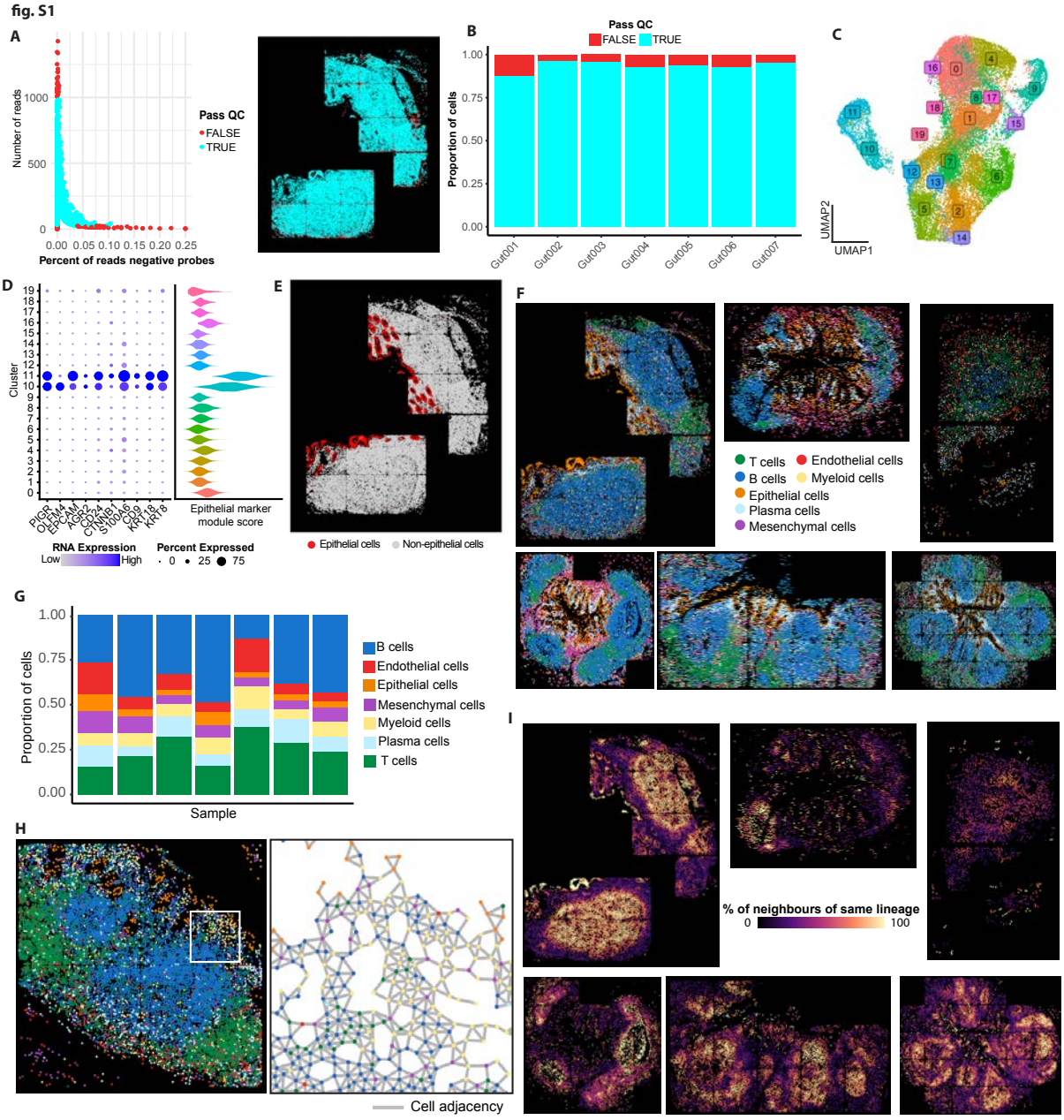


Fig. S1. Computational analysis of cells in GALT using CosMx

(A) Quality control (QC) of cells from a single representative sample in CosMx data, based on manual thresholding of reads per cell and percentage of reads belonging to negative probes (left). Resulting classifications of pass/fail QC were visualised back on the images (right). (B) Bar chart showing proportion of cells passing QC for each CosMx sample. (C) UMAP visualization of clusters from the same sample as shown in (A – labelled Gut004 in (B)). (D) Dot plot (left) showing expression of epithelial cell markers in clusters from (C). Genes are top 10 differential expressed genes from cells labelled as 'epithelial cells' in reference data used for lineage labelling in Fig. 1. Violin plot (right) showing module score per cluster for all epithelial markers. (E) Spatial plot

showing position of cells from clusters 10 and 11 in (D) marked as ‘Epithelial cells’. (F) Spatial plots for cell lineages for other CosMx samples – sample labelled Gut003 is shown in Fig. 1B. (G) Stack bar plot showing the proportion of major cell linages across individual samples using CosMx. (H) Spatial plot demonstrating construction of neighbor graphs by Delaunay triangulation. (I) Spatial plot showing percentage of neighbors of each cell which share the same lineage as the cell for CosMx samples – Gut003 is shown in Fig. 1G

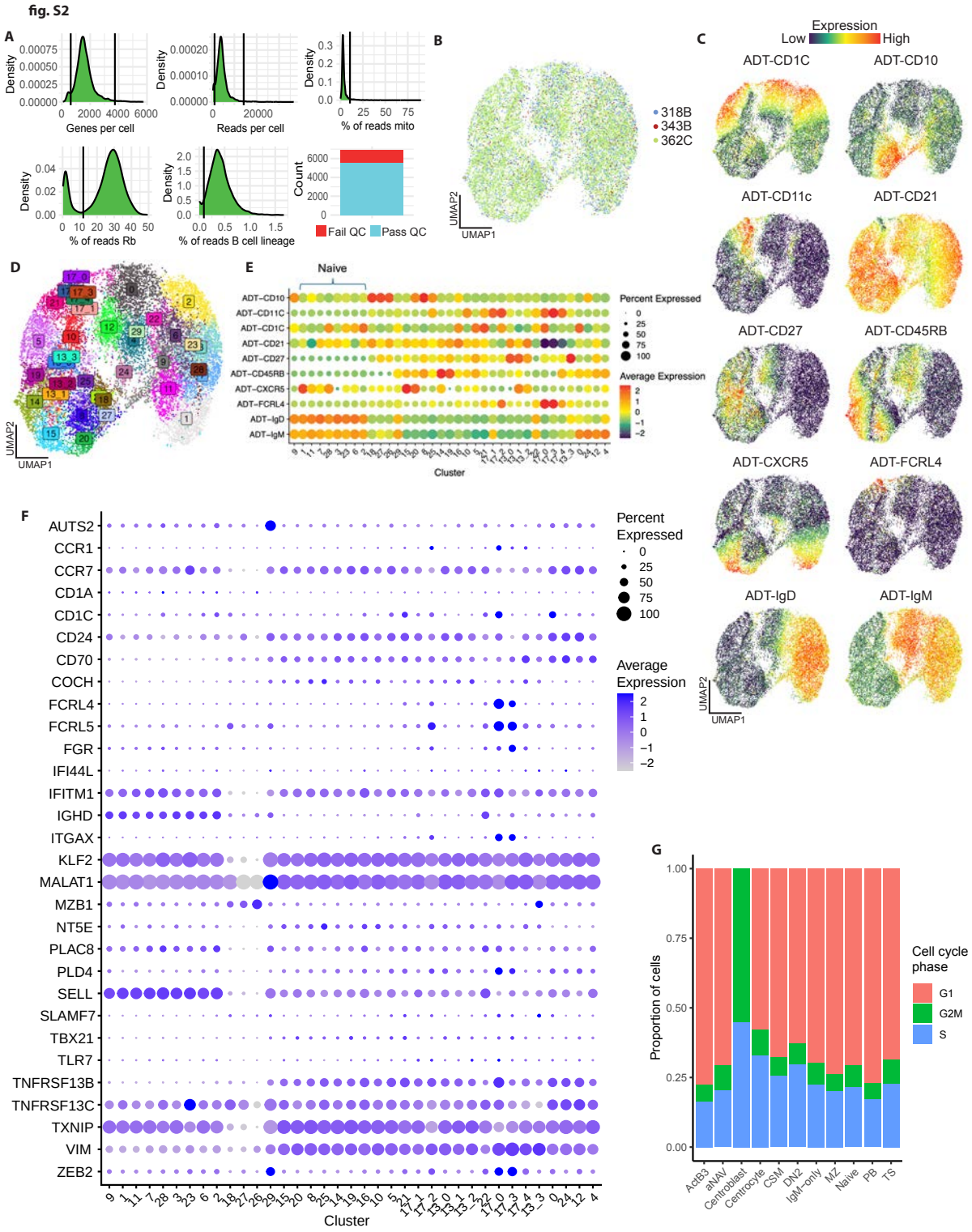


Fig. S2. Computational analysis of B cells in GALT using CITE-seq

(A) Quality control from a single representative sample, showing automatic thresholding for metrics: genes per cell, reads per cell, percentage of reads per cell classified as mitochondrial, percentage of reads per cell classified as ribosomal, percentage of reads per cell belonging to B

cell lineage genes (CD19, MS4A1, CD79A, CD79B). (B) UMAP visualization of B cells, showing cells split by donor of origin for confirmation of batch effect integration methods. (C) UMAP visualization of ADT surface antibody markers. (D) UMAP visualization of cells colored by cluster before manual cluster re-labeling. (E) Dotplot showing expression of ADT cell surface markers for each cluster in (D). (F) Dotplot showing expression of RNA markers for each cluster in (D). (G) Bar chart showing proportion of each labeled B cell subset belonging to cell cycle phases G1, G2M and S.

Fig. S3

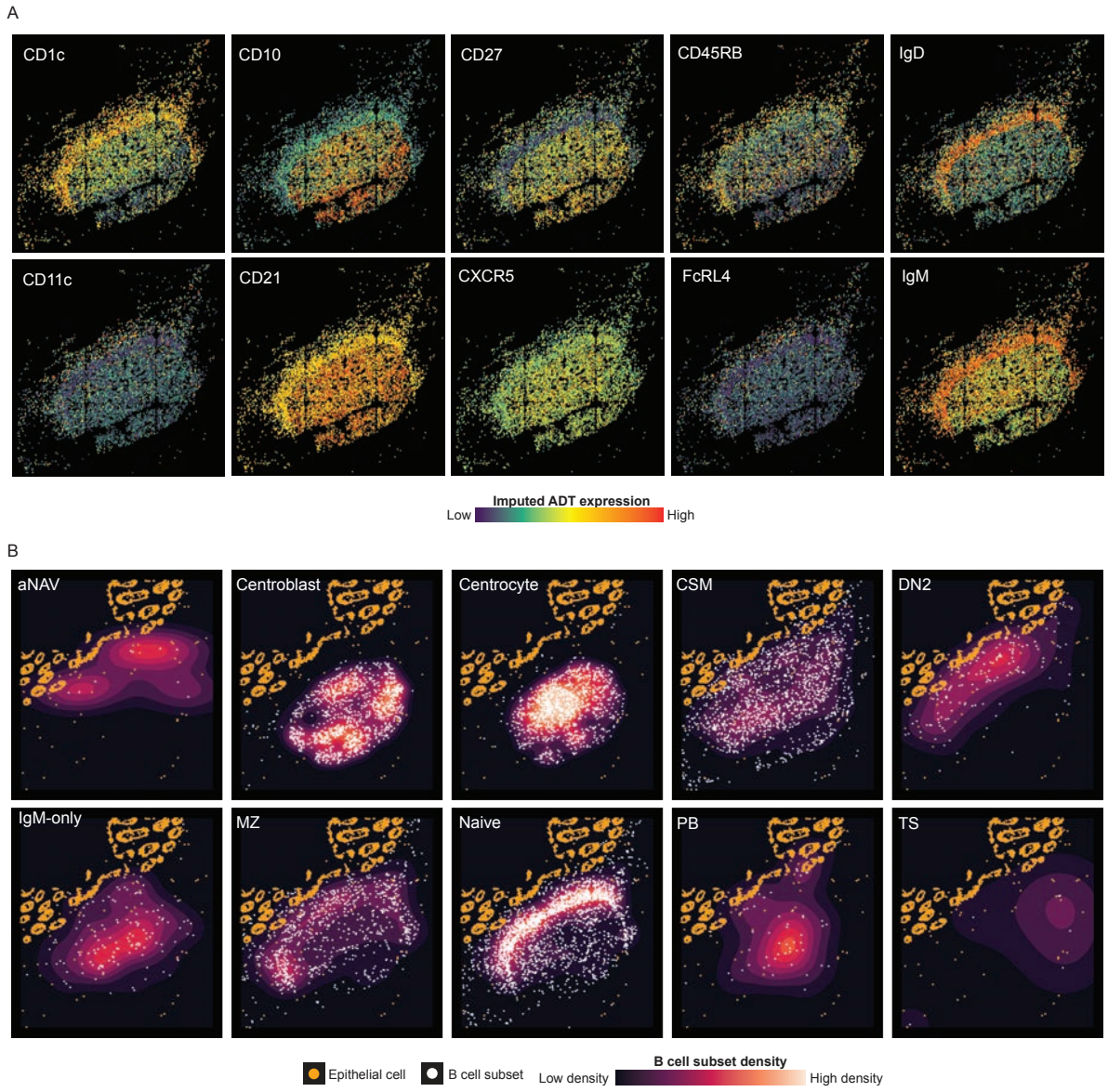


Fig. S3. Validation of imputed B cell subsets in GALT using CosMx

(A) Spatial visualization of imputed cell surface markers across B cell subsets in CosMx data. (B) B cell subset densities across the follicle shown in Fig. 2E.

fig. S4

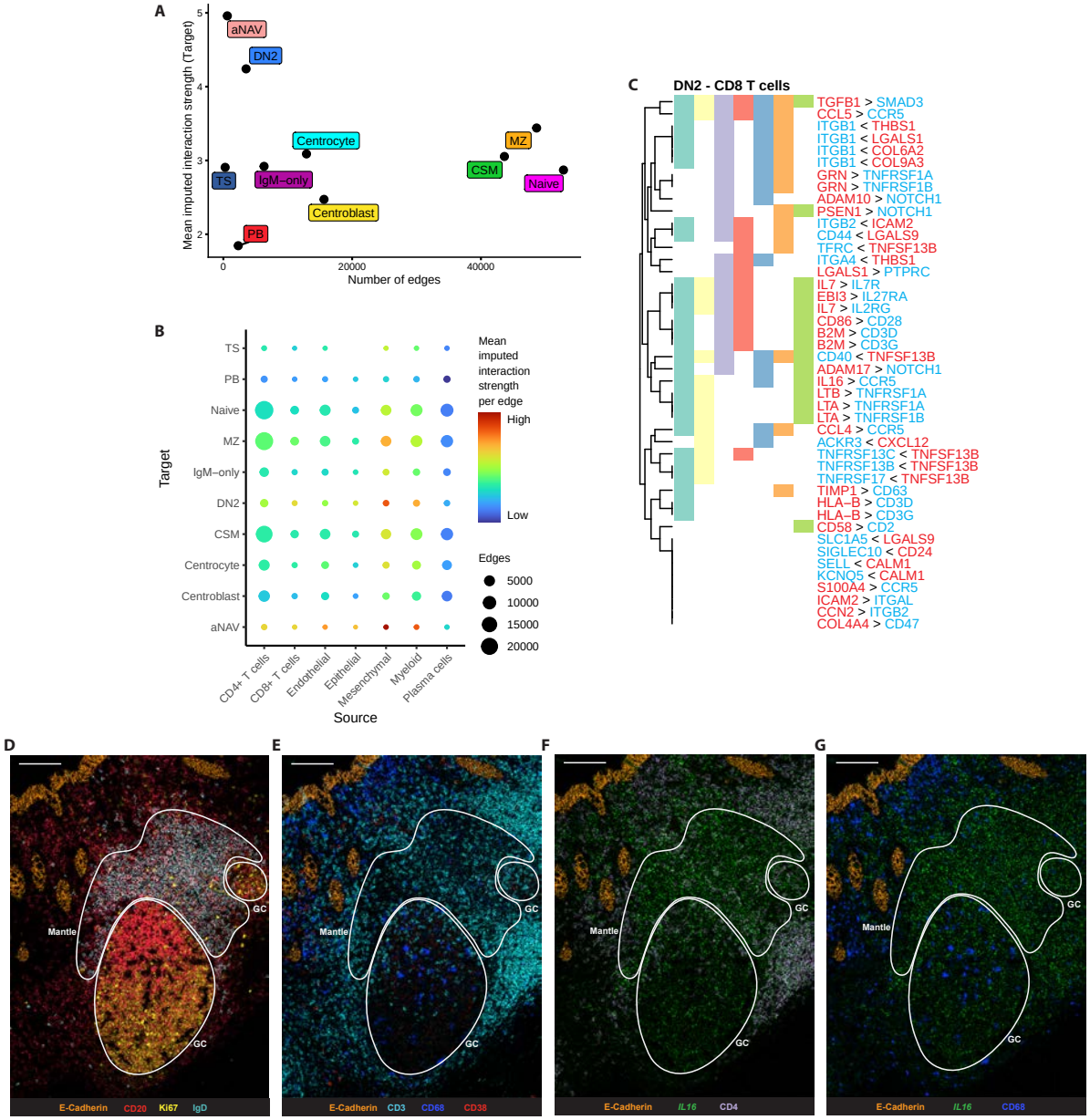


Fig. S4. Imputed interaction networks of B cell subsets and spatial validation of IL16 gene expression in follicular microenvironments

(A) Scatter plot showing the number of interaction edges (x-axis) and the mean imputed interaction strength (y-axis) for each B cell subset. Values include interactions where cells act as target (expressing imputed receptor). (B) Dot plot for B cell subset imputed interactions with B cells as source (expressing imputed ligand) and other lineages as the target (expressing observed receptor). (C) Ligand-receptor pairs present on DN2 interactions with $CD8^{+}$ T cells.

(D-G) Representative images generated by IMC and RNAscope of IL16 transcript expression in follicular architecture with germinal centers (GC) and mantle zones outlined in white. (D) B cell compartment (CD20) and proliferative status (Ki67). (E) Distribution of T cells (CD3), myeloid cells (CD68) and plasma cells (CD38) regions. (F) Spatial distribution of IL16 transcripts near $CD4^+$ T cells across follicular and GC areas. (G) IL16 transcript regions are spatially adjacent to $CD68^+$ myeloid cells within follicular microenvironments. Scale bars: 100 μm.

fig. S5

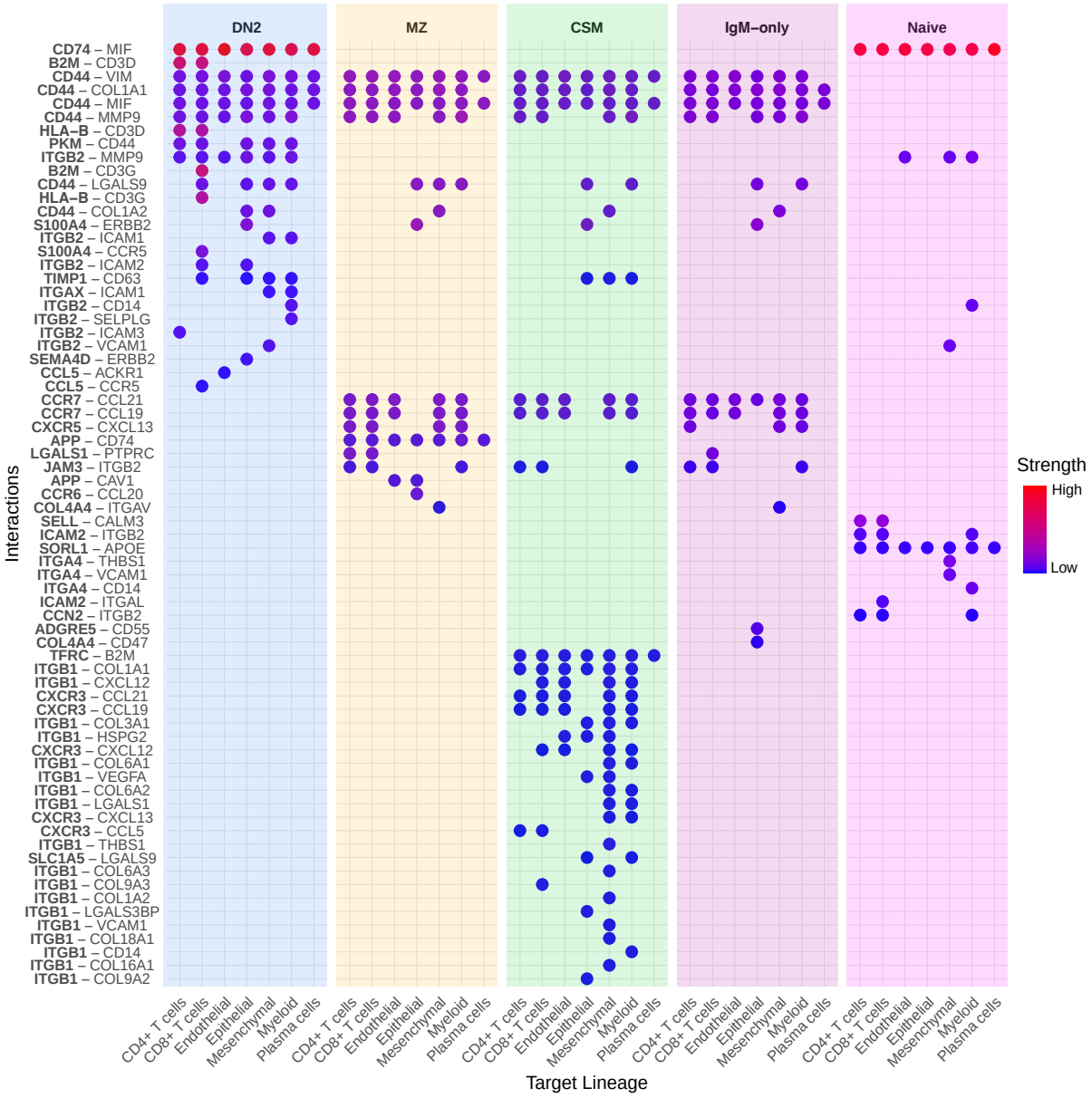


Fig. S5. Imputed interactions associated with antigen presentation and cell migration and/or maintenance function of significant B cell marker genes across selected B cell subsets

Dot plot showing the strength of imputed ligand-receptor interactions related to Antigen Presentation and Cell Migration and/or Maintenance involving B cell marker genes across five B cell subsets (DN2, MZ, CSM, IgM-only, and Naive). Dot color indicates interaction strength, with warmer colors representing stronger interactions.

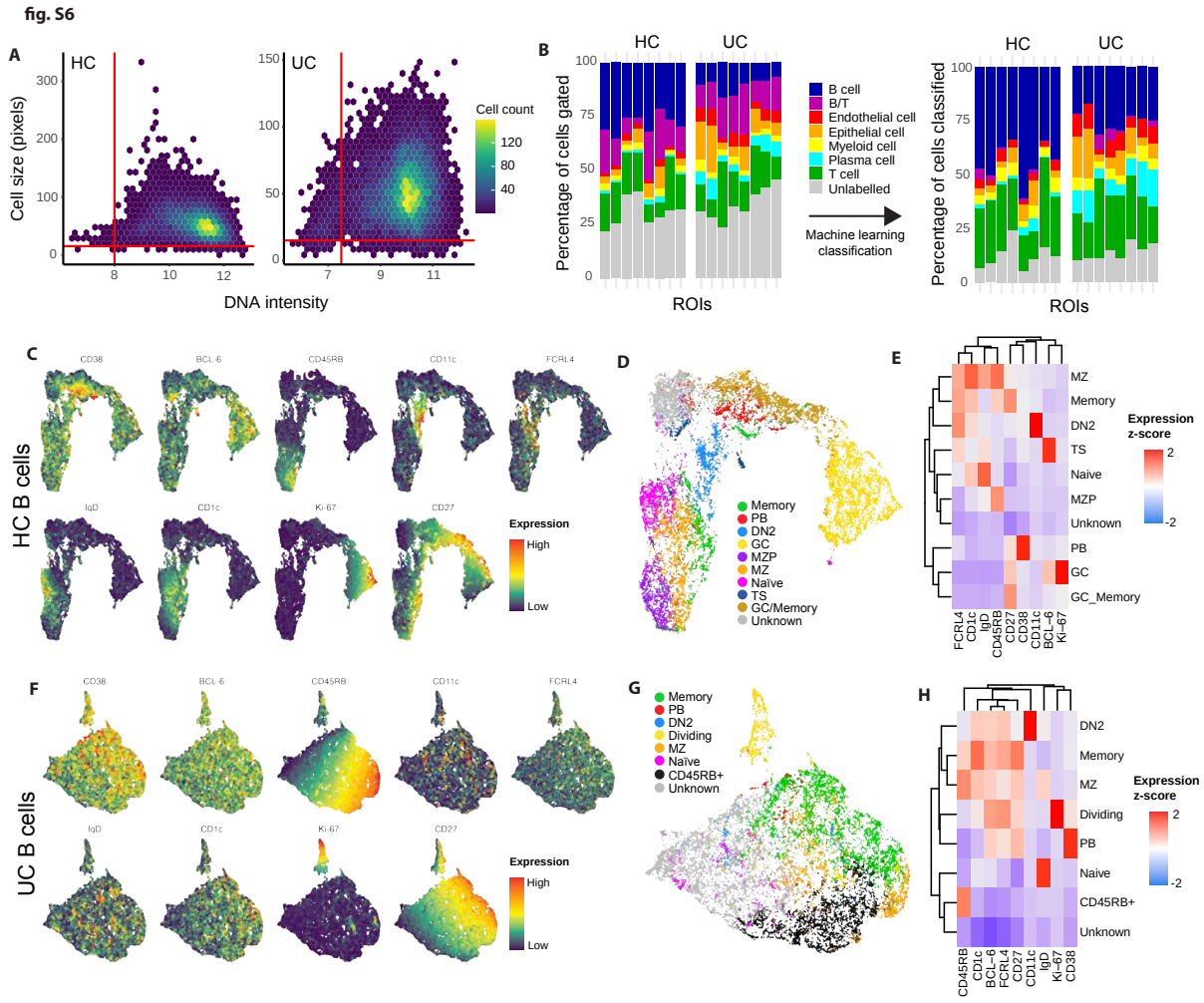


Fig. S6. Computational comparisons of GALT cells from ulcerative colitis patients and healthy controls

(A) Quality control of imaging mass cytometry data showing removal of segmented cells with low cell area and low DNA intensity (cell fragments). (B) B cell subsets classified in IMC data by manual gating (left) and subsequent machine learning classification (right). (C) UMAP showing expression of B cell subset markers in healthy appendix B cells in IMC. (D) UMAP showing B cell subset classification in healthy appendix B cells in IMC. (E) Heatmap showing expression of B cell subset markers in B cell subsets in healthy appendix B cells in IMC. (F) UMAP showing expression of B cell subset markers in UC appendix B cells in IMC. (G) UMAP showing B cell subset classification in UC appendix B cells in IMC. (H) Heatmap showing expression of B cell subset markers in B cell subsets in UC appendix B cells in IMC.

Table S1 Antibodies used in CITEseq experiment

ADT marker	Clone	Supplier	1/ dilution factor
ADT_IgD_TotalSeqC	IA6-2	Biolegend	20
ADT_IgM_TotalSeqC	MHM-88	Biolegend	20
ADT_CD10_TotalSeqC	HI10a	Biolegend	20
ADT_CD21_TotalSeqC	Bu32	Biolegend	20
ADT_CD1C_TotalSeqC	L161	Biolegend	20
ADT_CD27_TotalSeqC	Clone_323	Biolegend	20
ADT_CD11C_TotalSeqC	S-HCL-3	Biolegend	20
ADT_CXCR5_TotalSeqC	J252D4	Biolegend	20
ADT_FCRL4_TotalSeqC	413D2	Biolegend	20
ADT_CD45RB_TotalSeqC	MEM-55	Biolegend	20

Table S2 Antibodies used for immunofluoresence /confocal validation of interactions

Antibodies	Catalog #	Manufacturer	Species reactivity	Dilution	Antibodies
B7-2 (D-6)	sc-28347	Santa Cruz	Mouse	1:50	B7-2 (D-6)
Anti-GRN antibody	ab208777	Abcam	Rabbit	1:250	Anti-GRN antibody
Anti-EBI3 antobody	ab397195	Abcam	Rabbit	1:250	Anti-EBI3 antobody
Anti-CD20 antibody	ab244336	Abcam	Rabbit	1:1000	Anti-CD20 antibody
Purified anti-human CD20 Antibody	382802	BioLegend	Mouse	1:50	Purified anti-human CD20 Antibody
Donkey anti-Mouse IgG (H+L) Alexa Fluor™ Plus 555 - A32773	A32773	Thermo Fisher	Donkey	1:500	Donkey anti-Mouse IgG (H+L) Alexa Fluor™ Plus 555 - A32773
Donkey anti-Rabbit IgG (H+L) Alexa Fluor™ Plus 555 - A32794	A32794	Thermo Fisher	Donkey	1:500	Donkey anti-Rabbit IgG (H+L) Alexa Fluor™ Plus 555 - A32794
F(ab')2-Goat anti-Rabbit IgG (H+L) Alexa Fluor™ Plus 488 - A48282TR	A48282TR	Thermo Fisher	Goat	1:500	F(ab')2-Goat anti-Rabbit IgG (H+L) Alexa Fluor™ Plus 488 - A48282TR
F(ab')2-Goat anti-Mouse IgG (H+L) Alexa Fluor™ Plus 488 - A48286TR	A48286TR	Thermo Fisher	Goat	1:500	F(ab')2-Goat anti-Mouse IgG (H+L) Alexa Fluor™ Plus 488 - A48286TR

Table S3 Sample information

Appendix samples used for CITEseq:

Brain death donor (DBD) or cardiac death donor (DCD)	Disease	Age	Sex
DBD	Healthy	77	F
DBD	Healthy	70	F
DCD	Healthy	60	M

Patients with UC who underwent right hemicolectomy

Age at surgery	Sex	Disease duration (years)	Medication on admission
30	M	4	azathioprine, humira
28	M	1	azathioprine
47	F	8	mesalasine
27	F	16	mesalasine

In addition, twelve FFPE samples of normal human appendix were used for COSMX, for validation of imputed cellular interactions, and controls for comparison with UC appendix. No donor information is available for these samples.